# INVESTIGATION OF STABILITY, DYNAMICS AND SCOPE OF APPLICATION OF MYCOBACTERIAL PORIN MSPA: A HIGHLY VERSATILE BIOMOLECULAR RESOURCE

by

JAYAWEERALAGE AYOMI SHEAMILKA PERERA

B. Sc., The Open University of Sri Lanka, 2007

AN ABSTRACT OF A DISSERTATION

submitted in partial fulfillment of the requirements for the degree

DOCTOR OF PHILOSOPHY

Department of Chemistry
College of Arts and Sciences

KANSAS STATE UNIVERSITY
Manhattan, Kansas

2012

# Abstract

Porin A from *Mycobacterial smegmatis* (MspA) is an octameric trans-membrane channel protein and is one of the most stable porins known to date. MspA has been successfully isolated and purified to obtain liquid extracts and crystals using a modified extraction procedure. A full analytical assessment has been carried out to authenticate its' structure, including gel electrophoresis, spectroscopy (fluorescence, UV, FTIR, NMR), HPLC, Bradford protein assay, dynamic light scattering and X-ray crystallography. Nanoscopic vesicle formation of MspA molecules in aqueous media has been thoughroughly investigated. Temperature dependent dynamic light scattering experiments reveal that size of such vesicles is dependent on temperature but is independent of ionic strength of the medium. Zeta potential measurements reveal a steady build up of positive charge on the vesicle surface with increasing temperature.

For the first time, wild type (WT) MspA has been utilized as a channel forming agent. This phenomenon has future potential in DNA sequencing and the development of antimycobacterial drugs. Channel activity of WT MspA and mutant A96C MspA has been investigated and has shown to form stable channels across DPhPC lipid bilayers. Blocking of the channel current via external molecules (i.e. channel blocking) is an extremely important process, which helps to evaluate the biosensor ability of the pore. In this regard, two Ruthenium based compounds, $Ru(QP\text{-}C_2)_3^{8+}$ (i.e. RuC2) and $Ru(bpy)_3^{2+}$have been successfully employed as channel blocking agents. Both compounds show evidence for channel blocking of WT MspA. However, these results are not reproducible.

Three dimensional aggregation behavior of RuC2-MspA vesicles have been thoughroughly investigated. It is evident that addition of RuC2 significantly increases vesicle

size and polydispersity of MspA aggregates in solution. The results provide explanations onto the lack of channel blocking ability of MspA by RuC2.

Development of a ‘greener’ dye sensitized solar cell with the use of MspA as an electron carrier is investigated for the first time. A series of Ru(II)-phenanthroline-based dyes have been synthesized as non-toxic dyes in this regard. Chemical binding between the dyes and MspA has been achieved successfully. Two types of solar cell prototypes, i.e. $TiO_2$-based (Grätzel type) and FTO-based have been developed and tested. Significant current generation and conversion efficiencies have been achieved for both cell types. This marks the first development of a protein-based photovoltaic device, which has the potential to be developed as a new class of “hybrid soft solar cells”.

# INVESTIGATION OF STABILITY, DYNAMICS AND SCOPE OF APPLICATION OF MYCOBACTERIAL PORIN MSPA: A HIGHLY VERSATILE BIOMOLECULAR RESOURCE

by

JAYAWEERALAGE AYOMI SHEAMILKA PERERA

B. Sc., The Open University of Sri Lanka, 2007

A DISSERTATION

submitted in partial fulfillment of the requirements for the degree

DOCTOR OF PHILOSOPHY

Department of Chemistry
College of Arts and Sciences

KANSAS STATE UNIVERSITY
Manhattan, Kansas

2012

Approved by:

Major Professor
Dr. Stefan. H. Bossmann

# Copyright

# Abstract

Porin A from *Mycobacterial smegmatis* (MspA) is an octameric trans-membrane channel protein and is one of the most stable porins known to date. MspA has been successfully isolated and purified to obtain liquid extracts and crystals using a modified extraction procedure. A full analytical assessment has been carried out to authenticate its' structure, including gel electrophoresis, spectroscopy (fluorescence, UV, FTIR, NMR), HPLC, Bradford protein assay, dynamic light scattering and X-ray crystallography. Nanoscopic vesicle formation of MspA molecules in aqueous media has been thoughroughly investigated. Temperature dependent dynamic light scattering experiments reveal that size of such vesicles is dependent on temperature but is independent of ionic strength of the medium. Zeta potential measurements reveal a steady build up of positive charge on the vesicle surface with increasing temperature.

For the first time, wild type (WT) MspA has been utilized as a channel forming agent. This phenomenon has future potential in DNA sequencing and the development of antimycobacterial drugs. Channel activity of WT MspA and mutant A96C MspA has been investigated and has shown to form stable channels across DPhPC lipid bilayers. Blocking of the channel current via external molecules (i.e. channel blocking) is an extremely important process, which helps to evaluate the biosensor ability of the pore. In this regard, two Ruthenium based compounds, $Ru(QP\text{-}C_2)_3^{8+}$ (i.e. RuC2) and $Ru(bpy)_3^{2+}$have been successfully employed as channel blocking agents. Both compounds show evidence for channel blocking of WT MspA. However, these results are not reproducible.

Three dimensional aggregation behavior of RuC2-MspA vesicles have been thoughroughly investigated. It is evident that addition of RuC2 significantly increases vesicle

size and polydispersity of MspA aggregates in solution. The results provide explanations onto the lack of channel blocking ability of MspA by RuC2.

Development of a ‘greener’ dye sensitized solar cell with the use of MspA as an electron carrier is investigated for the first time. A series of Ru(II)-phenanthroline-based dyes have been synthesized as non-toxic dyes in this regard. Chemical binding between the dyes and MspA has been achieved successfully. Two types of solar cell prototypes, i.e. $TiO_2$-based (Grätzel type) and FTO-based have been developed and tested. Significant current generation and conversion efficiencies have been achieved for both cell types. This marks the first development of a protein-based photovoltaic device, which has the potential to be developed as a new class of “hybrid soft solar cells”.

# Table of Contents

# List of Figures

# List of Tables

# Acknowledgements

I would like to greatly acknowledge my research advisor and mentor Dr. Stefan H. Bossmann, for his tremendous encouragement and guidance rendered to me throughout my PhD. I am grateful to him for the trust and independence given to me, which was a strong influence in molding me into the researcher that I am today. The lessons I learned from him will forever urge me to strive for the best, not just in science but also in life.

I would also like to especially acknowledge the members of my PhD committee: Dr. Kenneth J. Klabunde, Dr. Deryl L. Troyer, Dr. Eric A. Maatta and Dr. Kevin B. Lease for their support and dedication.

Heartfelt gratitude is extended to Katherine Bossmann for her support, kindness and encouragement throughout the years. Special thanks goes out the members of the Bossmann group, both past and present, for their tremendous help and support. It has been a pleasure to work amongst such talented colleagues and wonderful friends.

I would like to acknowledge Dr. Daniel Higgins, Dr. Christer Aakeroy and Dr. Om Prakash, for allowing me to use their resources. I also thank Dr. Leila Maurmann, Mr. Ron Jackson and Mr. James Hodgson for their technical support and guidance. A warm thank you goes out to the staff and all my colleagues and friends at Department of Chemistry, who made it a pleasure to work there.

I also extend acknowledgements to my collaborators: Dr. Michael Niederweis, University of Alabama, Birmingham; Dr. Henry S. White, University of Utah; Dr. Francis D'Souza, University of North Texas; Dr. Claudia Turro, Ohio State University; Dr. Deryl L. Troyer, and Dr. Jun Li, who has contributed immensely to the success of my research.

I am grateful to my Alma Mata, Kansas State University and to the Department of Chemistry, for providing me with the invaluable opportunity to pursue my doctoral degree in this institution.

Last but not least I am forever in debt to my wonderful family: to my beloved parents for their constant love, support and belief in me and to my wonderful husband for his love, care and encouragement. I am also grateful to all other family and friends for their continuous support throughout the years.

# Dedication

Dedicated to *Amma* and *Thaththa* for a lifetime of unconditional love and support

# Chapter 1 - Extraction, Purification and Analytical Assessment of Mycobacterial Porin MspA

## 1.1 Background

### *1.1.1 Mycobacterium smegmatis*

Mycobacteria are well known for causing tuberculosis (*Mycobacterium tuberculosis*) and leprosy (*M. leprae*) and hence are of immense medical significance.[1] Tuberculosis is the cause of the highest number of deaths by an infectious disease per year in the world and it is estimated that approximately two billion people carry the disease.[2] Treatment of these diseases has been especially challenging, as mycobacteria are capable of forming impenetrable biofilms and feature outer cellular envelopes, which render them resistant to most treatment methods. As a result, the mycobacterial cell membrane has been thoroughly investigated over the years in order to understand its structure and function.[3,4] It has been found that the outer cell membrane of mycobacteria play a crucial role in protecting the cell against external toxic compounds. Traditionally mycobacteria were classified as Gram positive however, later experiments on genome comparison revealed that this classification was not accurate. At present they are placed as equidistant from Gram positive and negative bacteria.[5] Mycobacteria contain trans-membrane channel proteins or porins, which are used to uptake small, hydrophilic nutrients into the cell. These are usually of low concentration within the outer membranes. These porins were first found in *Mycobacterium chelonae*[6] and later on in extracts of *Mycobacterium smegmatis*.[7]

*M. smegmatis* is a species of non-pathogenic mycobacteria, which is commonly found in soil. Over the years it has been utilized by microbiologists as a tool to study pathogenic species of mycobacteria. Studies done on the outer cell membrane of *M. smegmatis* have revealed the presence of a porin which has been isolated, purified and named as MspA (porin A from *M. smegmatis*).[8] Other types of porins have also been found in this species but were present only in minute quantities. These have been named MspB, MspC and MspD and contain minor differences in structure to MspA.[9] The structure of MspA has been studied extensively and bares no significant resemblance to any other protein known to date.

### *1.1.2 Structure of MspA*

The initial experiments on MspA's structure have been performed using electron microscopy, which revealed a cylindrical structure.[10] Later on x-ray studies done on a mutant MspA strain (i.e. MspA A96R where Ala96 is replaced with Arg) provided a complex, detailed structural analysis.[11]

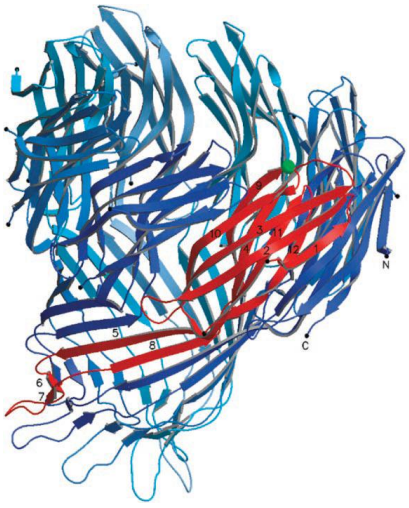


**Figure 1.1: Ribbon plot of MspA. Red area indicates a monomer. (Taken with permission from reference 11)**

MspA has been expressed in *Escherichia coli* and have shown to be consisting of 20 kDa monomers, which are assembled in octameric units to form a central channel.[11] Therefore total weight of the protein can be envisaged as 160 kDa. The shape of the protein resembles a 'goblet' with a wide rim consisting of 134 amino acid residues and a narrower stem followed by a base consisting of 50 residues. The porin is 96 Å (~10 nm) in height and the wide rim has an 88 Å diameter. Therefore MspA forms a 10 nm long channel across the mycolic acid layer in the mycobacterial outer membrane, which is identified as the longest protein channel known so far. The tilting of β barrels in the stem and base creates a constriction zone with an internal diameter of 10 Å. The widest diameter of the channel is 48 Å.

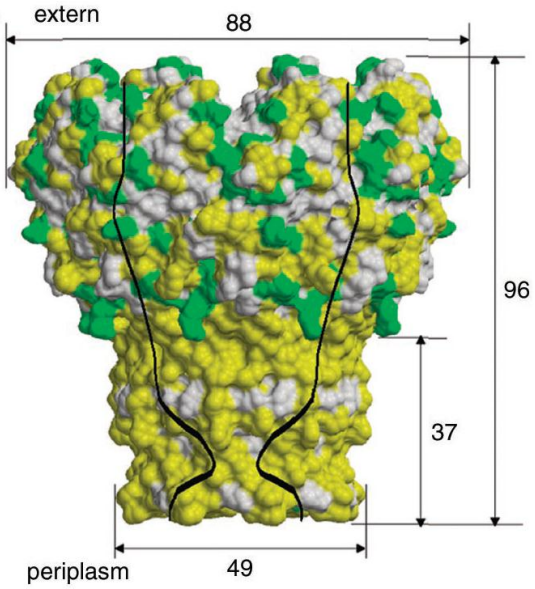


**Figure 1.2: Dimensions and hydrophobicity of MspA. Green - polar, yellow - non-polar. (Taken with permission from reference 11)**

The central channel of MspA is mostly polar with the exception of a single non-polar region along the periphery of the rim. The constriction zone bears a high negative charge due to Aspartate residues at positions 90 and 91. The surface polarity differs significantly in different

regions of MspA. The rim surface is largely polar and the stem and base are largely non-polar, thus allowing the porin to insert into lipid bilayer membranes. The polarity is generated mainly by 96 free carboxylates and 8 amino groups present on the surface of MspA.[1] There is evidence to suggest that MspA is the major transporter of electrolytes across the *M. smegmatis* cell membrane.[12] Understanding the structure and function of porins such as MspA is extremely important in the battle against tuberculosis. Both *M. tuberculosis* and *M. bovis*, which is also a species which spreads tuberculosis in animals, carries similar porins in their cell membranes. These are thought to play crucial roles in determining drug design methods to treat tuberculosis as small, polar drugs such as isoniazide, ethambutol, and pyrazinamide are known to pass through the porin constriction zones.[3]

### *1.1.3 Stability of MspA*

The extraction of MspA was achieved first with mild detergents at room temperature, but these were of low yield and included many contaminating proteins.[13] Later on non-ionic detergents, longer incubation times and temperatures as high as 90 °C rendered better yields with less contaminants.[14] The porin was able to retain its pore forming ability even after being exposed to harsh extraction procedures, therefore its remarkable stability was established early on. Methods were further developed to optimize the extraction procedure and test the limits of its stability.[15] High temperature seemed to be a crucial factor in determining the purity of the extracts as other proteins were denatured and removed by these conditions.

### *1.1.3.1 Stability of MspA against high temperatures and detergents*

During the extraction procedure, heating in detergents was necessary to obtain optimal purity of the protein. The extracts have been prepared at 30,40, 50, 60, 70, 80, 90 and 100 °C in PG05 buffer(0.5% Genapol, 100 mM $Na_2HPO_4/NaH_2PO_4$, 0.1 mM EDTA, 150 mM NaCl, pH 6.5) to determine the best extraction temperature.[15] It was evident that extracts heated at or above 80 °C gave the best results as observed by gel electrophoresis.

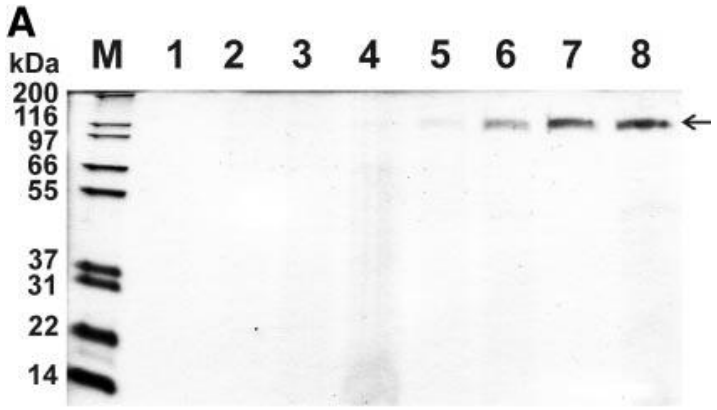


**Figure 1.3: Investigation of temperature stability of MspA extracts in PG05 buffer. M = molecular marker, lanes 1-8 = extracts obtained at 30, 40, 50, 60, 70, 80, 90, and 100 °C. The arrow indicates the MspA band. (Taken with permission from reference 14)**

MspA extracts in Genapol buffer were dissolved in various detergents to investigate the solubility and stability of the protein. Each mixture was heated at 100 °C for 30 minutes and subject to gel electrophoresis. (Please refer Appendix A for abbreviations and composition of detergents)

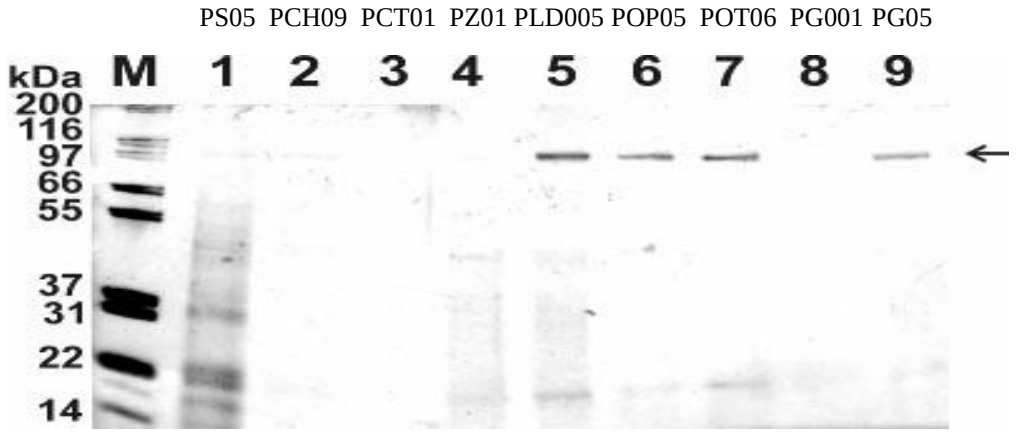


**Figure 1.4: Investigation of stability of MspA against various detergents. M = molecular marker, lanes 1-8 = detergents PS05, PCH09, PCT01, PZ01, PLD005, POP05, POT06, PG001 and PG05 respectively. (Taken with permission from reference14)**

It is evident that MspA retains its octameric structure even after boiling with buffers PLD005 POP05 POT06 and PG05.

### *1.1.3.2 Stability of MspA against extreme pH*

Resistance of MspA to denaturing in harsh pH conditions has been investigated in detail.[16] Wild type $mc^2155$ extracts of MspA have been incubated for 1 hour in various pH conditions and subjected to gel electrophoresis. Remarkably, the protein retains its octameric structure at a pH range of 2 to 14 as indicated by the characteristic gel band.

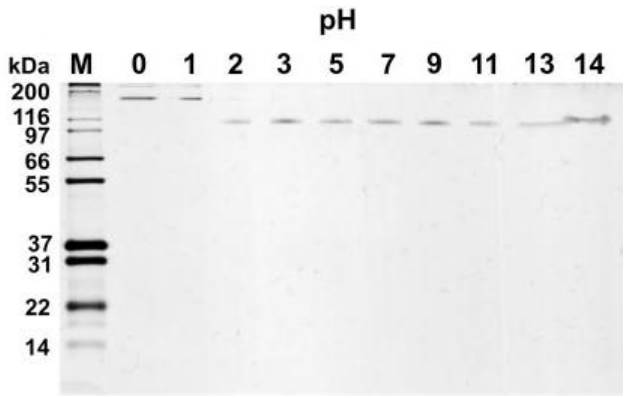


**Figure 1.5: Investigation of pH stability of wild type MspA. (Taken with permission from reference 16)**

These experiments provide evidence for the remarkable stability of MspA compared to other proteins and it was consequently classified as the most stable channel forming protein known so far.[16]

## 1.2 Experimental

Growth of the wild type *M. smegmatis* strain $mc^2$ 155 and mutant strain A96C was established successfully in our labs by utilizing previously published growth conditions. However, extraction of MspA according to procedures given by Niederweis *et al.* did not yield any porin according to gel electrophoresis observations. Therefore different extraction conditions were investigated in order to obtain pure MspA in high yield. A comprehensive set of analytical tools was employed to characterize and authenticate the presence of MspA.

### *1.2.1 Preparation of bacterial cultures and growth media*

*M. smegmatis* cultures that belong to wild type strain $mc^2$ 155 and mutant A96C strain were obtained from the laboratory of Dr. Michael Niederweis at University of Alabama, Birmingham. The cultures were inoculated onto Agar plates by streaking method and kept in incubator at 37.5 °C for 3-4 days until colonies developed. Liquid media 7H9 broth base was prepared for inoculation of the colonies.

In to a 1000 ml beaker, added 4.2 g of Middlebrook 7H9 broth base (purchased from Sigma-Aldrich) and 3 ml of 60% glycerol, followed by 900 ml of distilled water. The solution was stirred in to a homogeneous mixture, poured in to 1 l Nalgene bottles and autoclaved, then stored at 4 °C. For inoculation of small bacterial cultures, 50 ml of the 7H9 broth was mixed with 125 µl of 20% Tween 80 and 50 µl of hygromycin (prepared to a 50 µg/µl aqueous solution) under a laminar flow and vortexed for 1 minute. Two 10 ml culture tubes were each filled with 5 ml of this media and the *M. smegmatis* colonies were transferred via a sterilized needle into each tube. These were kept in a shaker at 37.5 °C and 75 rpm for 48 hours to obtained mature cultures. After 48 hours 0.5 ml of growth culture from each tube was transferred into two new culture tubes and mixed with 4.5 ml of prepared 7H9 media in order to refresh the cultures.

Scale up of the production of *M. smegmatis* cultures was achieved by inoculating the 'small' cultures prepared above into 'medium' and 'large' cultures. The 'medium' cultures were prepared by transferring 2 ml each from 'small' culture media (48 hours old) into a 125 ml culture flask adding up to 4 ml of culture-media. 36 ml of prepared growth media were added to this flask (total volume of 40 ml) and kept in shaker for 48 hours. 'Large' cultures were prepared

by transferring 40 ml of ‘medium’ culture into a 2 l culture flask followed by addition of 2.25 ml of 20% Tween 80 and 300 µl of hygromycin. Next 1 l of 7H9 broth was added to this flask and kept in shaker for 48 hours. All media preparations and inoculations were done under sterile conditions under the laminar flow.

### *1.2.2 Extraction of MspA from M. smegmatis*

Two 48 hour old ‘large’ culture flasks were emptied into large centrifuge bottles and centrifuged at 3696 rpm in 5 °C for 1 hour to separate the cells from the medium. The supernatant was discarded and 50 ml of PBS buffer was added to the cells and vortexed until dispersed. The mixture was then centrifuged at 10016 rpm in 5 °C for 1 hour then the supernatant was discarded and the cells were weighed. 3.5 ml of PEN buffer was added for every 1 g of cells. *n*-octyl-oligo-oxyethylene (nOPOE) detergent was added as 0.08% v/v of nOPOE/PEN ratio to obtain maximum extraction of protein. The mixture was then heated at 65 °C for 1 hour while stirring. Afterwards, the mixture was cooled for 5 minutes in freezer and centrifuged at 10016 rpm for 1 hour. The supernatant obtained was separated out and mixed with an equal volume of ice-cold acetone and kept in freezer (0 °C) overnight in order to precipitate the protein. The next day the mixture was centrifuged for 30 minutes at 10016 rpm in 5 °C. The supernatant was discarded and the precipitate was dissolved in PBS. The solution was then poured into 3000 MWCO ultra-filtration tubes and concentrated by centrifuging at 10016 rpm for 30-60 minutes until a constant volume was obtained. The protein extract was then stored and 4 °C followed by analysis via gel electrophoresis.

### *1.2.3 Analytical assessment of MspA*

The initial assessment of the presence of MspA was performed by gel electrophoresis technique using acrylic gels.

The separation gel was prepared as follows: First 3.3 ml of Acrylamide (30:1), 4.5 ml of 3x gel buffer, 2.25 ml of 60% glycerol and 3.3 ml of $H_2O$ were mixed well in a 15 ml centrifuge tube. Next, 0.015 ml of *N*,*N*,*N*,*N*-tetramethylethylenediamine (TEMED) was added and shaken well, followed by addition of 0.135 ml 10% APS and additional shaking. The mixture was then quickly transferred into a gel chamber followed by addition of a distilled water layer on top and kept for 30 minutes to solidify. After 30 minutes the water layer was poured out and a collection gel layer was added.

The collection gel was prepared as follows: 0.8 ml of Acrylamide (30:1), 2.6 ml of 3x gel buffer and 4.2 ml of $H_2O$ were mixed well in a 15 ml centrifuge tube. Next, added 0.015 ml of *N*,*N*,*N*,*N*-tetramethylethylenediamine (TEMED) and shook well, followed by addition of 0.160 ml 10% APS and shaking. This gel was added on top of the solidified separation gel and a gel comb was put on top to make wells. The gel was kept for 30 minutes then the comb was removed and samples were added into each alternating well.

Sample preparation for gel was done as follows: The protein extract was diluted by adding water into a desired dilution (ex. 5x, 10x, 20x etc.) 10 µl of diluted protein was mixed with 5 µl of loading buffer and vortexed for about 1 minute. 10 µl of the mixture was used to load one well of gel. A broad range protein molecular weight marker (purchased by Promega)

was used as a standard. The gel was run at 125 V and 400 mA for approximately 90 minutes. Next, the gel was soaked in a fixing solution (made with 500 ml ethanol, 400 ml $H_2O$, 100 ml acetic acid) and put in shaker for 1 hour. This was followed by a de-staining solution, which acts as a second fixing solution (500 ml methanol, 400 ml $H_2O$, 100 ml acetic acid) and kept in shaker overnight. The next day gel was soaked in a Coomassie blue stain for approximately 30 minutes. The gel was then de-stained for approximately 30 minutes or until bands were clearly visible.

Gel electrophoresis was used for a set of experiments to determine the optimum growth time, extraction time, use of hygromycin, as well as detection of mutant and crystalized protein. A $^1H$ NMR study was done for the wild type crystals of MspA for the first time (refer Appendix 1). FTIR data were also obtained for wild type extracts. X-ray diffraction data was obtained for powdered wild type MspA crystals.

HPLC was done using POROS® column of 10x10 mm (Purchased from Applied Biosystems) and detection was carried out at 254 nm with a flow rate of 0.5 ml/min. Buffer A (for $H_2O$ 1000 ml, HEPES 25 mM, NaCl 10 mM, 0.5% OPOE 500 µl, pH 7.5) and buffer B (for $H_2O$ 1000 ml, HEPES 25 mM, NaCl 2 mM, 0.5% OPOE 500 µl, pH 7.5) were used as solvents. Concentrations of wild type extracts were determined by Bradford assay.[17] The wild type was also analyzed using UV and Fluorescence. Dynamic light scattering and zeta potential measurements were done using ZetaPALS Zeta Potential Analyzer purchased by Brookhaven Instruments Corporation.

## 1.3 Results and Discussion

### *1.3.1 Gel electrophoresis*

The first detection of MspA wild type was achieved by gel electrophoresis as a single band close to 150 kDa.

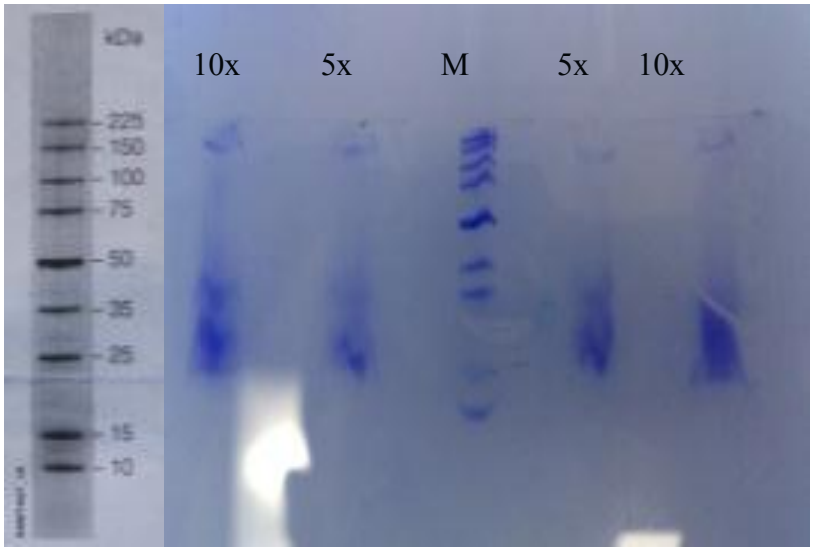


**Figure 1.6: First detection of wild type MspA via gel electrophoresis. (5x, 10x = 5 and 10 times diluted extract, M = molecular marker)**

Large cultures of *M. smegmatis* were extracted after 2, 3, 4, and 5 days of growth in order to investigate the optimum growth time which would produce maxim concentration of protein per extract. After the relevant growth period each culture was extracted and subjected to gel electrophoresis. The intensity of the protein bands is indicative of the amount of protein present in each extract. It was evident that cultures grown for 3 days gave a clean band of relatively high intensity. Cultures grown for 4 days gave the highest band intensity but contained two other faint bands corresponding to other contaminating proteins. Hence it was decided that 3 days of growth was the optimum time to obtain pure protein. All future extractions were done with 3 day old large cultures.

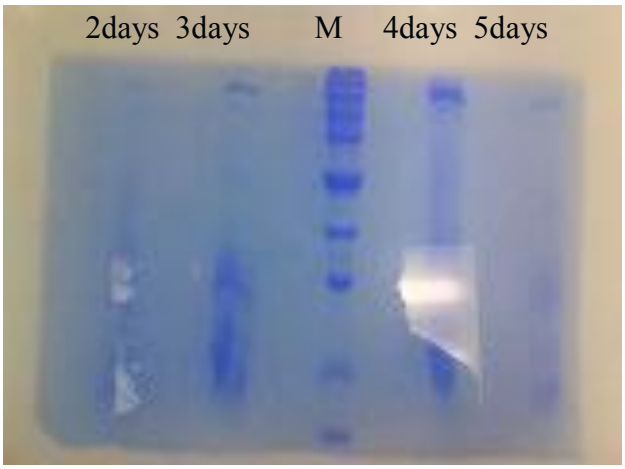


**Figure 1.7: Investigation of optimum growth time for *M. smegmatis* cultures**

The 3 day culture extract was tested at different dilutions in order to determine the concentration which gives the clearest band. It was found that 5x and 10x dilutions gave clear bands with less streaking. Two other bands of 20 kDa and 15 kDa were also observed in the gel. Since there are no other proteins reported for *M. smegmatis* other than MspA and its related porins and since they all have approximately similar molecular weights, it was concluded that these bands arise due to decomposition of octameric protein into monomers. The weight of an MspA monomer unit is 20 kDa.

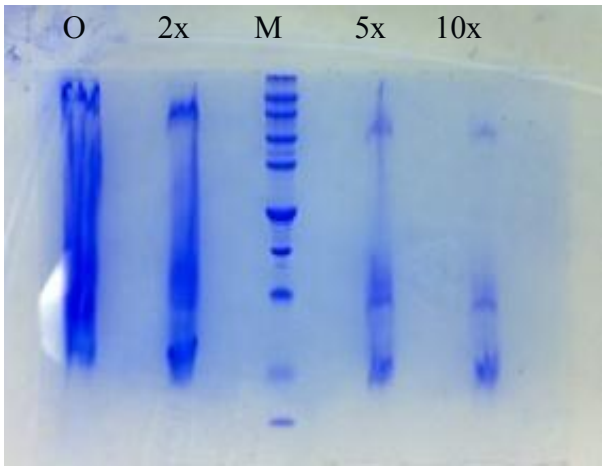


**Figure 1.8: Investigation of optimum MspA concentration for gel electrophoresis detection (O = undiluted MspA extract)**

Hygromycin is an antibiotic, which is added to the growth medium of *M. smegmatis*. The purpose of its addition is to prevent other aerobic bacteria from contaminating the cultures. Since *M. smegmatis* is highly resistant to hygromycin unlike most other bacteria, the cultures remain uncontaminated over long periods of time. For mutant strains such as A96C hygromycin is essential for growth.

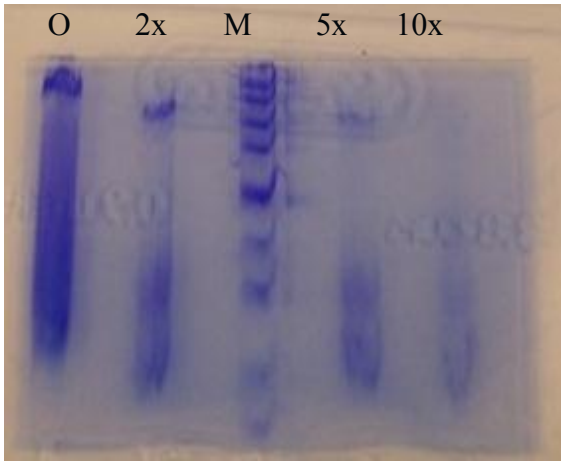


**Figure 1.9: Investigation of effect of hygromycin on MspA concentration**

An experiment was conducted in order to investigate whether reduction of the concentration of hygromycin used to prepare growth media would affect the concentration of extracted MspA. Two large cultures of mutant A96C strain were prepared without adding any hygromycin in the growth media and subjected to protein extraction. To our surprise the gel electrophoresis revealed significant levels of pure MspA. We believe that for the first time we obtained evidence for obtaining A96C MspA without hygromycin. However, the concentration of the 5x and 10x dilutions were significantly low hence, the overall amount of protein extracted was low. It is possible that certain point mutations in the bacterial strain may lead to adaptation of MspA expression without hygromycin.

Purified wild type MspA extracts were concentrated and dried at 4 °C for long periods of time which eventually lead to formation of crystals. This marks the first observation of crystallization of wild type MspA. Previous data of MspA crystals have been obtained for mutant strains.[10]

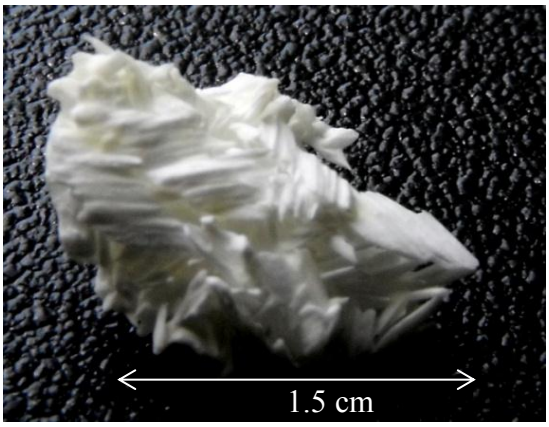


**Figure 1.10: Wild type MspA crystal**

The crystals were re-dissolved in 1x PBS buffer and subjected to gel electrophoresis. It was observed that the crystals consist of pure MspA.

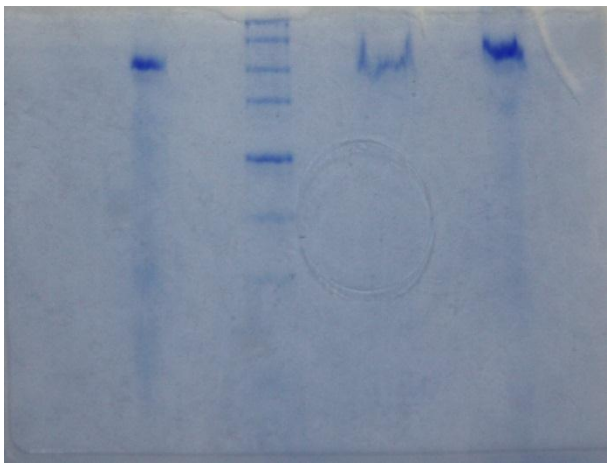

**Figure 1.11: Gel electrophoresis on wild type MspA crystals**

### *1.3.2 Bradford assay*

To determine the concentration of MspA in the extracted solutions, the Bradford assay was performed. The average concentration was found to be 616.35 µg/ml with 5.27% relative error and a standard deviation of 32.480µg/ml.

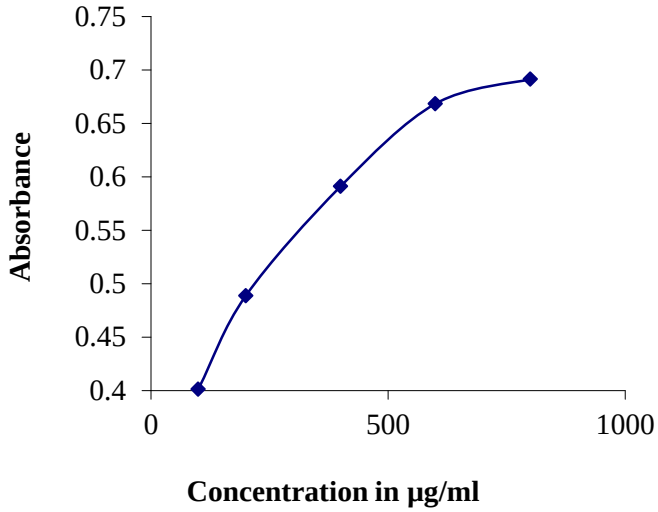


**Figure 1.12: Calibration curve for Bradford protein assay on wild type MspA**

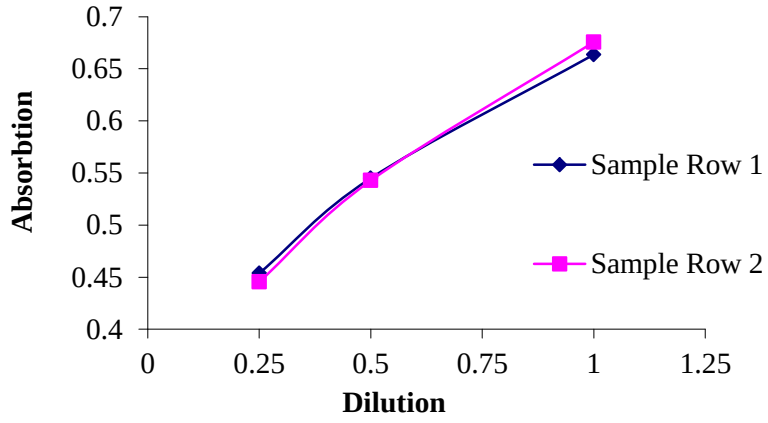


**Figure 1.13: Optical absorbance vs. dilution for wild type MspA extracts**

The experiments were repeated using mutant A96C MspA and a similar concentration within the limit error (± 5 relative percent) was found.

### *1.3.3 HPLC and UV/fluorescence measurements*

The UV measurement of wild type and A96C MspA in 1x PBS gave an absorption maximum at 258 nm (literature value: 254 nm in 1x PBS) was observed along with typical UV spectrum. This spectrum is typical for that of a tryptophan-rich protein.

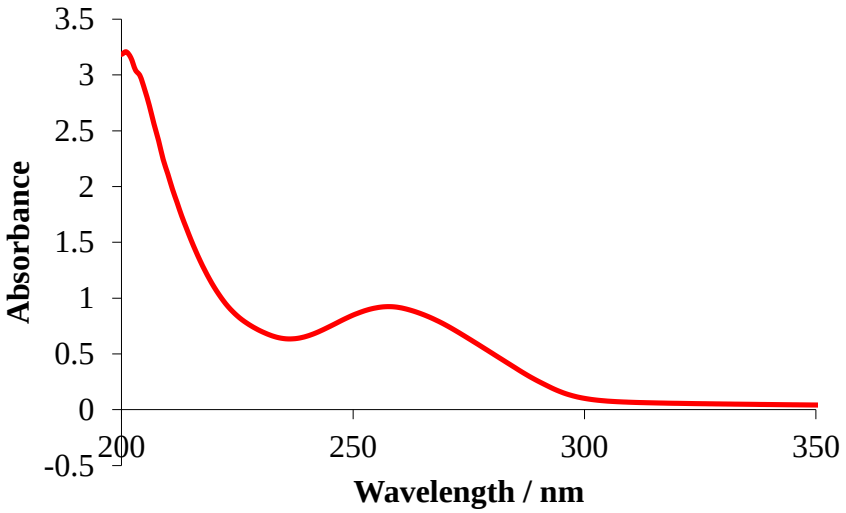


**Figure 1.14: UV absorption spectrum of wild type MspA**

Fluorescence measurement for wild type (WT) MspA also revealed a typical spectrum for a protein containing typtophan. It is noteworthy that in the spectrum of mutant A96C, the characteristic tryptophan excimers[18] (i.e. excited dimers[19]) were more pronounced than in the spectrum of WT MspA, indicating that there are slight differences in the structures of both octameric proteins. 24 of the 32 tryptophans in the MspA octamer are located within the upper rim. Slight structural changes of A96C, in comparison with WT MspA apparently result in a

significantly enhanced excimer peak. This is an excellent characterization method to distinguish between the wild type and mutant protein.

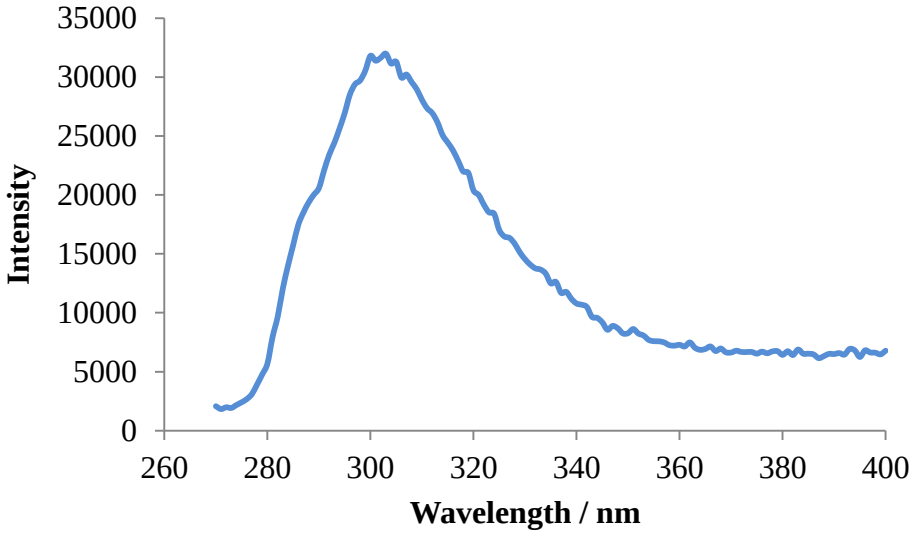


**Figure 1.15: Fluorescence-emission spectrum of wild type MspA**

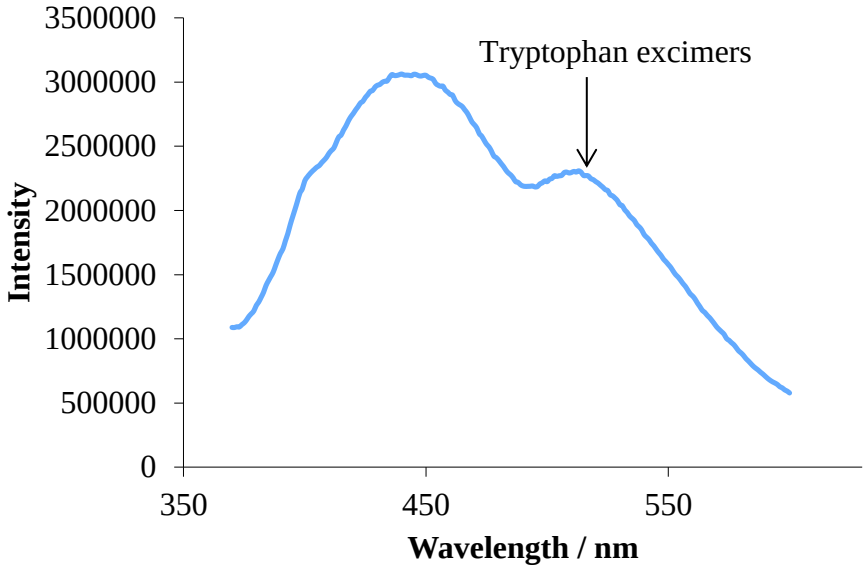


**Figure 1.16: Fluorescence-emission spectrum of mutant A96C MspA**

HPLC was performed for wild type MspA extracts using buffers A and B (refer experimental section 1.2.3) as solvents and detection at 254 nm.

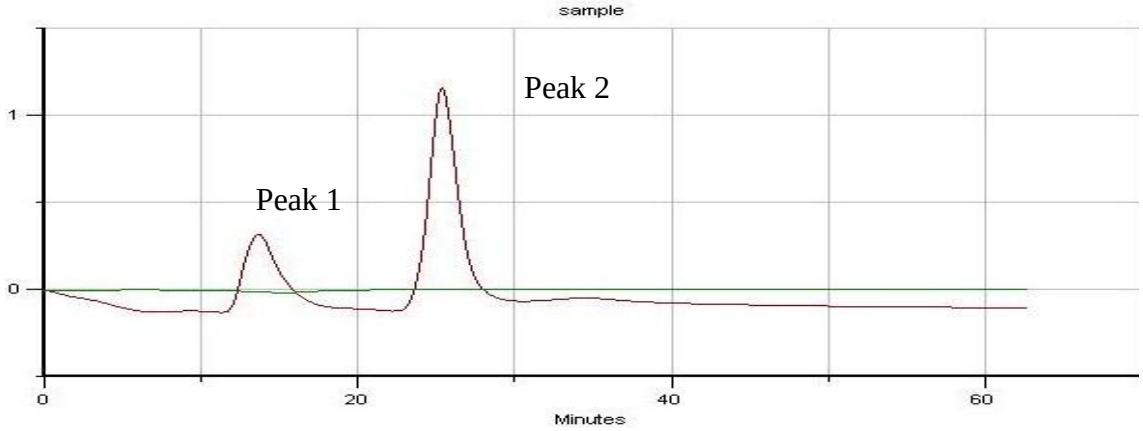


**Figure 1.17: HPLC data of wild type MspA**

Two peaks were observed from HPLC. Peak 1 which consisted of fractions 1 and 2 was identified as MspA and peak 2 which consisted of fractions 3, 4 and 5 was assumed to be the porin MspC based on literature.[11] UV and fluorescence measurements were repeated with combined fractions 1-2 and 3-5 and compared against the same protein extract which was not subject to HPLC purification.

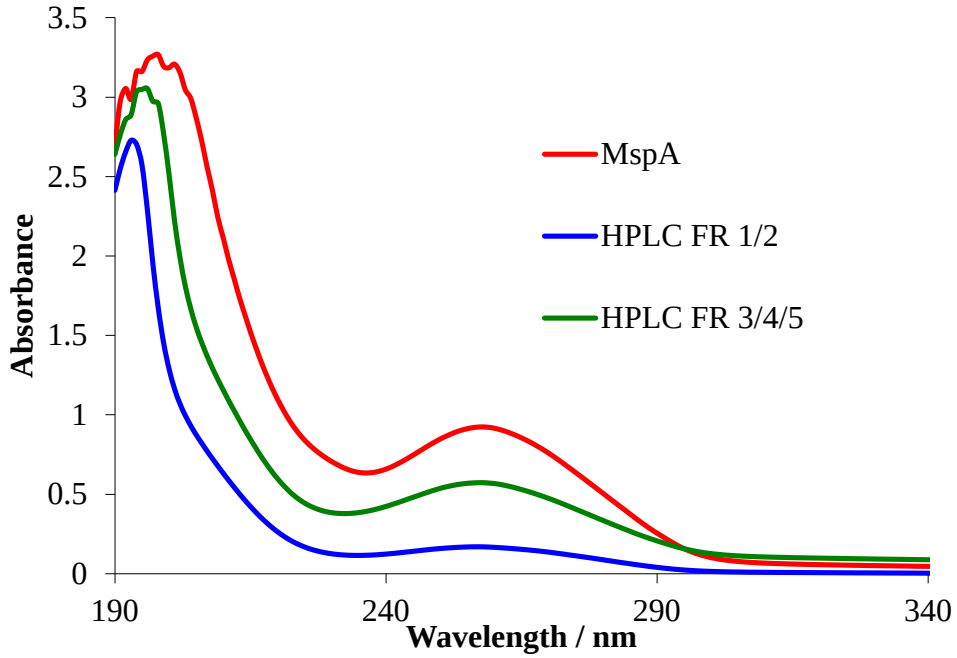


**Figure 1.18: UV spectra of combined HPLC fractions 1-2, 3-5 and unpurified MspA**

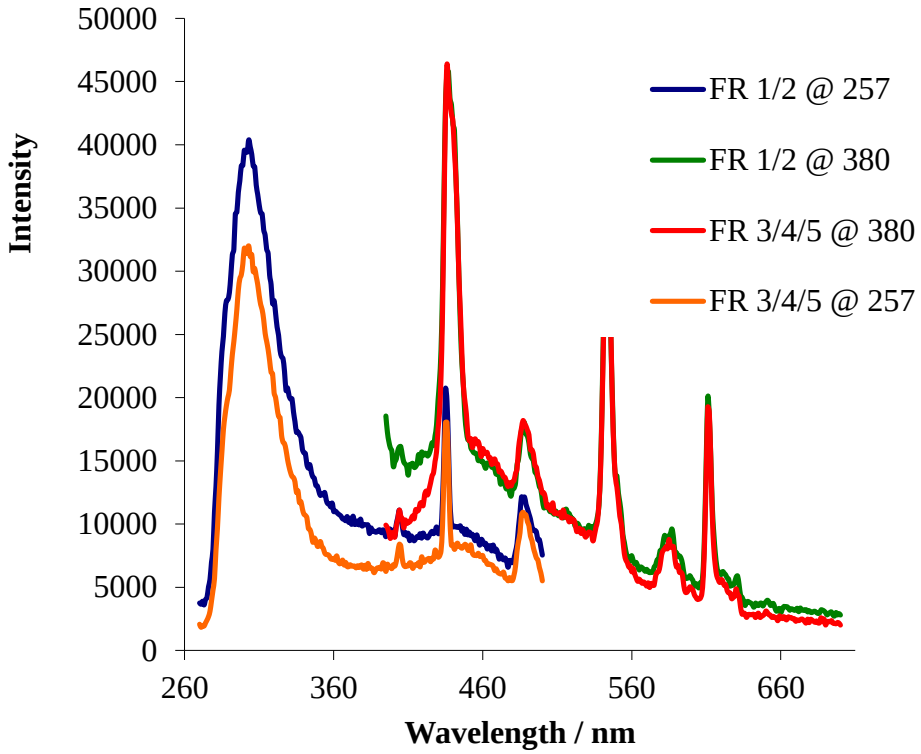


**Figure 1.19: Fluorescence spectra of combined HPLC fractions 1-2, 3-5 and unpurified MspA**

### *1.3.4 Dynamic light scattering studies*

Dynamic light scattering (DLS) experiments of wild type and A96C MspA gave an average particle size range of 110-150 nm in diameter in 1x PBS buffer for 50, 100 and 150 µl of MspA extract diluted in 2.0 ml of 1x PBS buffer. This indicates that the protein molecules are aggregated in an aqueous environment. DLS data also showed that the extracts were largely mono dispersed with a poly-dispersity range of 0.2-0.3% and scatter light evenly. These observations are further indicative of pure protein.

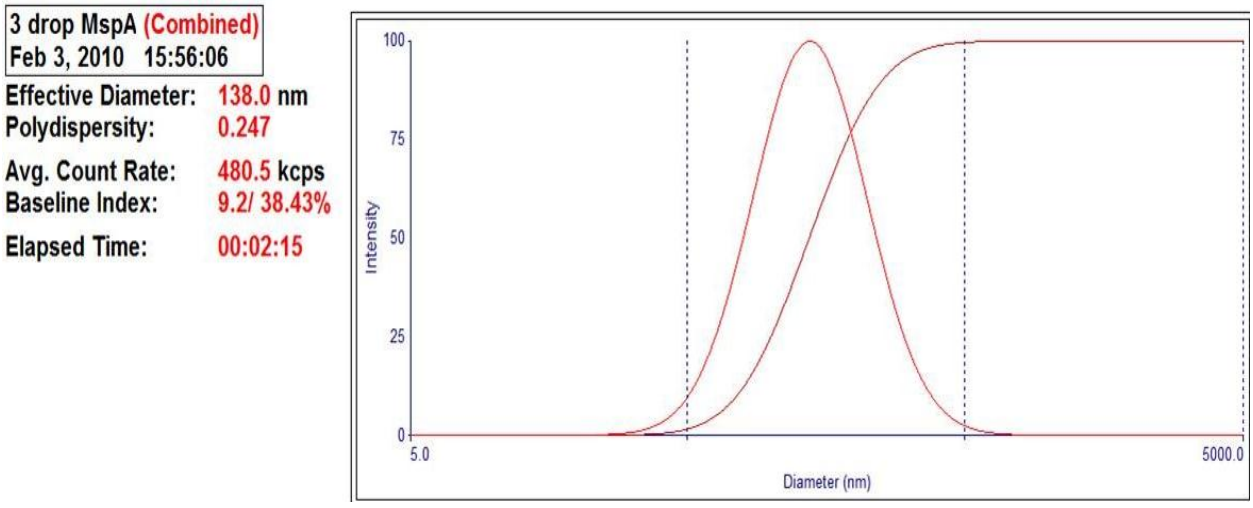


**Figure 1.20: Lognomial distribution of particles in wild type MspA extracts obtained from dynamic light scattering experiments**

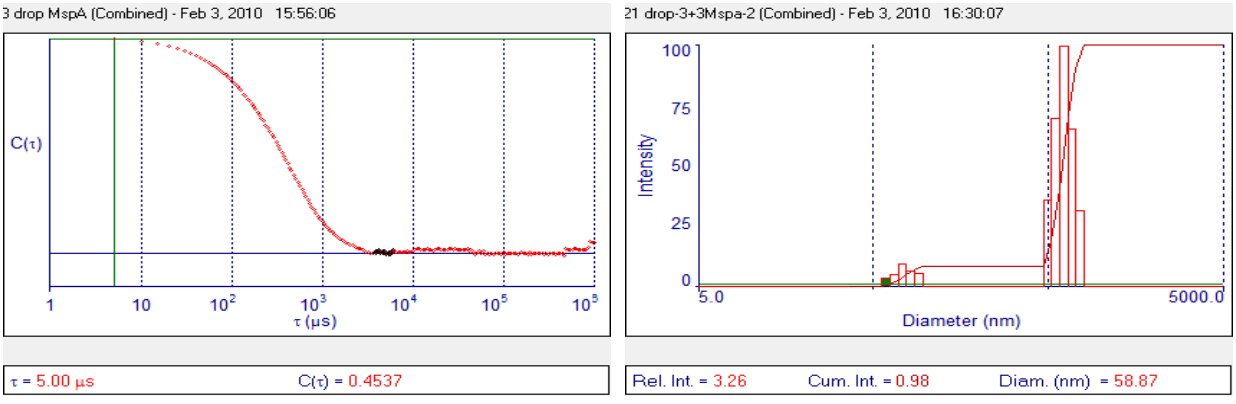


**Figure 1.21: Homogeneity (left) and monodispersity (right) of wild type MspA extracts demonstrated by dynamic light scattering experiments**

### *1.3.5 FTIR data*

FTIR data of a wild type MspA extract was obtained for the first time. A broad peak corresponding to hydrogen bonding of N-H and O-H was observed at ~3200 $cm^{-1}$. The carbonyl peak at 1642 $cm^{-1}$ is indicative of carboxylic acid/amide functional groups. In the carbonyl peak, shoulders were identified corresponding to α and β bending of protein. Peaks at ~1070-950 $cm^{-1}$ were characterized as corresponding crystalline water. The A96C MspA extract also showed similar trends in FTIR with the exception of crystalline water peaks.

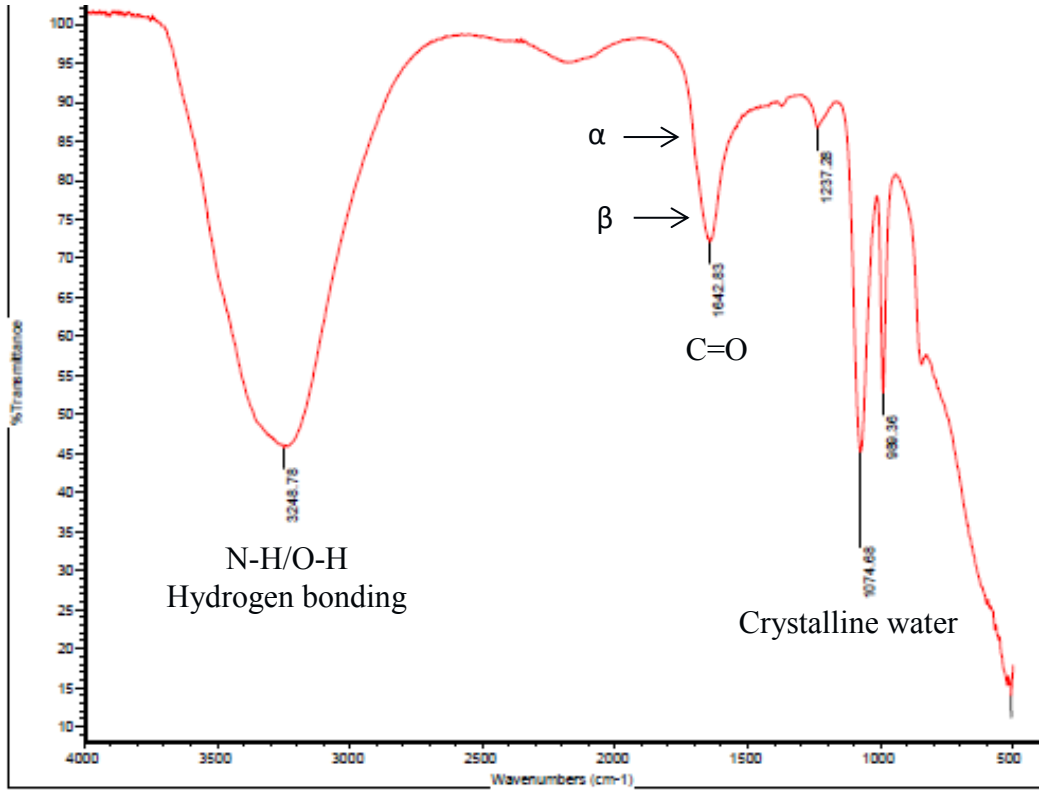


**Figure 1.22: FTIR spectrum of wild type MspA**

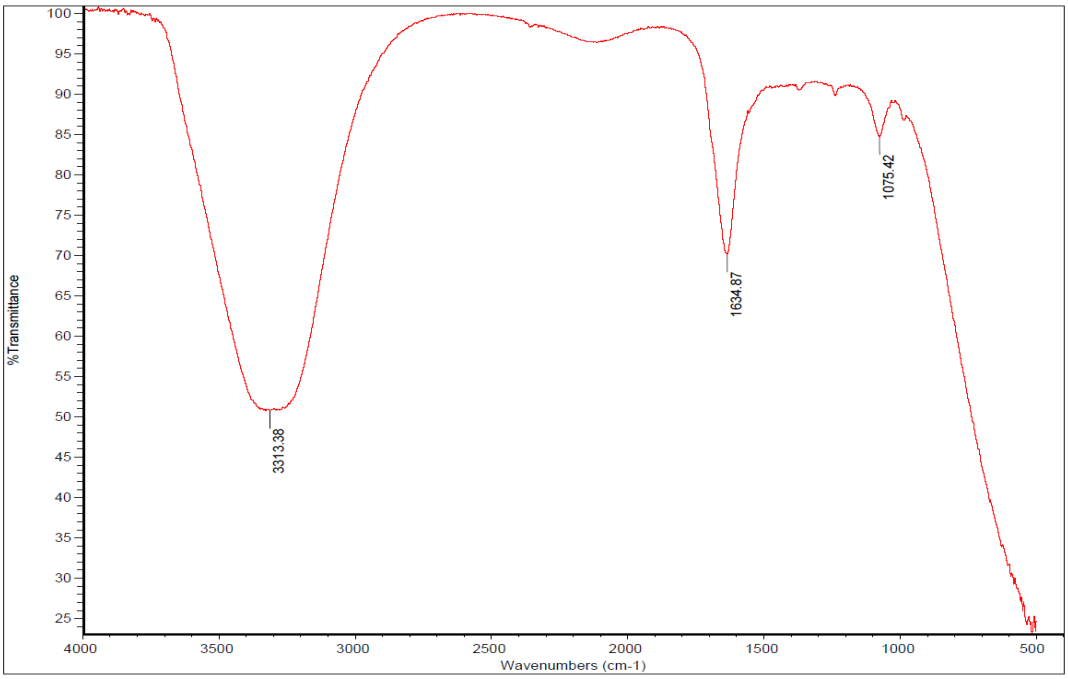


**Figure 1.23: FTIR spectrum of A96C MspA**

### *1.3.6 X-ray diffraction studies*

The crystals obtained for wild type MspA extracts were subject to a powder crystallogram. The spectrum depicted highly crystalline material without amorphous character indicating the high purity of the protein. This marks the first x-ray data obtained for wild type MspA.

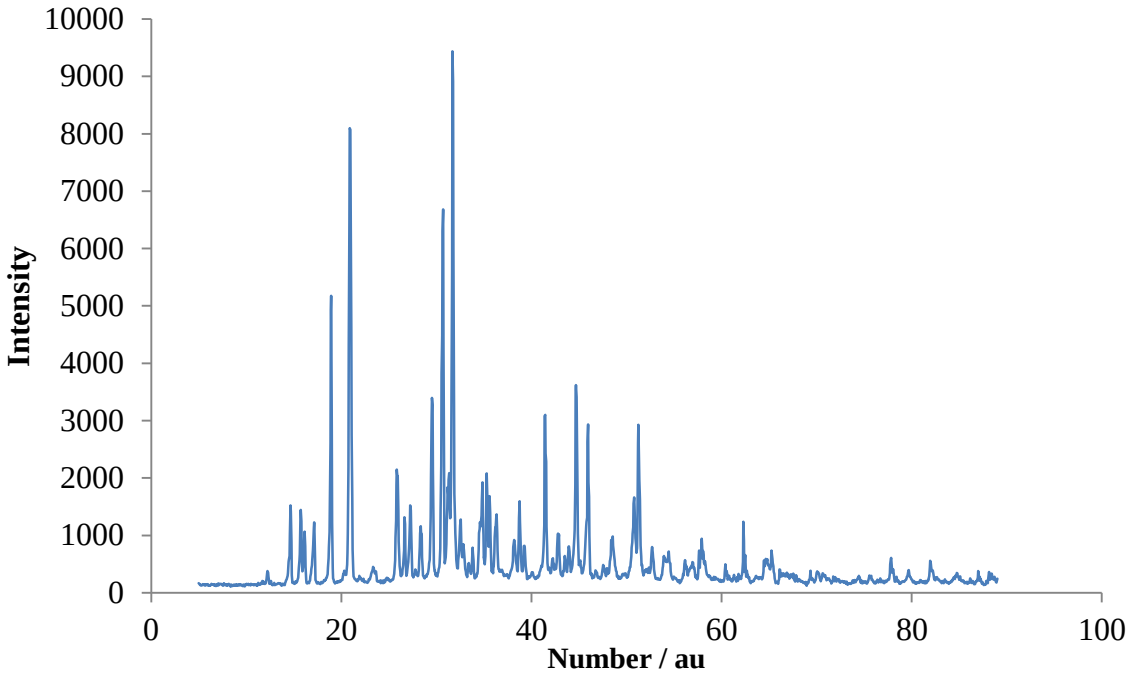


**Figure 1.24: Powder crystallogram of wild type MspA**

### *1.3.7 Proton NMR data*

No previous NMR data were available in literature for wild type MspA due to the fact that purity of these extracts did not render them suitable for NMR analysis. The modified extraction procedure employed in our labs gave highly pure wild type MspA, which lead to formation of crystals. A wild type MspA extract was lyophilized and re-dissolved in $D_2O$ and $^1H$ NMR spectrum was recorded. The amine and aliphatic protons were clearly identified. This marks the first evidence of a $^1H$ NMR obtained for wild type strain $mc^2$ 155 MspA.

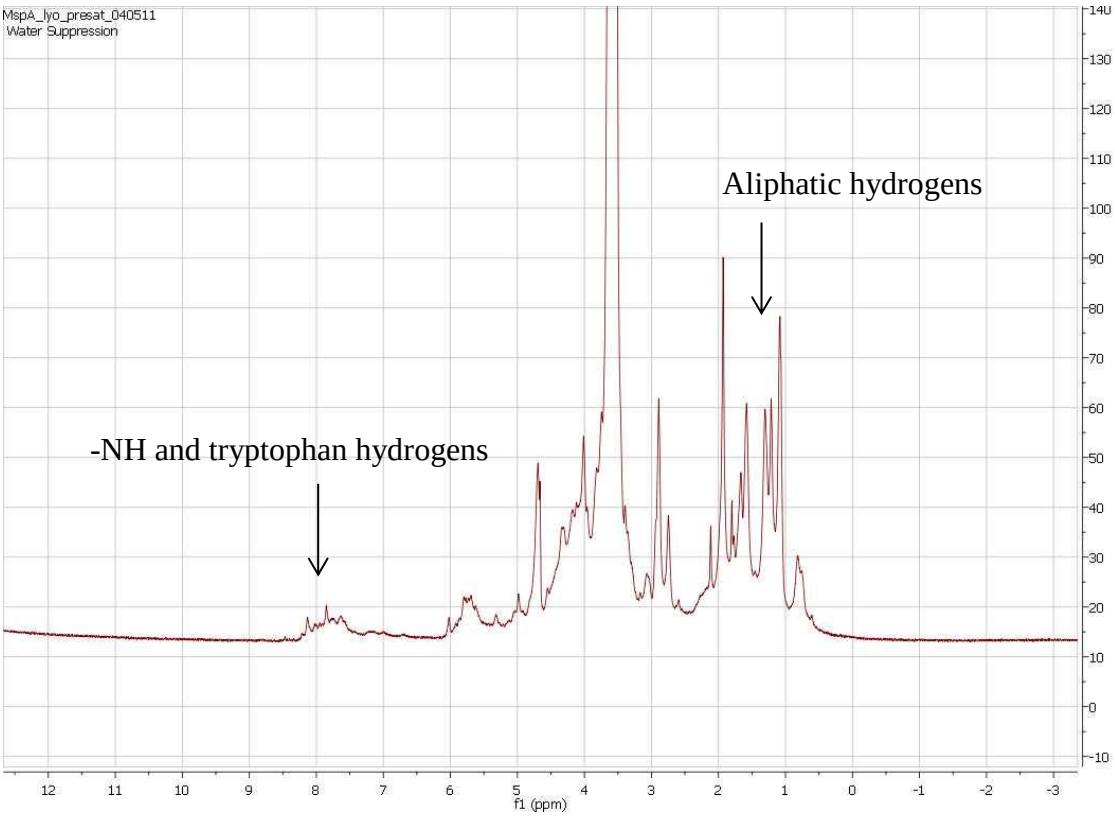


**Figure 1.25: $^{1}$H NMR spectrum of wild type MspA**

## 1.4 Conclusions

MspA from *Mycobacterium smegmatis* wild type strain mc$^2$ 155 and mutant strain A96C was extracted in high yield and high purity using a modified extraction procedure. Crystals from wild type MspA was obtained for the first time. A comprehensive analytical assessment was performed to authenticate the structure and dynamics of MspA. Initial protein detection was done using gel electrophoresis and a series electrophoresis experiments were used to determine the optimum growth time, extraction time, use of hygromycin, as well as detection of mutant and crystalized protein. Bradford assay was employed to obtain an average protein concentration of 0.6 mg/ml. UV, fluorescence, HPLC and FTIR studies provided further evidence for purity and characterization of MspA. Dynamic light scattering experiments provided insight into the

solution dynamics of wild type and mutant MspA. For the first time, proton NMR data of wild type MspA liquid extracts and X-ray diffraction data of wild type MspA crystals were obtained.

## 1.5 References


[1] Rastogi, N; Legrand, E.; Sola, C. "The mycobacteria: an introduction to nomenclature and

[2] Bleed, D.; Watt, C.; Dye, C. "Global tuberculosis control" (WHO Report, Geneva, **2001**).

[3] Lambert, P. A. "Cellular impermeability and uptake of biocides and antibiotics in Gram-positive bacteria and mycobacteria", *J. App. Microbiol.***2002**, *92*, 46s.

[4] Watanabe, M.; Aoyagi, Y.; Ridell, M.; Minnikin, D. E. "Separation and characterization of individual mycolic acids in representative mycobacteria", *Microbiology* **2001**, *147*, 1825.

[5] Fu, L. M.; Fu-Lia, C. S. "Is Mycobacterium tuberculosis a closer relative to Gram-positive or Gram-negative bacterial pathogens?",*Tuberculosis* **2002**, *82*, 85.

[6] Trias, J.; Jarlier, V.; Benz, R. "Porins in the cell wall of mycobacteria", *Science* **1992**, *258*, 1479.

[7] Trias, J. Benz, R. "Permeability of the cell wall of Mycobacterium smegmatis", *Mol. Microbiol.***1994**, *14*, 283.

[8] Niederwise M.; Danilchanka O.; Huff J.; Christian Hoffmann C.; Engelhardt, H. "Mycobacterial outer membranes: in search of proteins", *Mol. Microbiol.***1999**, *33*, 933.

[9] Stahl, C.;Kubetzko, S.; Kaps, I.; Seeber, S.; Engelhardt, H.; Niederweis, M. "MspA provides the main hydrophilic pathway through the cell wall of *Mycobacterium smegmatis*",*Mol. Microbiol.***2001**, *40*, 451.

[10] Engelhardt, H.; Heinz, C.; Niederweis, M. "A tetrameric porin limits the cell wall permeability of Mycobacterium smegmatis", *J. Biol. Chem.* **2002**, *277*, 37567.

[11] Faller M.; Niederweis M.; Schultz G. E. "The structure of a Mycobacterial outer membrane channel", *Science* **2004**, *303*, 1189-1192.

[12] Stephan J.; Mailaender C.; Etienne G.; Daffé M.; Niederweis M. "Multidrug resistance of a porin deletion mutant of Mycobacterium smegmatis", *Mol. Microbiol.***2001**, *40*, 451-464.

[13] Hjelmeland, L. M. "Solubilization of native membrane proteins", *Methods Enzymol.***1990**, *182*, 253–264.

[14] Heinz, C.; Niederweis, M. "Selective extraction and purification of a mycobacterial outer membrane protein", *Anal.Biochem.* **2000**, *285*, 113–120.

[15] Heinz, C.; Roth, E.; Niederweis, M., "Purification of porins from Mycobacterium smegmatis", *Methods in Molecular Biology* **2003**, *228*, 139-150.

[16] Heinz, C.;Engelhardt, H.; Niederweis, M. "The core of the tetrameric Mycobacterial porinMspAis an extremely stable β-sheet domain", *J. Biol. Chem.* **2003**, *278*, 8678-8685.

[17] Kruger, N. J., The protein protocols handbook, 2nd edition, Edited by Walker, J. M., Humana Press Inc., Totowa, NJ.

[18] Hutterer, R.; Hof, M.,"Fluorescence approaches for the characterization of the peripheral membrane binding of proteins applied for the blood coagulation protein prothrombin", *Springer Ser. Fluoresc.***2002**, *2*, 225.

[19] http://en.wikipedia.org/wiki/Excimer

# Chapter 2 - Supramolecular Binding Studies of MspA

## 2.1 Introduction

The surface chemistry of MspA allows various chemical binding options on both the outer and inner pore surface of the porin. These binding phenomena are rather complex as the protein tends to aggregate within itself in addition to binding with the analyte molecules. We have observed that MspA forms micelle-like structures at lower concentrations in aqueous media. (See figure below.)

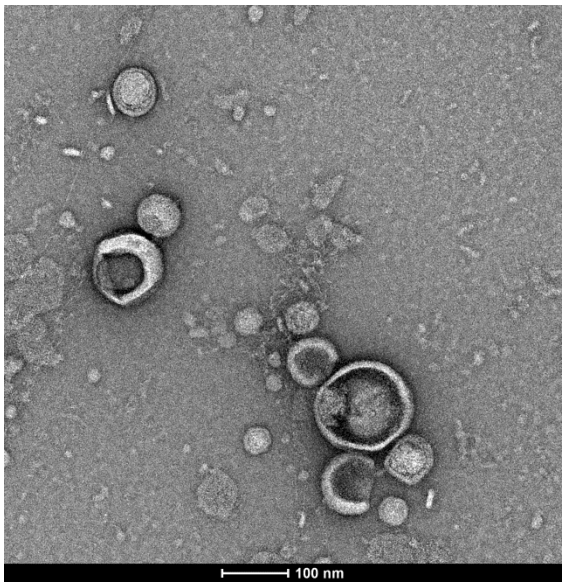


**Figure 2.1: TEM of vesicles formed from MspA on a carbon-coated 200-mesh copper grid**

The size of these aggregates can be controlled by varying the concentration of either the protein or the analyte or both. This behavior will be discussed in detail later on in this chapter.

In addition MspA also has the ability to insert within phospholipid bilayers[1] and polymer layers on surfaces.[2] Moreover, it is experimentally proven that MspA is capable of standing alone on surfaces such as mica without any supporting polymer or double layer.[3] It has also been experimentally proven that MspA has the ability to bind with gold nanoparticles[6,4] and Ruthenium polypridyl complexes.[5] Furthermore, the binding of "channel blocking agents" near the constriction zone of MspA has been discussed as a new strategy to combat mycobacterial infections, such as tuberculosis.[8] Although the presence of MspA homo-octamers on surfaces has been unambiguously proven by using TEM[5], AFM[6] and electrochemical techniques[6], only very little is known about the three-dimensional clustering behavior of MspA in aqueous environments. It has been established by TEM that MspA forms linear aggregates on surfaces showing a zipper-like pattern[7] (refer figure below). In this type of interaction, the strongly hydrophobic docking zones of MspA interact, shielding the proteins' stems from water. This behavior of MspA is in contrast to the behavior observed in aqueous buffers.

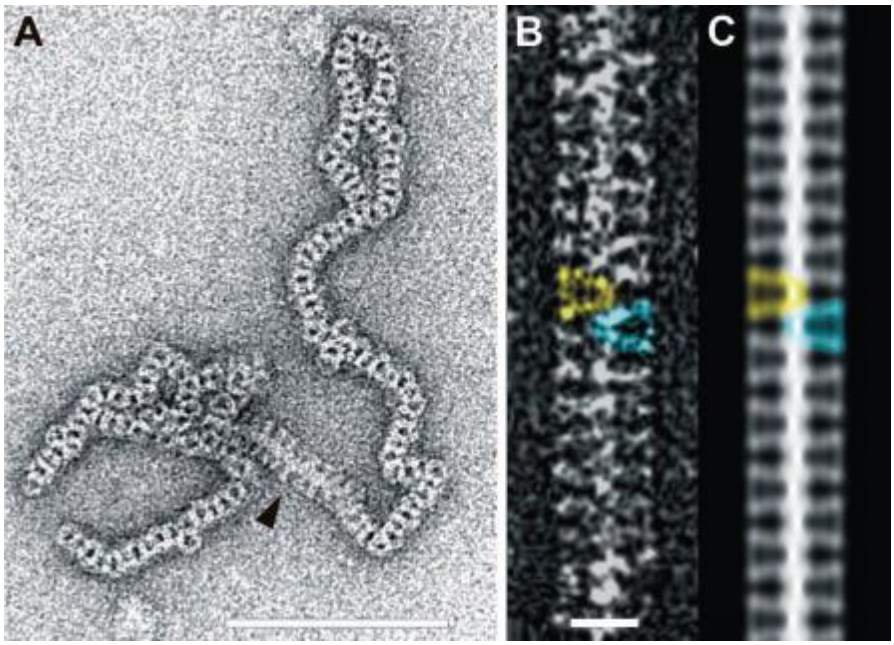


**Figure 2.2: Formation of 'zipper-like' structures of MspA: (scale bar represents 100 nm) A) reconstituted MspA in lipid media, B) and C) linear aggregate of MspA built from two rows of intercalating molecules. (Taken with permission from reference 28)**

Due to the high thermal stability of MspA[3], we were able to study the influence of ionic strength and especially the temperature on the size of the MspA-clusters and their zeta-potentials. The influence of temperature on the 3D-aggregation behavior of peptides is rarely discussed, because the temperature is well defined in many living organisms. Unlike MspA, most proteins cannot withstand higher temperatures and undergo denaturation, hence temperature dependent aggregation studies are largely limited. Designer proteins with tailored biophysical properties are becoming available to address this limitation[8] however, to date, temperature dependent studies on a wild type protein have not been made known. Thus new experiments on supramolecular aggregation behavior of pure wild type MspA and A96C MspA bound to Ruthenium(II)-polypyridyl complexes are discussed.

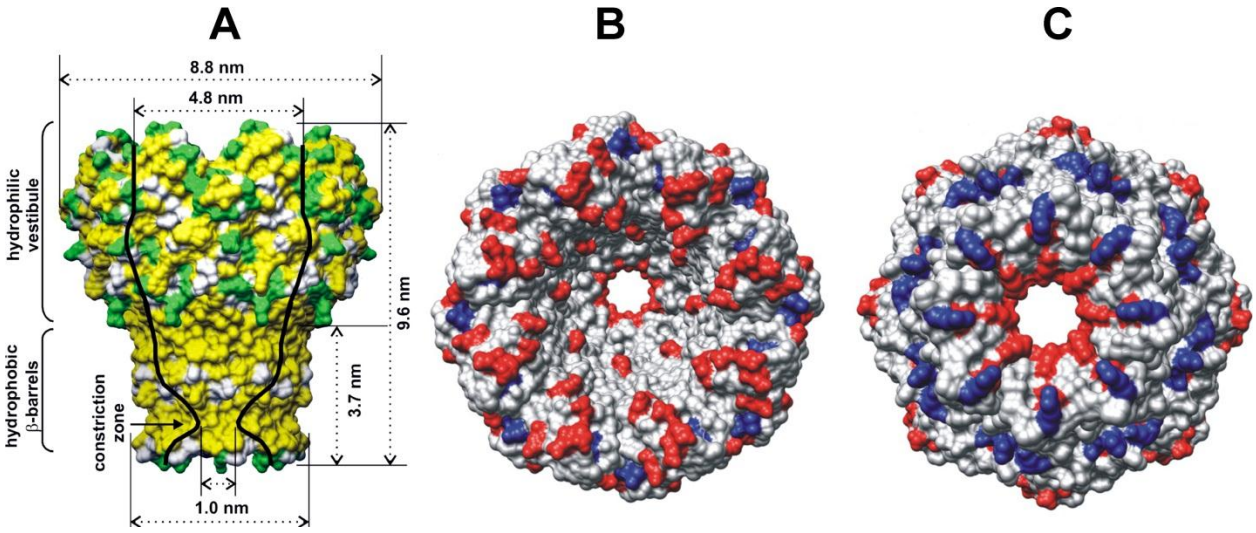


**Figure 2.3: The structure of the homo-octameric mycobacterial porinMspA: A) MspA is 9.6 nm in length and 8.8 nm in width. Its' "docking zone", which is formed by hydrophobic β-barrels, is located at the "stem". B) Structural model of the MspA pore viewed from the top generated using the UCSF Chimera software. Negatively and positively charged amino acids are shown in red and blue, respectively. Other amino acids are shown in gray. C) MspA pore viewed from the bottom. (Taken with permission from reference 2)**

MspA can also be chemically bound with dye molecules such as ethidium bromide and cyanine dyes. The significance of these studies is that these dyes are great imaging tools and gives us convenient means of characterizing and detecting MspA in a certain media. Cyanine dyes in particular have the advantage in that they are extremely biocompatible and can be engineered to be water soluble. This provides an efficient and cost effective detection of MspA in biological experiments.

Cyanines are a well-known class of fluorescent dyes that have wide-spread applications in bio-imaging. Synthesis of these compounds has been pioneered by Waggoner *et al.*[9,10] Cyanines are highly useful as fluorescent tags in biological media such as antibodies, DNA and proteins due their water solubility, photostability and pH insensitivity among many other advantages. The fact that sulfo-indo-cyanines show fluorescence signals much further from the

inherent auto-fluorescence signals given by biological media is a huge factor in their success as imaging reagents. Studies have been conducted to enhance and improve the binding between cyanines such as Cy3 and Cy5 to proteins for protein labeling.[11] The Bossmann group is continuously working on the synthesis and applications of improved cyanine dyes. Water soluble Cy3, Cy5 and Cy7 have been synthesized in our group recently.

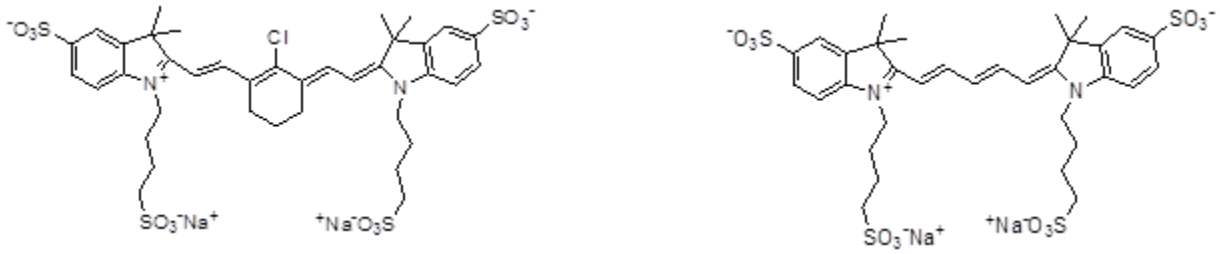


**Figure 2.4: Examples of Cy7 (left) and Cy5 (right) synthesized in the Bossmann labs**

Ethidium bromide is also a well-known dye used in biolmolecular labeling. However it is toxic to living organisms and therefore cannot be used for *in-vivo* studies. In particular, it is used as a fluorescent tag to label nucleic acid strains, which are analyzed by agarose gel electrophoresis.[12] It shows a significant increase in fluorescence intensity after binding with DNA and is hence a useful characterization tool.

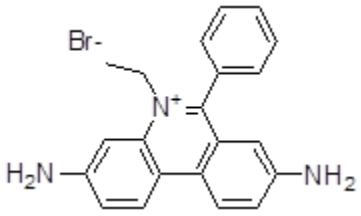


**Figure 2.5: Ethidium bromide**

Binding studies of wild type and A96C MspA with cyanines and ethidium bromide along with their characterization are discussed.

Binding of gold nanoparticles (diameter >5nm) into the inner pore of mutant Q126C MspA has been established previously.[4] The red color regions (refer figure 2.6) correspond to eight cysteine units found in Q126C mutant. The tryptophans within the upper rim region are shown in blue. The eight cysteine units greatly facilitate the binding of nanoparticles into the protein pore, as gold surfaces bind strongly with hydrophilic functional groups such as thiols.

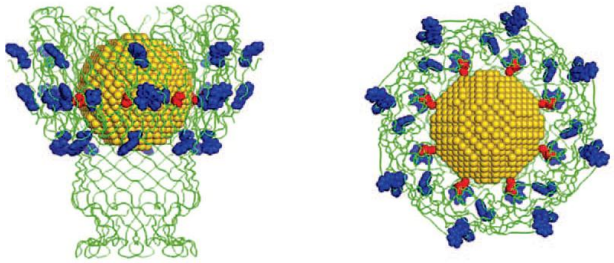

**Figure 2.6: MspA with bound gold nanoparticle (Taken with permission from reference 4)**

Protein-nanoparticle assemblies complement each other in that together they obtain better functionality and are easier to transport *in vivo*. Gold nanoparticle-protein assemblies are generally used for plasmonic hyperthermia studies and magnetic hyperthermia models, especially in cancer research.[4] Iron/iron oxide ($Fe/Fe_2O_3$) core/shell nanoparticles are also widely used for hyperthermia studies of similar nature.[13] These in particular provide attractive cancer research tools due largely to their biocompatibility. In this regard, binding studies of wild type MspA with iron/iron oxide core/shell nanoparticles have been conducted.

## 2.2 Experimental

### *2.2.1 Supramolecular aggregates of wild type MspA*

Dynamic light scattering and zeta potential measurements were done using ZetaPALS Zeta Potential Analyzer purchased by Brookhaven Instruments Corporation. One drop (50 μl) of wild type MspA extract (~0.6 mg/ml in 1x PBS) was diluted in 2.0 ml of deionized water and the average effective diameter of protein aggregates were recorded while increasing the temperature of the sample. The measurements were taken at increasing temperature values from 25 to 30, 35,40, 45, 50, 55, 60, 65 and 70 °C. The experiment was repeated using 2.0 ml of 1x PBS buffer solution instead of deionized water. Similarly, zeta potential was measured for wild type MspA extracts in both deionized water and 1x PBS solutions.

Transmission Electron Microscopy (TEM) was used to characterize the morphology of MspA aggregates in aqueous buffers. The TEM samples were prepared by immersing carbon-coated 200-mesh copper grids in aqueous solutions, counter staining by 2% uranyl acetate, followed by overnight drying in a desiccator. The dried grids were analyzed by Philips CM100 microscope operated at 100 kV.

### *2.2.2 Binding ethidium bromide to MspA*

In order to investigate whether a fluorescent tag could be bound to MspA, an experiment was conducted to bind the positively charged and highly fluorescent ethidium bromide with A96C MspA.

10 mg of ethidium bromide (purchased from Sigma Aldrich) was dissolved in 1 ml of $H_2O$. This was mixed with 20 mg of 1-Ethyl-3-(3-dimethylaminopropyl)carbodiimide hydrochloride (EDC) in 1 ml $H_2O$ and 20 mg of Hydroxybenzotriazole (HOBt) in 1 ml $H_2O$ and 1.3 ml THF. The overall volume was brought up to 5 ml. 250 µl of A96C MspA extract was added to this mixture and stirred at room temperature for 1 hour. The reaction mixture was put in a dialysis tube and immersed in 0.1x PBS buffer solution. Dialysis was performed for 48 hours and the remaining mixture of protein bound dye was subjected to UV and fluorescence analysis along with the corresponding unbound MspA and dye solutions.

### *2.2.3 Binding nanoparticle-ligand assemblies to MspA*

The iron/iron oxide ($Fe/Fe_3O_4$) core/shell nanoparticles were received from NanoScale Corporation. Synthesis of dopamine anchored tetraethylene glycol ligand and binding of ligand to nanoparticles was achieved in the Bossmann labs by Dr. Hongwang Wang according to procedures given in literature.[14,15,16]

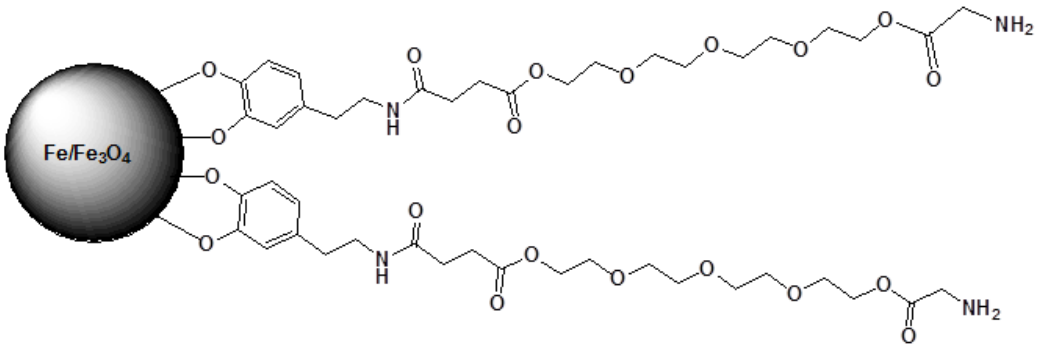


**Figure 2.7: Nanoparticle-ligand assembly used to bind with MspA (Taken with permission from reference 35)**

Next, the nanoparticle-ligand complex was chemically bound to A96C MspA via reaction between amine moiety of ligand with free carboxylate groups in the protein. This was achieved

by dispersing approximately 5 mg of nanoparticle-ligand complex in 2.0 ml of 1x PBS followed by the addition of 2.0 ml of either WT or A96C MspA extract with an approximate concentration of 0.6 mg/ml. The mixture was then stirred gently for 48 hours. Afterwards dialysis was performed using 0.1x PBS for 48 hours to concentrate the reaction mixture. Binding of nanoparticles to MspA was characterized by performing Dynamic light scattering (DLS) studies and UV/fluorescence measurements. The procedure for DLS measurements was similar to that described in section 2.2.1. However, as this was not a temperature dependent study the experiments were done at 25 ºC and in de-ionized water medium. One experiment was carried out at 55 ºC as a comparison study.

### *2.2.4 Binding cyanine dyes to MspA*

Water soluble cyanine dyes Cy7-1 and Cy-2 synthesized in our labs were employed for all measurements.

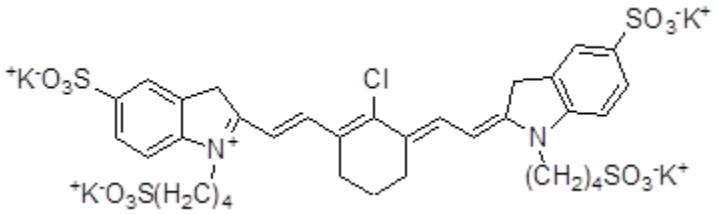


**Figure 2.8: Water soluble cyanine dye Cy7-1**

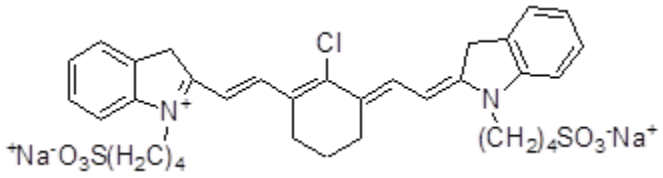


**Figure 2.9: Water soluble cyanine dye Cy7-2**

400 µl of Cy7-1 solution was mixed with 400 µl of A96C MspA and diluted up to 2.0 ml with distilled water. Similarly, 400 µl of Cy7-2 was mixed with 400 µl of A96C MspA and 1.2 ml of distilled water for a total volume of 2.0 ml. The solutions were stirred at room temperature for 24 hours. Next, the mixtures were filtered with ultra-filtration tubes with a molecular weight cut off of 10,000 in order to separate the unbound dye molecules and water from the bound protein-dye assemblies. The filtered samples were subjected to UV and fluorescence measurements as well as optical density studies to determine whether binding between the cyanine dyes and MspA has occurred.

## 2.3 Results and Discussion

### *2.3.1 Supramolecular aggregates of MspA*

#### *2.3.1.1 Temperature dependent solution dynamics of wild type MspA extracts*

The MspA-octamer is formed by 96 negatively charged and 8 positively charged amino acids.[17] R165 and E127, as well as R161 and E39 form salt bridges, which greatly stabilize its tertiary structure.[2] Whereas the negative charges are predominantly found within the interior of the "goblet", positive charges are concentrated in the stem and the periplasmatic loop region of MspA (Figure 2.3). These charges are responsible for the aggregation behavior of MspA molecules in various environments.

In order to investigate the solution dynamics of MspA aggregates in polar solvents, a series of temperature dependent dynamic light scattering experiments were carried out. It was

evident that increasing the temperature up to a certain extent causes the protein particles to aggregate but with further increase in temperature the particles dis-aggregate due to increased vibrational energy. This behavior is analog to the behavior of magnetic nanoparticles, which dis-aggregate after exceeding their Curie temperature ($T_c$).[18] However, it is important to clarify that the aggregation behavior of MspA discussed herein, was found to be a result of hydrophobic interaction and not of magnetic interaction.

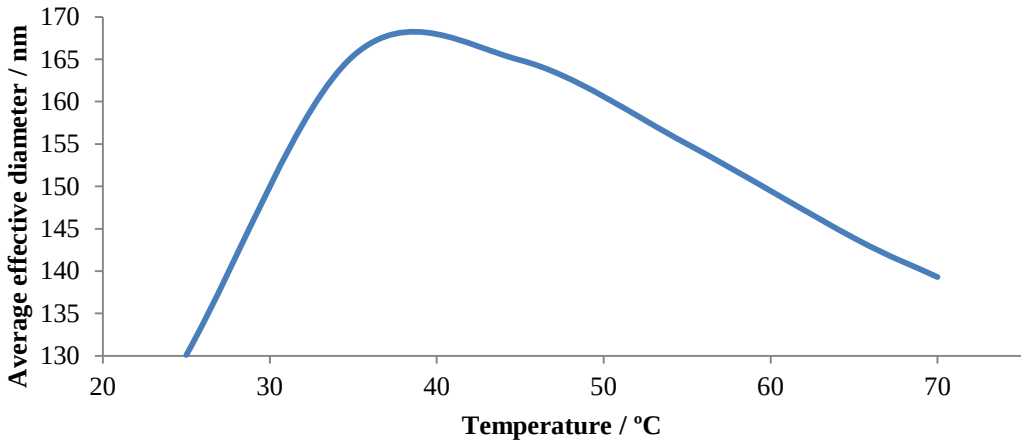


**Figure 2.10: Temperature dependent dynamic light scattering data of wild type MspA in de-ionized water**

In order to investigate whether or not there is a difference in particle size in different environments, the experiments were repeated in de-ionized water and in 1x PBS. Both media show similar patterns of clustering behavior. Although in general, the aggregations tend to be higher in PBS than in water, this difference is not clearly discernible due to experimental error. Hence it can be concluded that the aggregation behavior of MspA molecules in aqueous media is not dependent on the ionization of the medium but is a caused by hydrophobic attraction. The difference of aggregation is more marked in room temperature than any other thermal state.

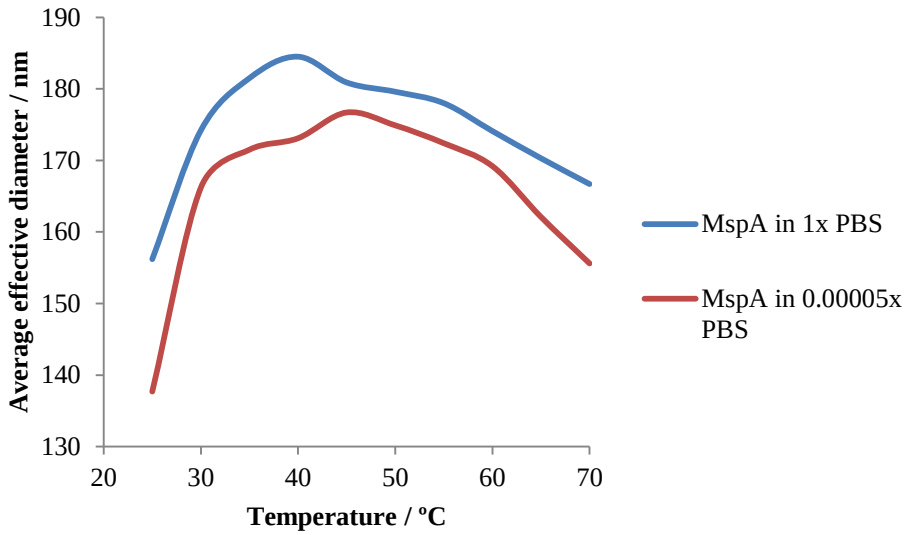


**Figure 2.11: Temperature dependent comparison study of MspA aggregates in 1x PBS and de-ionized (i.e. $5x10^{-5}$ x PBS) water**

Interestingly, the maxima of the supramolecular structures formed were observed at 40 ºC (standard 1x PBS) and 45 ºC (diluted MspA extract in de-ionized water). The aggregate diameters in both media were approximately 180 nm and were not distinguishable due to experimental error. Since it is evident that aggregation proceeds independent of the ionic strength of the medium, it is reasonable to assume that hydrophobic clustering is the major mechanism behind the observed aggregation behavior of MspA. The critical micellar concentration (cmc) is below 7.5 x $10^{-9}$ M (1.35 mg $L^{-1}$), which is approximately 300 times smaller than the cmc of sodium dodecyl sulfate (SDS) in PBS.[19] The packing parameter (P) is a concept that is widely used in surface chemistry to explain and predict the nature, shape and size of surfactant molecular aggregates in solution.[20] Calculation of packing parameter for these aggregates can be achieved by applying a semi-quantitative predictive model of forming supramolecular aggregates to MspA as given by the following equation:

$$P = \frac{V_0}{a_0 I_0}$$

**Equation 2.1: P: packing parameter, $V_0$: surfactant tail volume, $a_0$: area at the aggregate interface, $I_0$: tail length.**

$I_0$ is known (3.7 nm) and $V_0$ can be calculated using the geometric parameters of MspA known from literature (refer Chapter 1 and figure 2.12) and is found to be 69.7 $nm^3$. Also $a_0$ is calculated to be 60.8 $nm^2$.

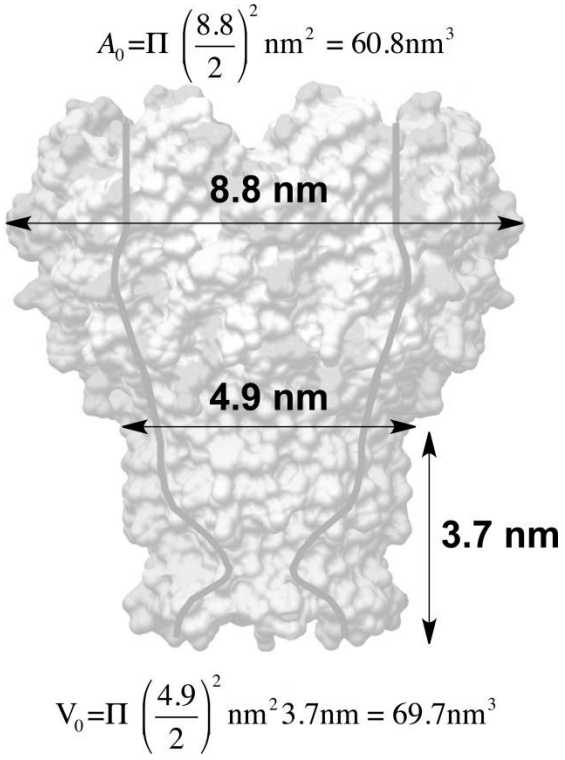


**Figure 2.12: Dimensions of MspA used for calculation of $V_0$ and $A_0$**

It is important to point out that $V_0/I_0$ is a constant for a given surfactant and the only variable that resembles the unique nature of the surfactant in packing parameter is the area $a_0$.

The latter is not a mere representation of the surfactant geometry, but rather of equilibrium free energy and is directly influenced by the interaction of surfactant head groups. The packing parameter of MspA is thus calculated to be 0.31, which is indicative of surfactants forming spherical or ellipsoidal micelles. Indeed, TEM characterization of MspA aggregates clearly indicated the presence of micellar-like structures (refer figure 2.1). However, MspA micelles formed appear to be spherical bilayer vesicles and not simple spherical vesicles as predicted by the packing parameter value. According to literature data, micelles that are formed by surfactant bilayers should have a packing parameter within the range of 0.5 to 1.0.[21] Thus there seems to be a marked discrepancy. This issue is discussed in detail in section 2.4.

#### *2.3.1.2 Zeta potential measurements of wild type MspA*

Zeta potential of a bilayer surfactant vesicle is the electric potential between the slipping plane in the interfacial double layer and the bulk solution.[22] The zeta potential data for the two mediums (i.e. de-ionized water/diluted PBS and 1x PBS) measured shows marked difference in values, unlike the particle sizing values. The more ionized buffer medium gives larger surface ionization values than the de-ionized water medium.

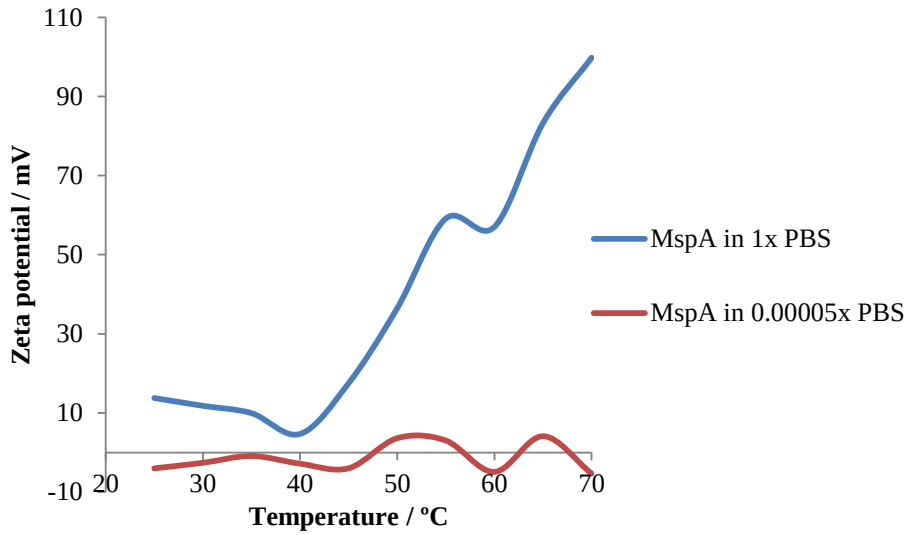


**Figure 2.13: Temperature dependent zeta potential measurements of WT MspA in 1x and $5x10^{-5}$x PBS**

For the de-ionized water medium (i.e. 5 x $10^{-5}$ x PBS) the zeta potential (ζ) values oscillate around the zero charge in de-ionized water in the temperature range from 25 to 45 ºC. This oscillation becomes more pronounced after 45 ºC. The observed oscillations are reproducible (experimental error ± 5 mV at each respective temperature). They are indicative of a complicated interplay between deprotonation of MspA's carboxylic acid groups and increased protonation of MspA's amine functions. Both effects increase with increasing temperature. The enhanced macromolecular motion of MspA with increasing temperature may lead to a changing dynamics of forming and breaking hydrogen bonds as the temperature is increased. A clear cut explanation in this regard cannot be provided at this stage.

However, in 1x PBS there is a marked difference in ζ values, especially at higher temperatures. A remarkable increase in zeta potential is observed beyond 40 ºC in 1x PBS medium. At 70 ºC zeta potential value measured is 99.79 mV, which is significantly high for a

protein solution. It is an indication of the high stability of MspA vesicles in this medium. The temperature dependence of the zeta potential is indicative of an endergonic adsorption process of cations ($Na^+$ and $K^+$) at MspA. The observed increase of ζ as a function of temperature is completely reversible. The aggregation number of the vesicles formed by MspA varied between *N*=1100 and *N*=2500 for the reported diameters (refer section 2.4). Although the aggregation behavior of MspA as a function of temperature is apparently governed by the hydrophobic effect, we have observed evidence for a strong influence of the ionic strength in the surface charges of MspA vesicles.

It is noteworthy that the remarkable difference of the surface charges of MspA vesicles in diluted PBS and 1x PBS only results in slightly different diameters, as shown in figure 2.11. The size of the MspA vesicles decreases in both media, however, the decrease is stronger in diluted PBS than in 1x PBS, indicating that charge-attraction/repulsion does not contribute significantly to $\left(\frac{D\mu^0}{kT}\right)_{\text{Head Groups}}$ (refer section 2.4), although it is the strongest interactive force (±5-8 kJ $mol^{-1}$ per bridge/repulsion) in supramolecular binding.[20] The pH of both media (5 x $10^{-5}$ x PBS and 1 x PBS) was measured to be 7.20 at 25 ºC. Therefore, we assume that similar number of hydrogen bonding events occurs between MspA - "heads" in the bilayer, when forming vesicles from both media. Hydrogen bonds between side chains of proteins have a typical strength of 4-5 kJ $mol^{-1}$ per bridge.[20] At this point we cannot distinguish between the effects of charge-attraction/repulsion and hydrogen bonding on the supramolecular attraction of MspA vestibules when forming the bilayer. In addition, different types of attraction/repulsion may exist between MspAs on the same and the opposite side of the bilayer, because the charge distribution at

MspA's surface is not isotropic (see Figure 2.3). The increase of the vesicles' diameters in both, diluted and standard PBS between 25 ºC and 40 ºC (1 x PBS) or 45 ºC (5 x $10^{-5}$ x PBS) could be caused by a thermal activation step required for vesicle formation. Since MspA is a large surfactant, the requirement for thermal activation is comprehensible. It should also be noted that many classic vesicles/liposomes are not in their thermodynamic minimum.[23]

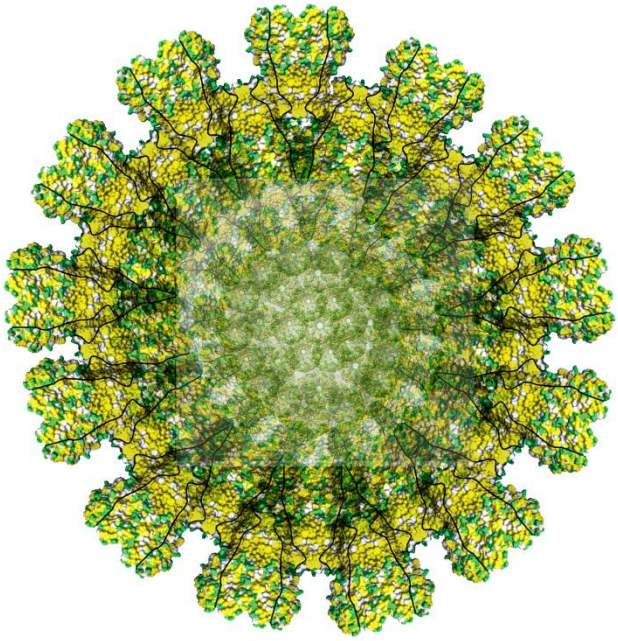

**Figure 2.14: Diagram depicting liposome-like MspA aggregate found to exist in aqueous buffers**

### *2.3.2 Ethidium bromide – MspA assemblies*

Evidence for binding of ethidium bromide to MspA was obtained by examining the fluorescence excitation spectra of unbound MspA and ethidium bromide vs. the bound MspA-ethidium bromide assembly. The unbound samples show characteristic fluorescence behavior. The MspA-dye assembly excitation peak shows a clear red shift from the unbound dye peak,

which is a characteristic feature of protein-dye assemblies. The tryptophan excimers of A96C MspA also contribute to this peak.

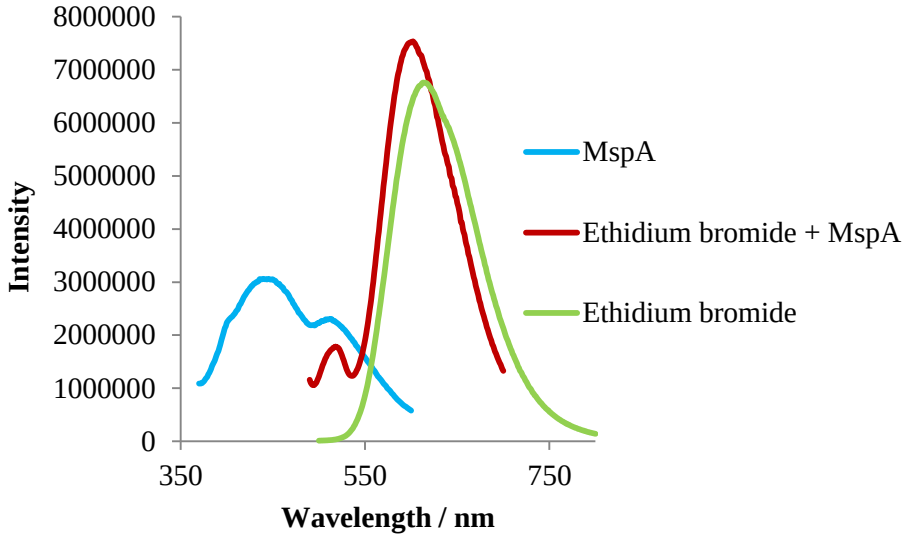


**Figure 2.15: Fluorescence excitation spectra for A96C MspA, A96C MspA bound to ethidium bromide and ethidium bromide**

### *2.3.3 Nanoparticle-linker – MspA assemblies*

Dynamic light scattering experiments revealed that the particle size of MspA-nanoparticle assemblies were significantly higher than the unbound protein particle sizes. The results are summarized below:

**Table 2.1: Summary of results for DLS experiments of MspA-nanoparticle-linker assemblies**

| Protein type | Volume of protein/ protein-nanoparticle-linker added / µl | Time between experiments / min | Average effective diameter of particles / nm |
|---|---|---|---|
| Unbound WT MspA | 150 | - | 138.0 |
| Nanoparticle-linker bound WT MspA | 150 | - | 527.7 |
| | 300 | - | 421.4 |
| Unbound A96C | 150 | - | 148.9 |

| | | | |
|---|---|---|---|
| MspA Nanoparticle-linker bound A96C MspA | 150 | - | 515.1 |
| | | 2 | 360.4 |
| | | 4 | 345.8 |
| | | 6 | 323.0 |

At room temperature, the unbound protein shows typical aggregation behavior as discussed in section 2.2.1. Interestingly, addition of excess MspA causes the particles to dis-aggregate and the average particle size decreases. It is possible that the excess charges added by the higher number of protein molecules result in attraction forces that disrupt the aggregates, leading to reduced particle sizes. It is evident from the above data that binding of the nanoparticle-linker complex to the protein significantly increases its' particle size in solution. It was also observed that these aggregates gradually dis-aggregate over time.

### *2.3.4 Cyanine dye – MspA assemblies*

Establishment of chemical binding between MspA and cyanine dyes were characterized using gel electrophoresis. The charges on cyanines affect the surface chemistry on the protein, causing possible dis-aggregation, hence the bound samples appear approximately 50 kDa lower than the unbound MspA bands. (Refer Figure 2.16)

Evidence of binding was also detected with fluorescence excitation measurements and clearly indicates maxima shifts for unbound and bound protein. (Refer Figure 2.17)

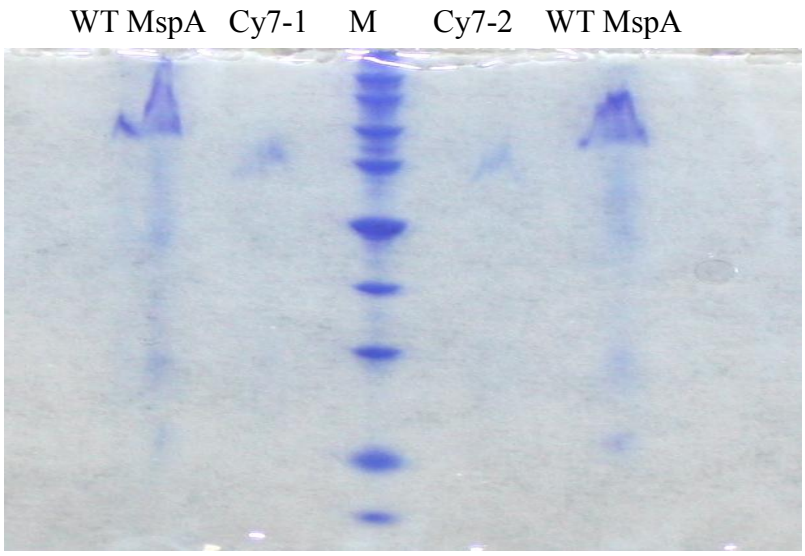


**Figure 2.16: Gel showing binding of Cy7-1 and Cy7-2 with WT MspA**

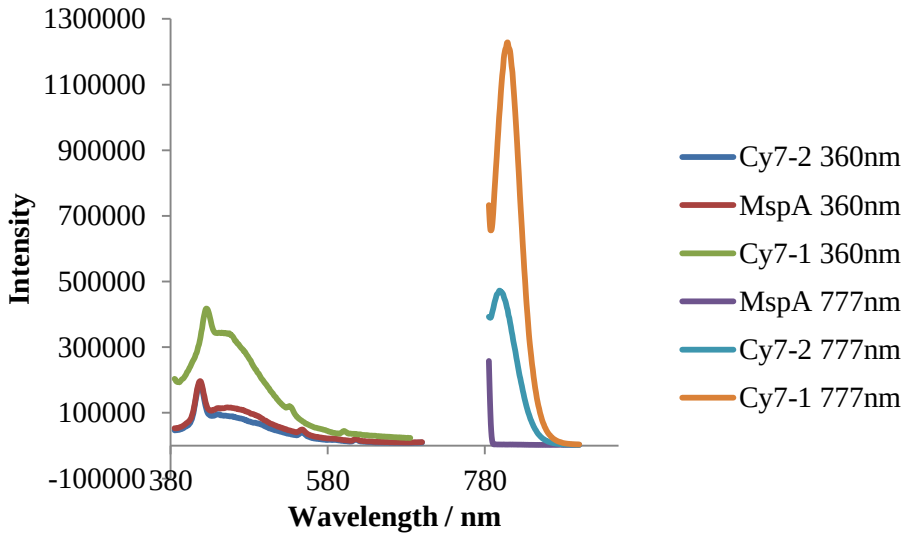


**Figure 2.17: Fluorescence excitation spectra of MspA, MspA+Cy7-1 and MspA+Cy7-2 detected at 360 nm and 777 nm respectively**

Optical density measurements for MspA bound Cy7-1 and Cy7-2 was measured with increased concentration in order to detect concentration effects. (Refer graphs below)

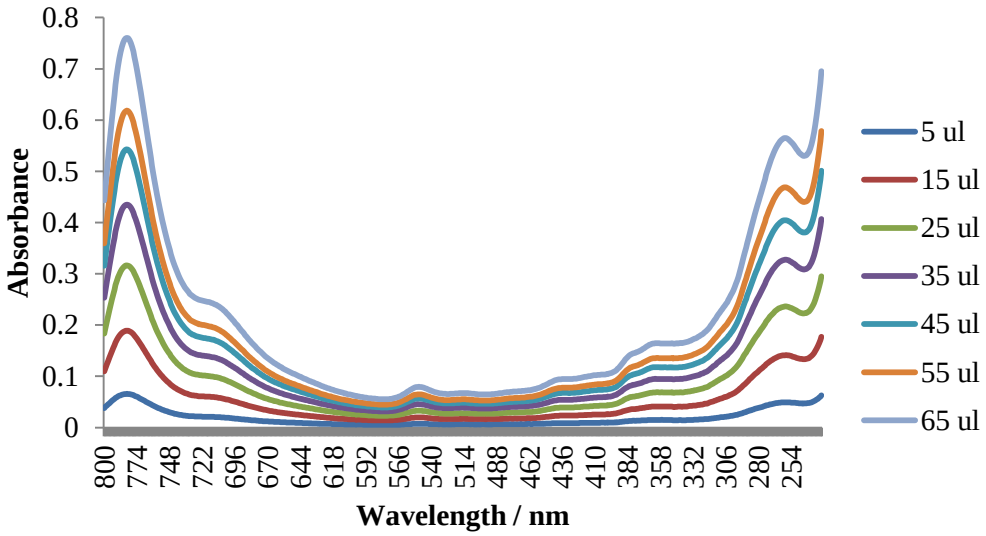


**Figure 2.18: Optical density measurements of MspA+Cy7-1**

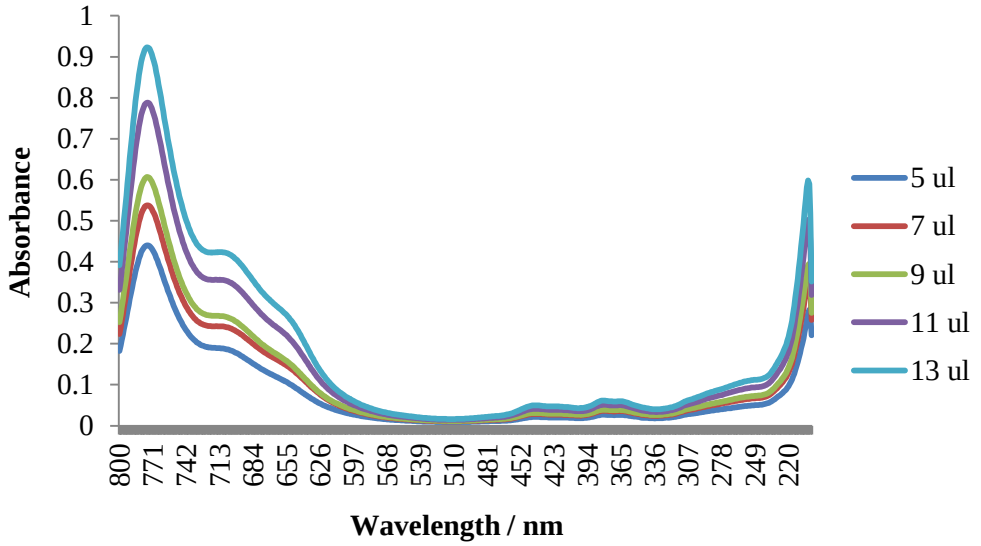


**Figure 2.19: Optical density measurements of MspA+Cy7-2**

It is clearly evident that both dyes show enhanced absorption with increasing concentrations. Hence introduction of cyanine dyes is an efficient technique to improve the overall absorption of MspA. This provides a convenient means of detecting MspA at lower protein concentrations. It is also an efficient and biocompatible imaging method for MspA.

## 2.4 Discussion: An explanation to the discrepancy of theoretical and experimental packing parameter value of MspA

As discussed in the introduction, MspA forms linear aggregates in a zipper-like pattern on surfaces.[7] This behavior is indicative of a packing parameter that is very close to 1.0.[24] Whereas the "docking zone" of MspA is formed by very stable hydrophobic β-barrels, the hydrophilic vestibule (the surfactant's "head") can potentially be deformed when single MspA proteins aggregate. Protein deformation is often observed during crystallization.[23] The formation of a bilayer is evidence for attractive interactions between MspA units. Predicting the geometry of supramolecular aggregates formed by one type of surfactant is assuming that the charged head groups show charge- and/or sterical repulsion.[23] However, the observed formation of vesicles indicates that the interactions of the vestibules are attractive and not repulsive. Furthermore, the formation of vesicles is not a function of ionic strength, as MspA forms vesicles in both diluted and 1x PBS in a similar manner.

### *2.4.1 Aggregation number as a function of vesicle radius*

We have calculated the aggregation number *N* of MspA-octamers that form a unilamellar vesicle as a function of the vesicles' diameter according to the following equation:

$$N = \frac{4\pi r_e^2}{A} + \frac{4\pi r_i^2}{A}$$

**Equation 2.2: Calculation of aggregation number *N* of MspA**

In here, $r_e$ is the external radius of the vesicle, which is consistent with its diameter divided by 2. $r_i$ is the inner radius of the vesicle, which is $r_e^2 - 2\ (L_{MspA} - L_{dz})$ ($L_{MspA}$: length of

MspA = 9.6 nm; $L_{dz}$: length of the docking zone = 3.7 nm, see Figure 2.3). Also area occupied by one MspA-octamer: 72.4 $nm^2$. This calculation is based on the assumption that the docking zones are in contact in the vesicles' double layer. This interaction causes the centers of MspA within either the external or the internal layer to be 9.6 nm apart from each other, forming a simple packing pattern (see figure below). The largest diameter of MspA is 8.8 nm.[2]

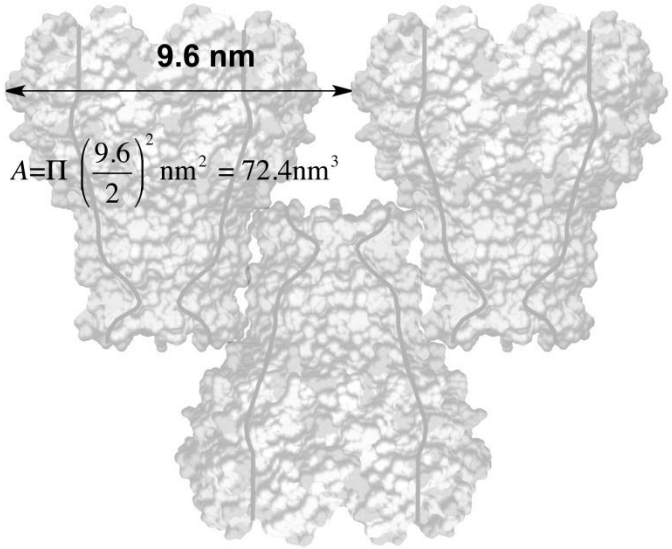


**Figure 2.20: Distance between two neighboring MspA octamer units in the outer layer of a vesicle's double layer, and effective size of MspA within that layer**

The inner radius $r_i$ is smaller than the external radius $r_e$ by twice the lengths of MspA minus the extension of the docking zone, because MspA forms aggregates showing a zipper-like pattern in which the hydrophobic docking zones are in contact with each other.[7]

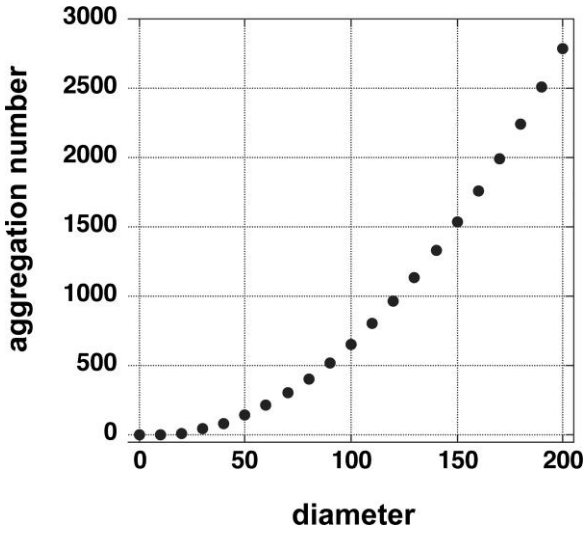


**Figure 2.21: Estimated number of MspA-octamers forming a unilamellar vesicle (the presence of one MspA double layer is assumed) as a function of vesicle radius, according to equation 2.2**

According to equation 2.2 and Figure 2.21, the aggregation number *N* varies between approximately *N*=1100 and *N*=2500 of the known diameters for MspA.

### *2.4.2 The Hydrophobic Effect is Responsible for Vesicle Formation by MspA*

In describing the self-assembly process by the free energy model originally developed by C. Tanford[25] and assuming that the residual contact of the water with the hydrophobic constriction zone is negligible after vesicle formation, the change in the chemical potential ($\Delta\mu^0$) during supramolecular aggregation is dependent on the transfer of MspA from the aqueous phase into the MspA-bilayer and the interaction of the headgroups.

$$\left(\frac{\Delta m^{0}}{kT}\right) = \left(\frac{\Delta m^{0}}{kT}\right)_{\text{Transfer}} + \left(\frac{\Delta m^{0}}{kT}\right)_{\text{Head Groups}}$$

**Equation 2.3: Calculation of chemical potential ($\Delta\mu^0$): k = Boltzmann constant, T = temperature in K**

$\left(\frac{\Delta m^{0}}{kT}\right)_{\text{Transfer}}$ is negative, because the solvation of extended hydrophobic surfaces has a disruptive effect on water structure. The transfer of MspA from the aqueous phase to the bilayer is the thermodynamic driving force of vesicle formation. Whereas the hydrogen bond network of water around an alkane of modest length (e.g. $C_6H_{14}$) is not distorted significantly, the solvation of extended hydrophobic structures has a disruptive effect on water structure because it prohibits the formation of an extended hydrogen bonding network. Huang and Chandler have established that the excess chemical potential decreases monotonically with temperature for structures with radii R > 1 nm, as this is the case with the "docking zone" of MspA (r =1.85 nm).[26]

$\left(\frac{\Delta m^{0}}{kT}\right)_{\text{Head Groups}}$ is describing the energetic contribution arising from the interactions of the vestibules of MspA in the bilayer. Due to the presence of polar amino acid side chains at the exterior of MspA's "head", hydrogen bonding[27] and charge attraction/repulsion[28] could be potentially responsible for the discrepancy of the calculated packing parameter P = 0.31 and the experimental finding that vesicles are formed.

## 2.5 Conclusions

TEM has provided experimental evidence that the mycobacterial porin MspA forms vesicles at low concentrations from aqueous buffers. The size of the MspA vesicles is strongly dependent on temperature, but not on the ionization of the aqueous buffer medium. The hydrodynamic maximum of the vesicles has been determined by dynamic light scattering to approximately 180 nm. It occurs at 40 ºC (1x PBS) and 45 ºC (diluted PBS). The occurrence of a temperature maximum is indicative of a thermal activation step required for the formation of bilayers from MspA. The above speculation is reasonable, as MspA is a rather large surfactant of 9.6 nm in length and 8.8nm in diameter. Due to the complexity and large size of MspA molecules, size and shape of its vesicles cannot be predicted, using simple surface chemistry principles. Zeta potential measurements show that increasing the temperature favors reversible cation ($Na^+$, $K^+$) adsorption at MspA in 1x PBS. It is noteworthy that the corresponding significant increase in $\zeta$ does not significantly affect the hydrodynamic diameter of the vesicles.

Binding and characterization of MspA with dyes such as ethidium bromide and cyanines have been achieved. These have the potential to be developed as efficient detection and imaging techniques for MspA. The above results are significant in utilization of MspA in cancer detection. Binding of nanoparticle-linker assemblies to MspA has also been successfully achieved. These are significant in potential applications of cancer treatment via hyperthermia.

## 2.6 References


[1] Stahl, C.; Kubetzko, S.; Kaps, I.; Seeber, S.; Engelhardt, H.; Niederweis, M. "MspA provides the main hydrophilic pathway through the cell wall of *Mycobacterium smegmatis*", *Mol. Microbiol.* **2001**, *40*, 451.

[2] Bossmann, S. H.; Janik, K.; Pokhrel, M. R.; Heinz, C.; Niederweis, M. "Reconstitution of a porin from Mycobacterium smegmatis at HOPG covered with hydrophobic host layers", *Surf. Interface Anal.* **2004**, *36*, 127.

[3] Basel, M. T.; Dani, R. K.; Kang, M.; Pavlenok, M.; Chikan, V.; Smith, P. E.; Niederweis, M.; Bossmann, S. H. "Direct observation of gold nanoparticle assemblies with the porinMspA on Mica", *ACS Nano* **2009**, *3*, 462.

[4] Dani, R. K.; Kang, M.; Kalita, M.; Smith, P. E.; Bossmann, S. H.; Chikan, V. "MspAporin-gold nanoparticle assemblies: Enhanced binding through a controlled cysteine mutation", *Nano Lett.* **2008**, *8*, 1229.

[5] Pokhrel, M. R.; Gamage, P.; Kalita, M.; Shi, A.; Bossmann, S. H. "Developing new strategies for the treatment of tuberculosis employing ruthenium(II)quaterpyridyl complexes", *J. Nepal Chem. Soc.* **2009**, *23*, 2.

[6] Woerner, M.; Lioubashevski, O.; Basel, M. T.; Niebler, S.; Gogritchiani, E.; Egner, N.; Heinz, C.; Hoferer, J.; Cipolloni, M.; Janik, K.; Katz, E.; Braun, A. M.; Willner, I.; Niederweis, M.; Bossmann, S. H. "Characterization of nanostructured surfaces generated by reconstitution of the porinMspA from Mycobacterium smegmatis", *Small* **2007**, *3*, 1084.

[7] Engelhardt, H.; Heinz, C.; Niederweis, M. "A tetrameric porin limits the cell wall permeability of *Mycobacterium smegmatis*", *J. Biol. Chem.***2002**, *277*, 37567-72

[8] Senes, A. "Computational design of membrane proteins", *Curr.Opin.Struct.Biol.* **2011**, *21*, 460.

[9] Ernst, L. A.; Gupta, R. K.; Mujumdar, R. B.; Waggoner, A. S. "Cyanine dye labeling reagents for sulfhydryl groups", *Cytometry* **1989**, *10*, 3-10.

[10] Mujumdar, R. B., Ernst, L. A., Mujumdar, S. R., Lewis, C. J., and Waggoner, A. S. "Cyanine dye labeling reagents: sulfoindocyaninesuccinimidyl esters", *Bioconjugate Chem.* **1993**, *4*, 105-111.

[11]Toutchkine A.; Nalbant P.; Hahn K. M. "Facile synthesis of thiol-reactive Cy3 and Cy5 derivatives with enhanced water solubility", *Bioconjugate Chem.*, **2002**, *13*(3), 387–391.

[12] http://en.wikipedia.org/wiki/Ethidium_bromide

[13]DerylL .Troyer and Stefan H .Bossmann, Chapter 5."Utilization of magnetic nanoparticles for cancer therapy in nanomedicine and cancer",Edited by Victor R .Preedy, Science Publishers **2011**.

[14] Wang, H.; "I. Studies of NHC-palladium(IV) species in C-H bond activation process II. Synthesis of functionalized bimagnetic core/shell iron/iron oxide nanoparticles for the treatment of cancer", Department of Chemistry, Kansas State University, **2009**.

[15] Fernandez, C.; Nieto, O.; Rivas, E.; Montenegro, G.; Fontenla, J. A.; Fernandez-Mayoralas, A. "Synthesis and biological studies of glycosyl dopamine derivatives as potential antiparkinsonian agents", *Carbohydrate Research*, **2000**, *327*, 353-365.

[16] Xu, C.; Xu, K.; Gu, H.; Zhang, R.; Liu, H.; Zhang, X.; Guo, Z.; Xu, B. "Dopamine as a robust anchor to immobilize functional molecules on the iron oxide shell of magnetic nanoparticles", *J. Am. Chem. Soc.***2004**, *126*, 9938-9939.

[17] Rastogi, N.; Legrand, E.; Sola, C. "The mycobacteria: an introduction to nomenclature and pathogenesis", *Rev Sci Tech***2001**, *20*, 21.

[18] Buschow, K. H. J. (**2001**), *Encyclopedia of materials : science and technology*, Elsevier. ISBN 0-08-043152-6.

[19] Bayrak, Y. "Micelle formation in sodium dodecyl sulfate and dodecyltrimethylammonium bromide at different temperatures", *Turk. J. Chem.* **2003**, *27*, 487.

[20] Israelachvilli, J. N.; Mitchell, D. J.; Ninham, B. W. "Theory of self-assembly of hydrocarbon amphiphiles into micelles and bilayers", *J. Chem. Soc., Faraday Trans. 2* **1976**, *72*, 1525.

[21] Svenson, S. "Self-Assembly and Self-Organization: Important Processes, But Can We Predict Them?", *J. Dispersion Sci. Technol.* **2004**, *25*, 101.

[22] Kirby, B.J. (2010). *Micro- and Nanoscale Fluid Mechanics: Transport in Microfluidic Devices.*. Cambridge University Press.ISBN 978-0-521-11903-0.http://www.kirbyresearch.com/textbook.

[23] Luisi, P. L. "Are Micelles and Vesicles Chemical Equilibrium Systems?",*Journal of Chemical Education* **2001**, *78*, 380.

[24] Tachibana, M.; Kojima, K. "Growth, defects and mechanical properties of protein single crystals", *Curr.Top.Cryst.Growth Res.* **2002**, *6*, 35.

[25] Tanford, C. "The hydrophobic effect: Formation of micelles and biological membranes", John Wiley & Sons: New York, **1973**.

[26] Huang, D. M.; Chandler, D. "Temperature and length scale dependence of hydrophobic effects and their possible implications for protein folding", *Proc. Natl. Acad. Sci. U. S. A.* **2000**, *97*, 8324.

[27] Bowie, J. U. "Membrane protein folding: how important are hydrogen bonds?", *Curr. Opin.Struct.Biol.* **2011**, *21*, 42.

[28] Schneider, H. J. "Binding mechanisms in supramolecular complexes", *Angew.Chem., Int. Ed.* **2009**, *48*, 3924.

# Chapter 3 - Channel Activity and Channel Blocking Studies of MspA

## 3.1 Background

### *3.1.1 Channel activity of porins*

Channel activity of a porin is essentially its ability to transport electrolytes through its pore under specific voltage and pressure conditions, while being immersed in a lipid bilayer. These electrolytes can be small inorganic ions, large organic molecules such as proteins or molecular fragments such as single stranded (ss) DNA or RNA fragments. The first single molecule channel activity measurement with reproducible results was done by Hayden and Hladky in 1970.[1] In this study they used the antibiotics nonactin, nystatin and gramicidin (Figure 3.1) as channel forming molecules and the bilayers were formed with either lecithin or glycerol solutions. NaCl and KCl were employed as electrolytes.

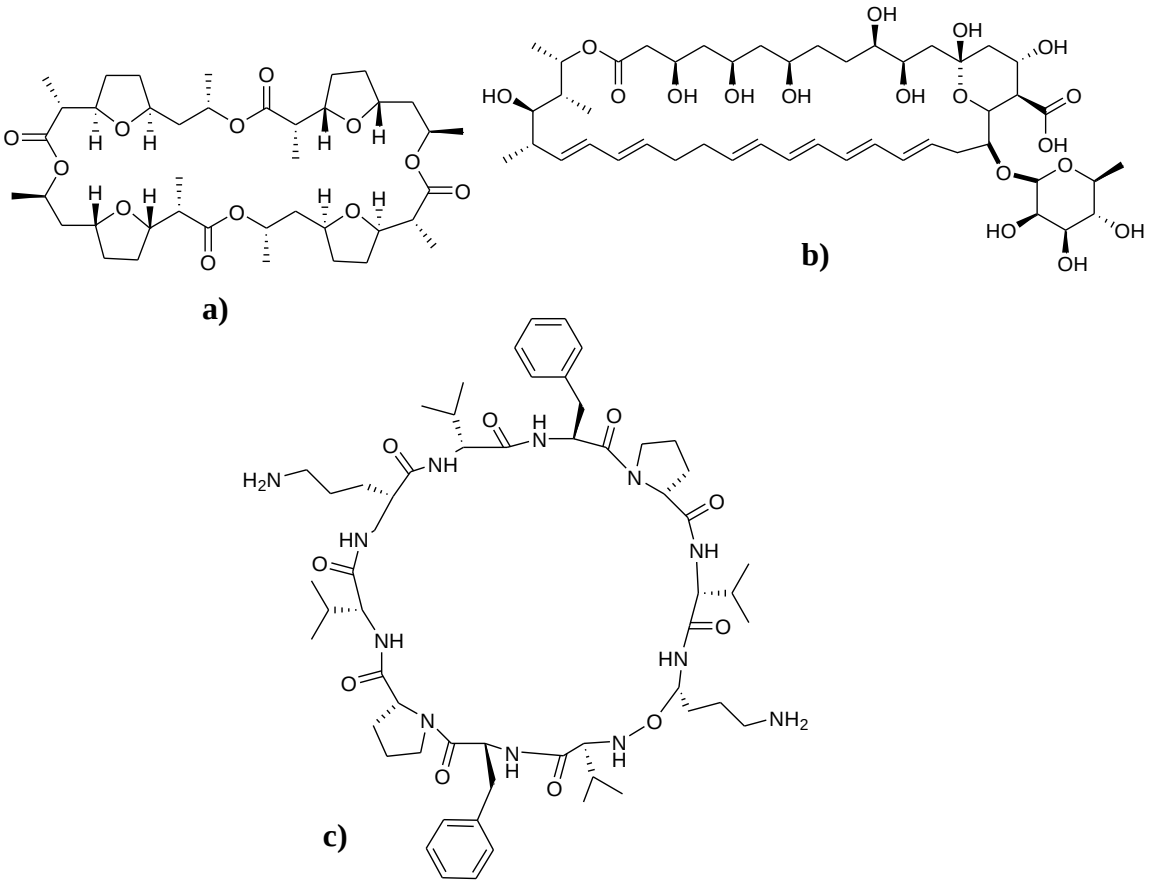


**Figure 3.1: a) Nonactive b) Nystatin c) Gramicidin S**

Continuous research in this field eventually led to the development of 'stochastic sensing' as a major discipline in analytical chemistry. This is essentially the detection of binding of an analyte molecule (ex. small electrolytes such as KCl or large organic molecules like ss-DNA or protein) to a receptor (ex. channel forming antibiotic or protein), thereby identifying various characteristics of the analyte.[2] The applications of stochastic sensing range from defense applications and environmental applications to medicine.

Over the years porins have gained prominence as channel activity research tools. The Staphylococcal porin α-hemolysin (αHL) has been utilized extensively in this regard.

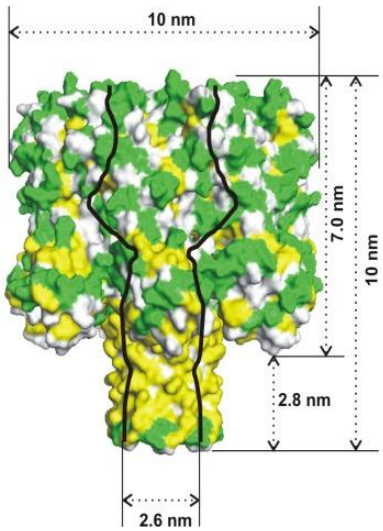


**Figure 3.2: Structure of α-hemolysin (Taken with permission from reference 3)**

α-Hemolysin is a heptameric porin found in the outer cell membrane of *Staphylococcus aureus*. It consists of 293 amino acid residues and is capable of assembling itself into lipid bilayers.[3] The inner pore of αHL can be engineered to control the channel blocking by the analyte. Due to its unique dimensions, αHL allows the passage of a wide range of analytes including single stranded nucleic acids, globular organic molecules (~2 kDa) as well as various cyclodextrins.

### *3.1.2 Basic principles of channel activity measurement*

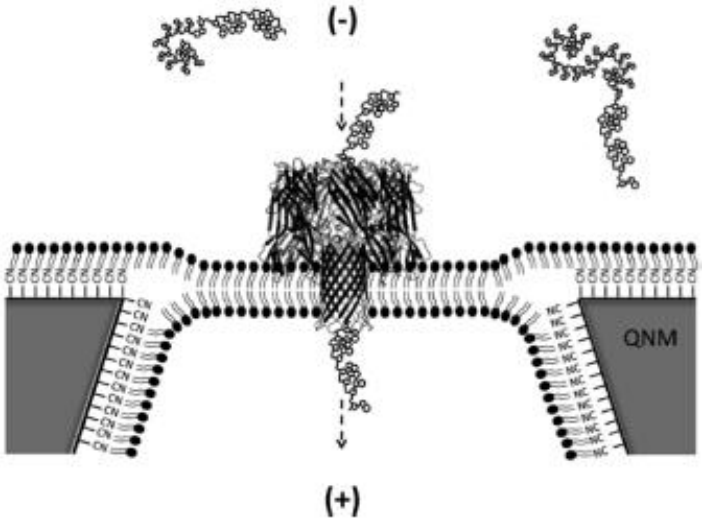


**Figure 3.3: Schematic representation of a channel activity experiment. ss-DNA is translocated through αHL pore, immersed in a lipid bilayer, which in turn is supported on a quartznanopore (Taken with permission from reference 4)**

In order to obtain a uniform lipid bilayer, two individual lipid layers need to be held together firmly from the top and bottom along an orifice of a solid support. For this purpose, an engineered quartz nanopore is usually employed. Construction of such nanopores has been studied extensively by Henry S. White et al.[4] A nanopore is engineered from fused quartz membranes (quartz capillary) with a diameter usually ranging from 10-1000 nm. Next, the pore is cleaned and dipped in a silanizing agent in order to introduce a silanized layer along the inside and outside surfaces of the nanopore orifice. 3-Cyanopropyldimethylcholrosilane is often used as a silanizing agent.

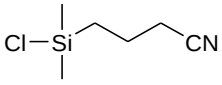


**Figure 3.4: Silanizing agent 3-cyanopropyldimethylcholrosilane[3]**

Next, a lipid solution such as DPhPC is applied to the nanopore with the aid of a plastic pipette tip (DPhPC = 1,2-diphytanoyl-*sn*-glycero-3-phosphocholine). The cyanine groups of the silanized layer bind with the hydrophilic tails of the lipid along the outside and inside of the pore, thereby forming a bilayer. The bilayer containing a nanopore is then introduced onto a voltage setup. (Figure 3.5)

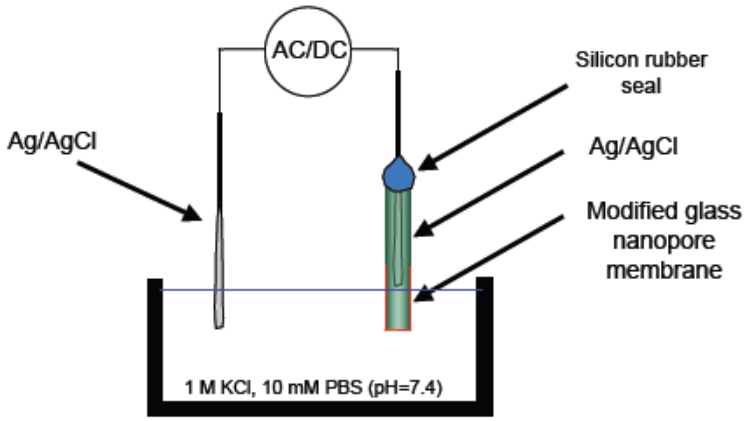


**Figure 3.5: Experimental setup for a channel activity measurement (Taken with permission from reference 3)**

A solution of αHL is added to the electrolyte container and a certain voltage and pressure is applied. Under these conditions, the porin assembles itself in the bilayer, forming a channel across it. Whether or not a porin channel is formed on the bilayer and how many porins are immersed at one particular time etc. can be detected by measuring the conductance across the membrane. (Figure 3.6)

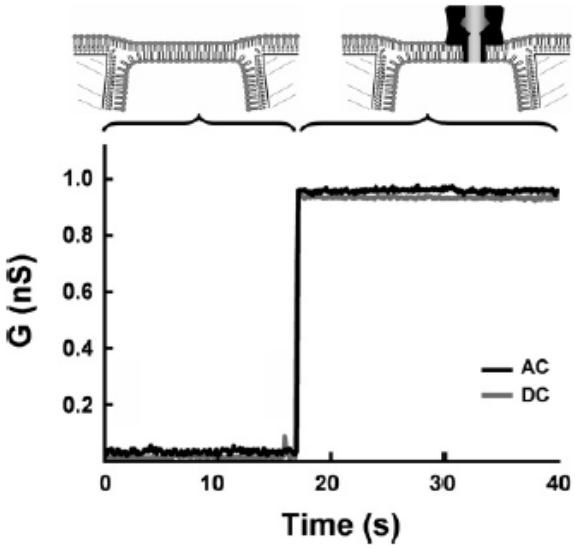


**Figure 3.6: Schematic representation of a conductance measurement across a lipid bilayer during a channel activity study (Taken with permission from reference 8)**

The conductance should read zero across the bilayer, but when a porin is immersed a steady conductance reading can be observed. This reading can appear either as positive or negative, depending on the direction of the applied current. There are several advantages to using engineered glass nanopores over synthetic porous material such as teflon.[4] Quartz nanopores help to generate a lipid bilayer which is less susceptible to mechanical vibration and they have better voltage stability (breaks at 0.8 V) as well as higher lifetimes (days to weeks). Also smaller bilayers limit the number of protein insertions at one time. This significantly simplifies signal analysis.

### *3.1.3 Nucleic acid translocation through α-Hemolysin pore*

Single molecule analysis is an important application of porin channel activity. By reading the change in conductance while the molecules pass through the pore, its dynamic properties and structure can be determined. ss-DNA or RNA molecules can be electrophoretically driven through αHL pore[4, 5] (Figure 3.3). Since these are large molecules, they occupy a large space in

the pore, thereby blocking the ionic current which passes through the pore. Hence this phenomenon is called ‘channel blocking’ or ‘gating’. Generally the channel current would reduce to ~90% of the open channel value during a blockade event. Each nucleotide would give a distinctly different current signal hence by identifying the different current signals the sequence of the nucleotides can be determined. The number of blockades is directly correlated to number of nucleic acid molecules added and the duration of blockade is proportional to the length of the nucleic acid.

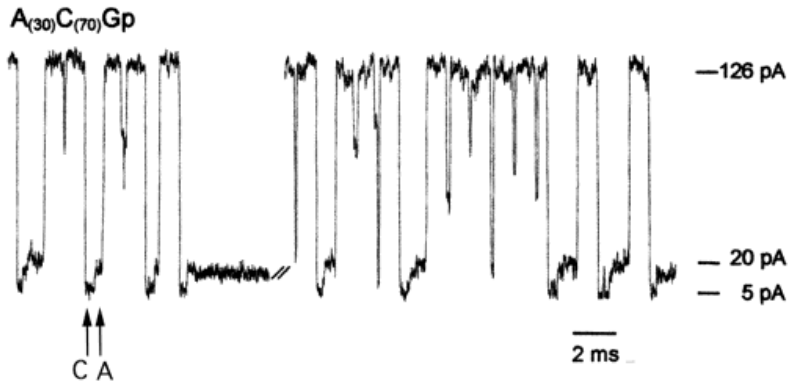


**Figure 3.7: Typical blockade signals for RNA A(30)C(70)Gp (Taken with permission from reference 5)**

Each point above corresponds to blocking of the αHL channel by a single RNA molecule. The signals given by polyC (poly-cytosine) are distinctly different from signals given by polyA (poly-adenine). Accordingly, this method provides a fast and inexpensive way to determine a nucleic acid sequence.

By measuring the duration of the blockade signal a “binding constant” (k) between the protein pore and the analyte can be calculated. The binding constant is a measure of the strength of the non-covalent interaction of the channel with the channel blocking agent. The longer the

blockade signal (t) the higher the interaction. This interaction is often reversible and can be represented by an equilibrium as follows:

$$\text{Analyte} + \text{Protein} \underset{k_{off}}{\overset{k_{on}}{\rightleftharpoons}} \text{Analyte-Protein (non-covalent complex)}$$

Where, $k_{on}$ and $k_{off}$ are the association and dissociation rate constants (or binding constants) respectively.[6] The relationship between the blockade duration t and $k_{on}$ can be depicted as $t = 1/k_{on}[A]$, where [A] is the analyte concentration present.

White *et al.* have conducted various experiments to increase the sensitivity and accuracy of channel activity measurements.[7] Although each nucleotide (i.e. Adenine, Guanine, Thymine, Cytosine) should theoretically give a different current signal in a blockade event, the actual signal values are only <10% different from each other and are thus difficult to identify. Also under typical experimental conditions, ss-DNA/RNA translocates rather fast through the channel (2-20 μs per base at room temperature), adding to the difficulty of identification. Studies have shown that increasing the viscosity of the electrolyte solution will decrease the speed of DNA translocation significantly, thereby improving the signal-to-noise (SNR) ratio of the conductance reading. Translocation of polyA in 1M KCl containing 63 vol % glycerol has shown a decrease of 20 times in velocity. This clearly indicates the correlation between viscosity of electrolyte solution and translocation speed. Thus a significant SNR improvement can be achieved. (Figure 3.8) Another method to increase SNR is to use a separate DC (direct current) bias to control binding rates while employing another AC bias to record the ion channel conductivity.[8]

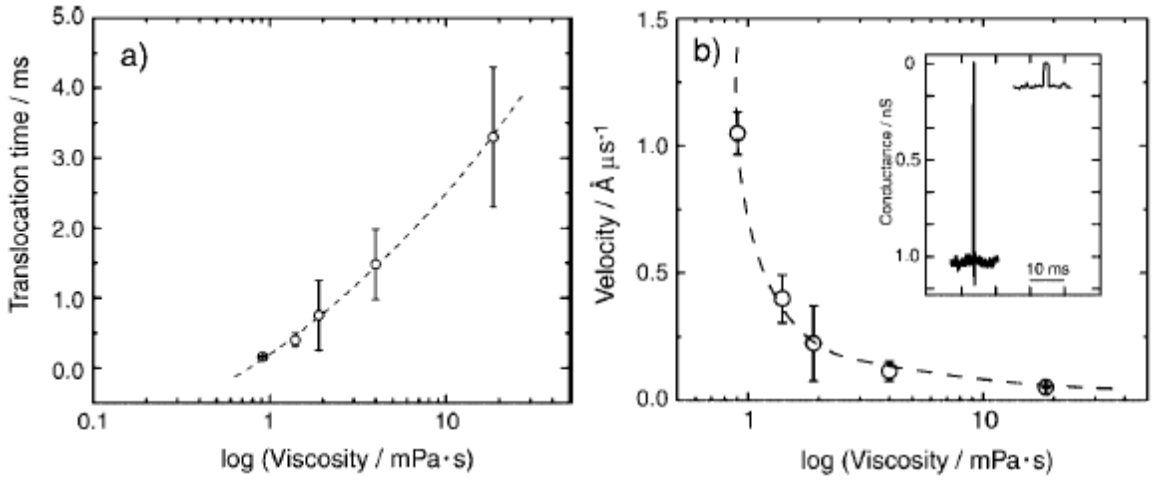


**Figure 3.8: Translocation time a) and viscosity b) of poly-(dA)50 as a function of bulk solution viscosity (Taken with permission from reference 7)**

### *3.1.4 Use of MspA as a channel forming agent*

Over the years MspA has proven to be an excellent candidate for channel activity studies.[8] Due to its high stability and unique structure, MspA has more favorable characteristics for DNA translocation than αHL. The constriction zone of MspA is approximately 1 nm long and 1 nm wide and opens up on either side to larger diameters. This is a highly favorable geometry to accurately read a nucleotide sequence, since the current blocking occurs at a narrow region (Figure 1.2). In αHL however, there's a longer narrow region, which is 4 nm long and 1-2 nm wide, and this is immediately followed by a 1 nm constriction zone (Figure 3.2). This long narrow region would block current altogether and may give misleading results during a conductance measurement. Moreover, research indicates that MspA can be subjected to point mutation where we can engineer specific sites of the porin to bind with a specific analyte exchanging amino acids (ex. MspA-A96C, MspA-Q126C etc.).[9] The ability of MspA to retain its channel forming nature even after being exposed to extreme physical conditions such as 0-14

pH, extraction at 100 °C for 30 min and incubation at 80 °C in 2% SDS are also favorable factors.

Wild type (WT) MspA has shown an average open channel conductance of 4.9 nS at 1M KCl at 20 °C. However translocation of ss-DNA through WT porin has been unsuccessful. A reason for the above was envisaged as the negative charge at the constriction zone. Hence the mutant D90N/D91N/D93N (M1MspA) was expressed where the aspartates of the WT inside the constriction zone were replaced with asparagines. Constructed ss-DNA hairpins have been successfully driven through this pore.[9]

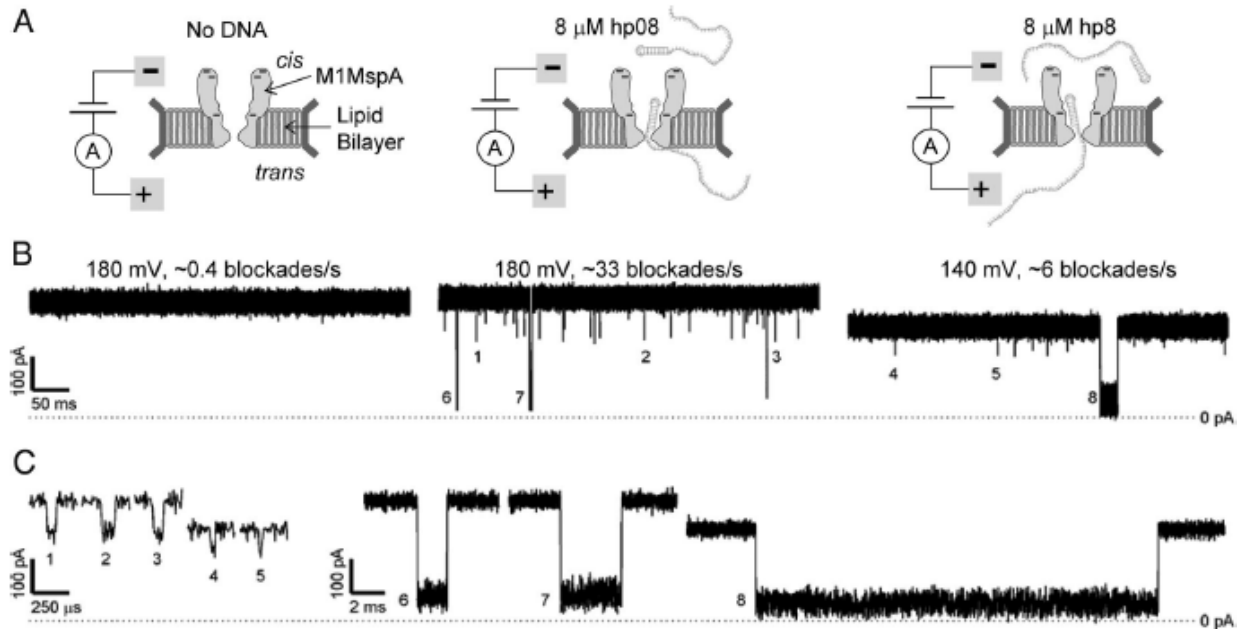


**Figure 3.9: Translocation of ss-DNA with M1MspA: A) Schematic representation of experiments, B) Representation of ionic current signals, C) Expanded blockades from B (Taken with permission from reference 9)**

We recently re-investigated the channel activity of WT MspA in order to re-establish and improve its channel forming and current conducting ability. Another purpose for this study was

to compare and validate the new extraction procedure for MspA against the previously reported procedure by comparing the current conductance values.

### *3.1.5 Channel blocking studies of wild type MspA*

Binding of Ruthenium(II) based polypyridine complexes inside the MspA pore, thereby blocking its channel has been reported previously.[10] These experiments have been aimed towards developing an alternate treatment method to combat mycobacterial infections as well as to develop nanostructures capable of luminescence. Since MspA plays a crucial role in transportation of electrolytes in and out of the mycobacterial cell, blocking its pore disrupts the basic metabolic processes of the cell and eventually leads to its death. Since *M. smegmatis* bears genetic resemblance to *M. tuberculosis*, channel blocking strategies developed on MspA could eventually lead to viable treatment options for tuberculosis.

A series of Ruthenium complexes consisting of several positive charges have been synthesized to achieve optimum binding at the MspA constriction zone.[11] Compound $Ru(QP\text{-}C_2)_3^{8+}$ (also abbreviated as RuC2) in particular shows significant binding with the protein inner pore.

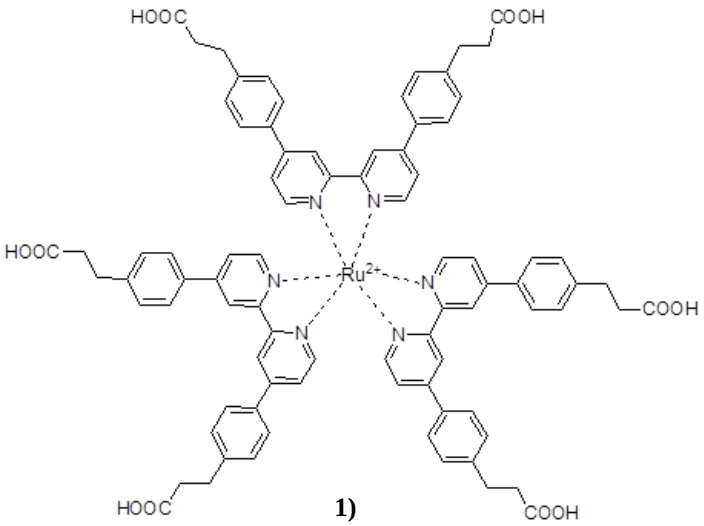


**Figure 3.10: tris(N,N'''-bis(carboxyethyl)-4,4':2,2'':4'',4'''-Quarterpyridine-N',N''-dium-N',N''')ruthenium(II) octachloride [$Ru(QP\text{-}C_2)_3^{8+}$]**

The positively charged Ruthenium complex would bind preferably with the negatively charged MspA inner pore. Characterization of binding has been established by HPLC and luminescence studies. The binding constant between $Ru(QP\text{-}C_2)_3^{8+}$ and MspA has been found to be $5.8 \times 10^9$ $M^{-1}$. Luminescence data shows a marked bathochromic shift of the maxima of the MspA bound sample, compared to the unbound dye.

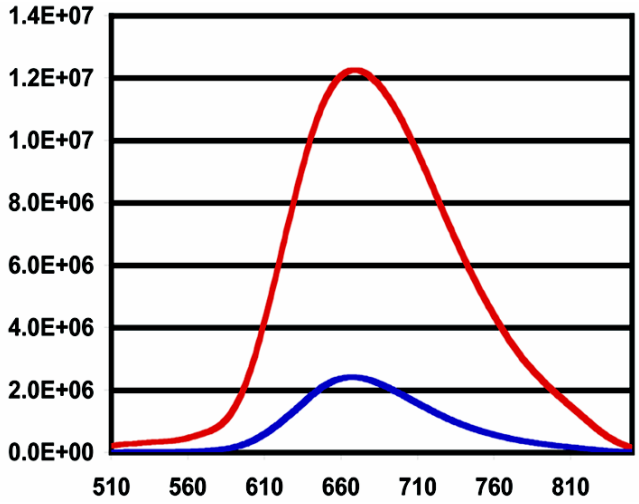


**Figure 3.11: Luminescence spectrum of RuC2. Red - in presence of MspA, blue - without MspA. (Taken with permission from reference 11)**

This red shift is said to occur due to interaction between protein and metal complex. The ligand-field surrounding the Ruthenium center is extended as a result of this interaction consequently causing the bathochromic shift.[12] The luminescence data also indicates a significant increase in intensity of the protein bound dye. Since the sample is in aqueous medium, the luminescence that arises due to the metal to ligand charge transfer of the dye is partially quenched by the water molecules.[13] However, when the dye complex binds to the protein, it loses part of its hydrate coating. This is the reason for the enhanced luminescence observed in the bound sample. This overall behavior is typically observed for protein bound Ruthenium(II) polypyridyl complexes.[11]

Convenient binding, favorable geometry and simplicity of binding characterization makes Ruthenium(II) polypyridyl complexes the ideal candidates to be used as MspA channel blocking agents.

## 3.2 Experimental

All channel activity and channel blocking experiments were conducted in collaboration with Dr. Henry S. White and co-workers at University of Utah at Salt Lake City, Utah.

All MspA extracts used for this study were HPLC purified and had a concentration of 0.1 mg/ml. Experiments were performed in 1mM KCl, 10mM PBS (pH 7-8), 1M KCl/30mM PBS (pH 7.4) and 1M KCl/10mM HEPES (pH 8). MspA extracts were diluted to concentrations ranging from 2 ng/ml to 1.5 mg/ml. The lipid bilayer was made from 1,2-diphytanoyl-*sn*-glycero-3-phosphocholine and was obtained from Avanti Polar Lipids, Inc. The experiments were performed on an EBS (Electronic BioSciences) system.

Channel blocking studies of MspA were conducted with two Ruthenium based blocking agents; *tris*(*N*,*N*'''-dipropyl-4,4':2,2'':4'',4'''-quarterpyridine-*N*',*N*''-dium-*N*',*N*''')Ruthenium(II)

octachloride [$Ru(QP\text{-}C_2)_3^{8+}$] and Ruthenium(II)-*tris*-bipyridine [$Ru(bpy)_3^{2+}$]. The synthesis of $Ru(QP\text{-}C_2)_3^{8+}$ had been achieved previously according to the procedure published by Bossmann *et al.* in 2005.[14] Synthesis of $Ru(bpy)_3^{2+}$ had also been achieved previously in the Bossmann labs according to procedure given by Dürr *et al.*[15]

## 3.3 Results and Discussion

### *3.3.1 Channel activity experiments of wild type MspA*

During the first attempt of channel blocking experiments of wild type MspA done in 2010, the value of channel conducting current varied significantly with each separate experiment.

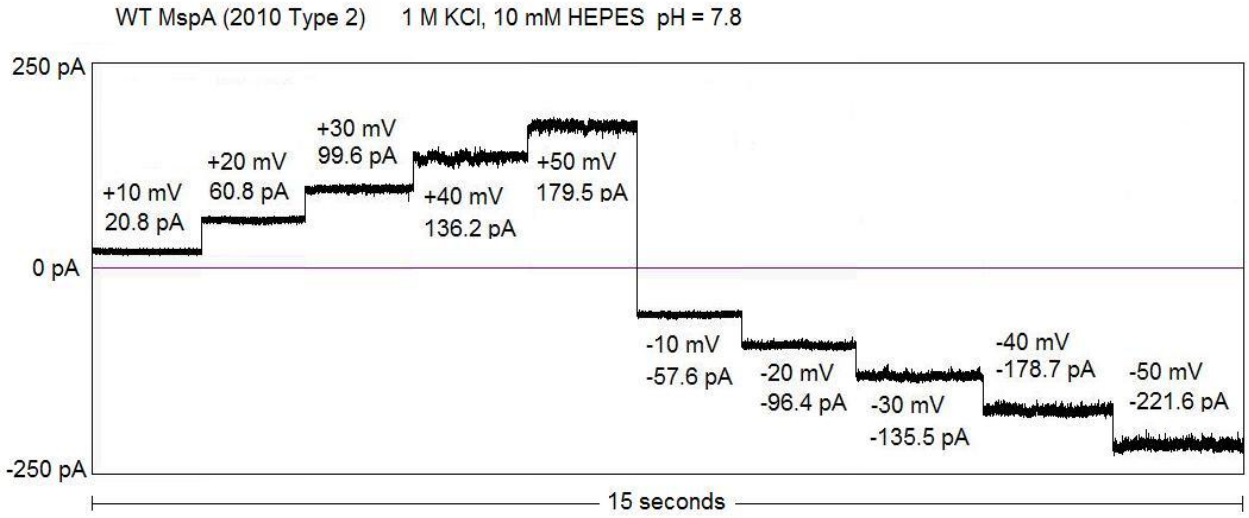


**Figure 3.12: I.T. trace showing conductance of WT MspA (Unpublished, 2010, Perera, A. S. *et al.*)**

Two major conductance populations were observed during the study. One was of lower value with an average conductance of ~1 nS and was categorized as Type 1. These were more frequent and formed highly stable and reproducible insertions. The other population was of higher conductance value of ~4 nS and was categorized as Type 2. These were much less in

frequency of occurrence and once occurred, did not last long periods of time. Both types of channels did not show gating behavior until higher voltages of >100 mV were applied. The above observations were significantly different from the literature values which were previously reported. A comparison is given in the table below.

| | WT MspA in literature | WT MspA 2010 |
|---|---|---|
| Average conductance | ~ 5 nS | ~ 1 nS |
| Maximum conductance | 5.2 nS | 5.75 mV |
| Occurrence of gating | < 100 mV | No gating at < 100 mV |

**Table 3.1: Comparison of experimental and literature values for pore conductance and gating behavior of WT MspA**

Although channel forming ability of wild type MspA in a lipid bilayer was successfully demonstrated, several concerns still remained after completion of this study:

For certain MspA extracts, insertion onto the bilayer were not observed. When insertion did occur, it was not always reproducible and in some cases the bilayer ruptured after a short time. Conductance values varied greatly and isolated populations of low conductance (~1 nS) and high conductance (~4 nS) were observed for some samples. The low conductance channels were observed more than the high conductance channels. This was not in agreement with the previous literature value of ~4.9 nS. It was assumed that impurities in the protein may cause these effects hence research was conducted to further optimize the extraction procedure. Extracts heated at 65 °C for 1 hour (instead of 100 °C 30 min) using a detergent concentration of 0.08% (instead of 0.05%) rendered the most pure protein (characterized by gel electrophoresis). These extracts were further purified by HPLC and channel activity studies were repeated with the optimized protein extracts. Indeed the results obtained afterwards were much improved. Stable

insertions, which lasted up to 2-3 hours were observed. The conductance reading gave a steady average of ~350 pA (see figure below).

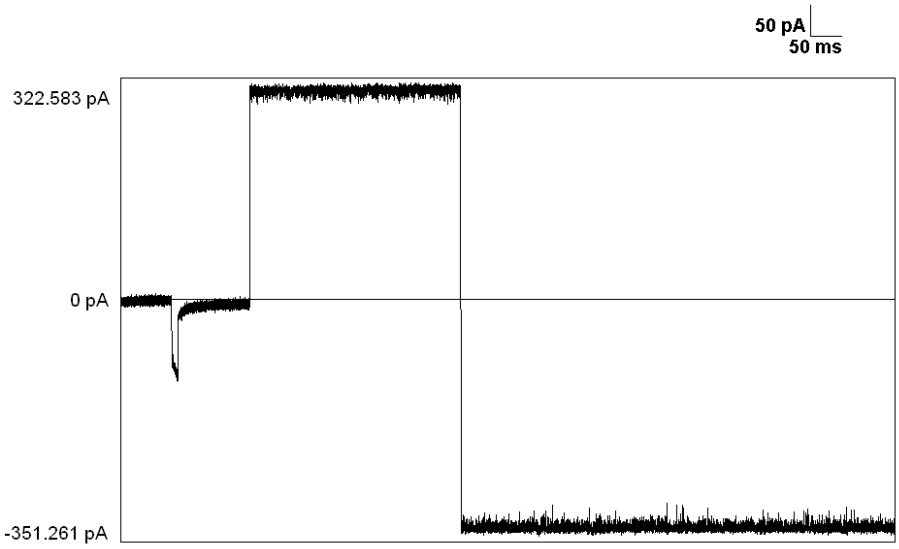


**Figure 3.13: I.T. trace showing conductance of WT MspA (Unpublished, 2011, Perera, A. S. *et al.*)**

It is also noteworthy to observe that at the applied voltage and KCl concentration, MspA has an open ion channel current of about -350 pA, thus showing when a single insertion has been obtained. Due to the asymmetric geometry of the protein, which is roughly conical in shape, ion current rectification takes place, so that when the polarity is flipped from positive to negative, the current value for the positive polarity has an absolute value less than that of the negative polarity, which is again, as stated above -350 pA.

It is reasonable to assume that purity of the protein leads to more stable and frequent bilayer insertions. Hence it became apparent that the new extraction procedure renders higher quality protein.

### *3.3.2 Channel blocking experiments of wild type MspA*

The channel blocking of MspA was also re-investigated with Ru(II) complexes, $Ru(QP\text{-}C_2)_3^{8+}$ (or RuC2) and $Ru(bpy)_3^{2+}$ which were previously synthesized in the Bossmann labs. The objective of this study was to utilize a positively charged blocking agent to counteract the negative charges of the aspartates present inside the MspA pore, thereby allowing the binding molecule to enter into the pore and bind at the constriction zone. As mentioned Chapter 1 WT MspA contain three aspartate groups close to its constriction zone. In particular aspartates D90 and D91 at the constriction zone contribute to a high negative charge at this site. Each monomer has two aspartates hence the octamer has sixteen overall.[16]

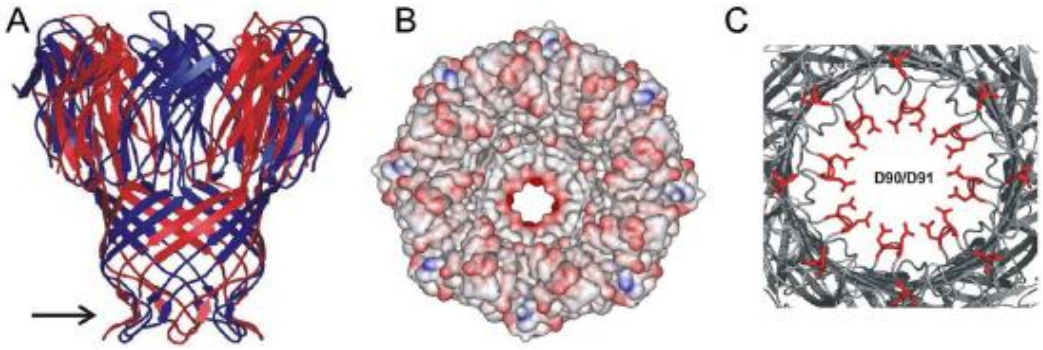


**Figure 3.14: A) Arrow depicts constriction zone of MspA, B) Top view of MspA, red color regions indicate negative charges from carboxylates and blue regions indicate positive charges from ammine groups, C) Aspartates D90 and D91 at constriction zone (note: D93 cannot be seen here) (Taken with permission from reference 16)**

In order to be an effective channel blocker for MspA, the binding complex needs to be within 2-5 nm of diameter and contain flexible bonds to allow substitute mobility. Most importantly, it should have a considerably high positive charge per molecule. Considering the above requirements, several Ruthenium based complexes have been synthesized in the Bossmann labs, two of which were used for this study and are discussed below.

### *3.3.3 Synthesis of tris(N,N'''-dipropyl-4,4':2,2'':4'',4'''-quarterpyridine-N',N''-dium-N',N''')Ruthenium(II) octachloride [Ru(QP-$C_2$)$_3^{8+}$]*

Synthesis of [Ru(QP-$C_2$)$_3^{8+}$] (or RuC2) has been achieved previously in the Bossmann labs according the procedure given in scheme 3.1.[11]

**Scheme.3.1: Synthesis of tris(N,N'''-dipropyl-4,4':2,2'':4'',4'''-quarterpyridine-N',N''-dium-N',N''')Ruthenium(II) octachloride [Ru(QP-$C_2$)$_3^{8+}$]**

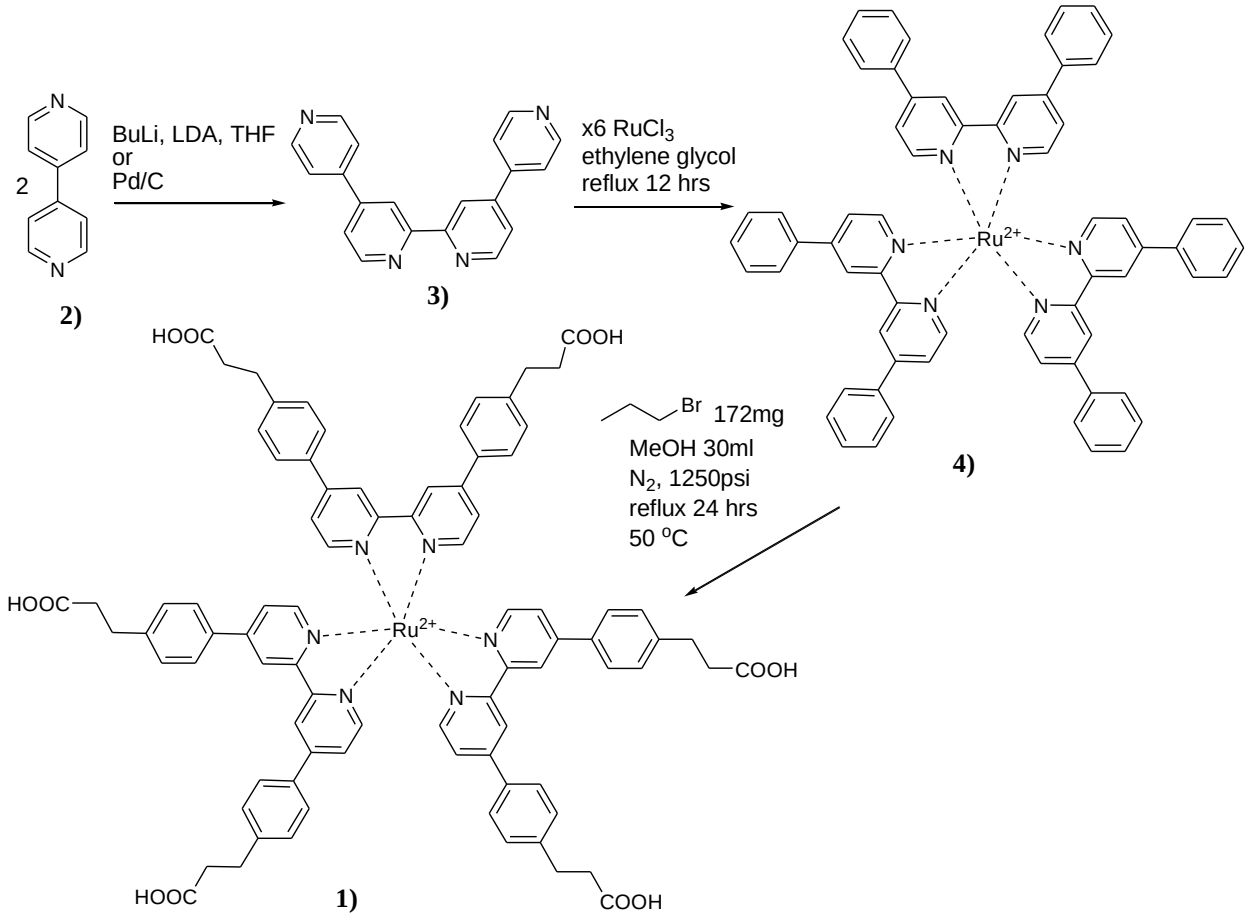


### *3.3.4 Synthesis of Ru(bpy)$_3^{2+}$*

Another compound which was used for MspA channel blocking was Ru(bpy)$_3^{2+}$. This complex is highly stable and has a high excited state lifetime.[17] It is kinetically inert and

thermodynamically stable, making it an excellent candidate for many photophysical applications. Its structure is simple and synthesis is uncomplicated.

**Scheme 3.2: Synthesis of$Ru(bpy)_3^{2+}$**

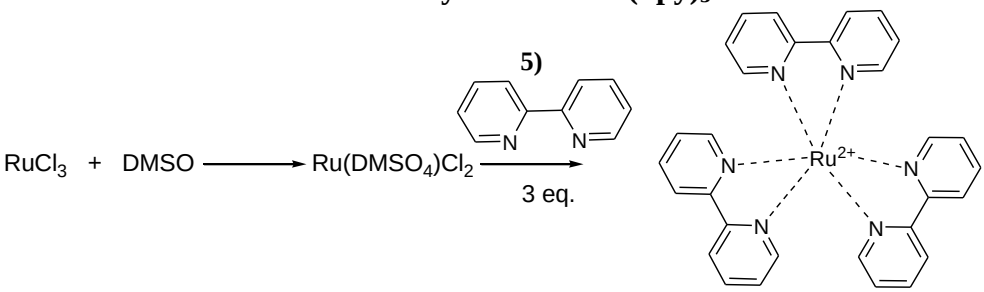


**6)**

### *3.3.5 Discussion*

Initial experiments were carried out in 2010 in order to detect gating by $Ru(QP\text{-}C_2)_3^{8+}$ and $Ru(bpy)_3^{2+}$ with WT MspA. Both dyes were tested using concentrations of 0.02 μM, 10 μM and 25 μM solutions. The presence of $Ru(QP\text{-}C_2)_3^{8+}$ was successfully detected using WT MspA using the 25 μM concentration. The figure below depicts what we observed to be $Ru(QP\text{-}C_2)_3^{8+}$ blockade of the WT MspA channel. Detection occurred at an applied voltage of 10-25 mV.

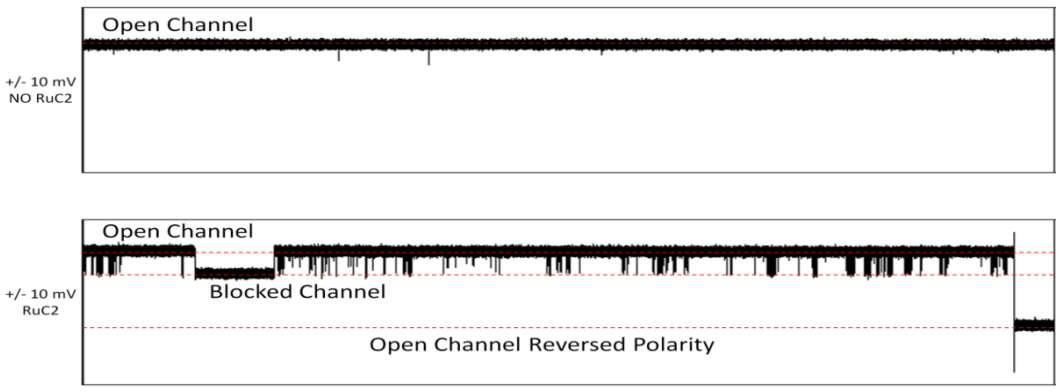


**Figure 3.15: Gating of WT MspA with $Ru(QP\text{-}C_2)_3^{8+}$(Unpublished Perera, A. S. *et al.*)**

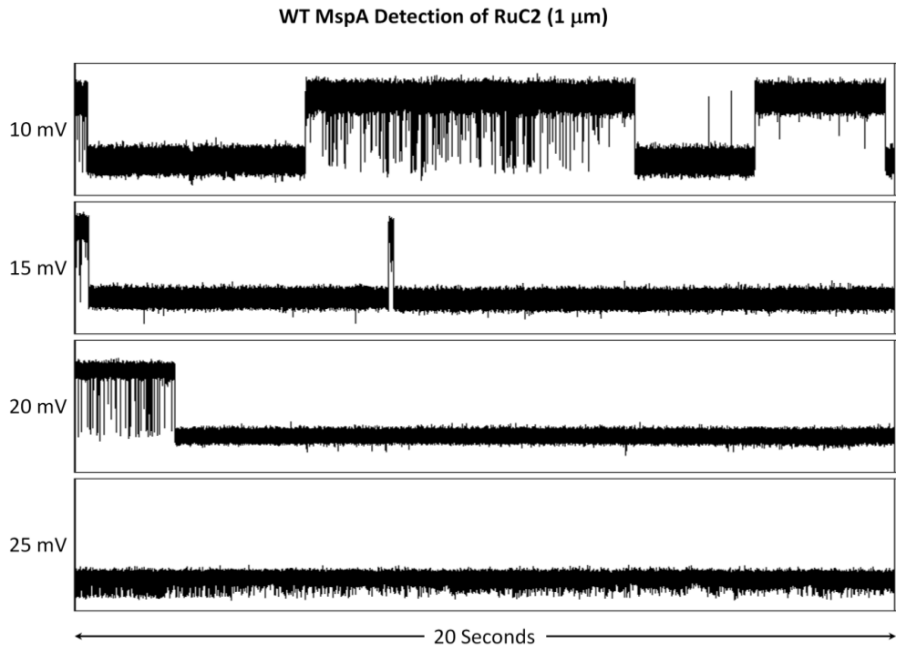


**Figure 3.16: Detection of $Ru(QP\text{-}C_2)_3^{8+}$(RuC2) as a function of applied voltage (Unpublished Perera, A. S. *et al.*)**

Similar observations were made for $Ru(bpy)_3^{2+}$ with WT MspA. These experiments were performed in 1M KCl/10mM HEPES (pH 8), and the complex was detected at a concentration of 1 μM at an applied voltage of 10-25 mV.

Several questions remained unanswered for the channel blocking experiments as well. Although both Ruthenium compounds showed evidence of gating, the results were inconsistent. Two types of events were observed, short events (< 1 ms) and long events (> 1 ms). When the voltage was increased, the longer events became long until the channel did not open (~30 mV). In instances where the channel was open, the short events remained, regardless of changes to the voltage. These results are somewhat ambiguous. Certain extracts showed no gating at all. In certain other cases, concentration of the Ruthenium complex had to be greatly increased in order to observe gating. Understandably, these blocking events did not last long and the bilayer

ruptured after few minutes. For example, we observed that adding ≥50 mM of the Ru complex ruptured the bilayer, and it was not possible to reform the bilayer with the high concentration of Ru(II) complex present.

Consequently, it is obvious that in order to obtain steady channel blocking events, further improvements were needed in the protein quality as well as in the blocking agent. These experiments were repeated in 2011 using MspA extracted by the improved procedure. The initial experiments were conducted with $Ru(QP\text{-}C_2)_3^{8+}$(or RuC2) and revealed a series of small periodic blockade events which were reminiscent of blocking of MspA pore by the Ruthenium complex.

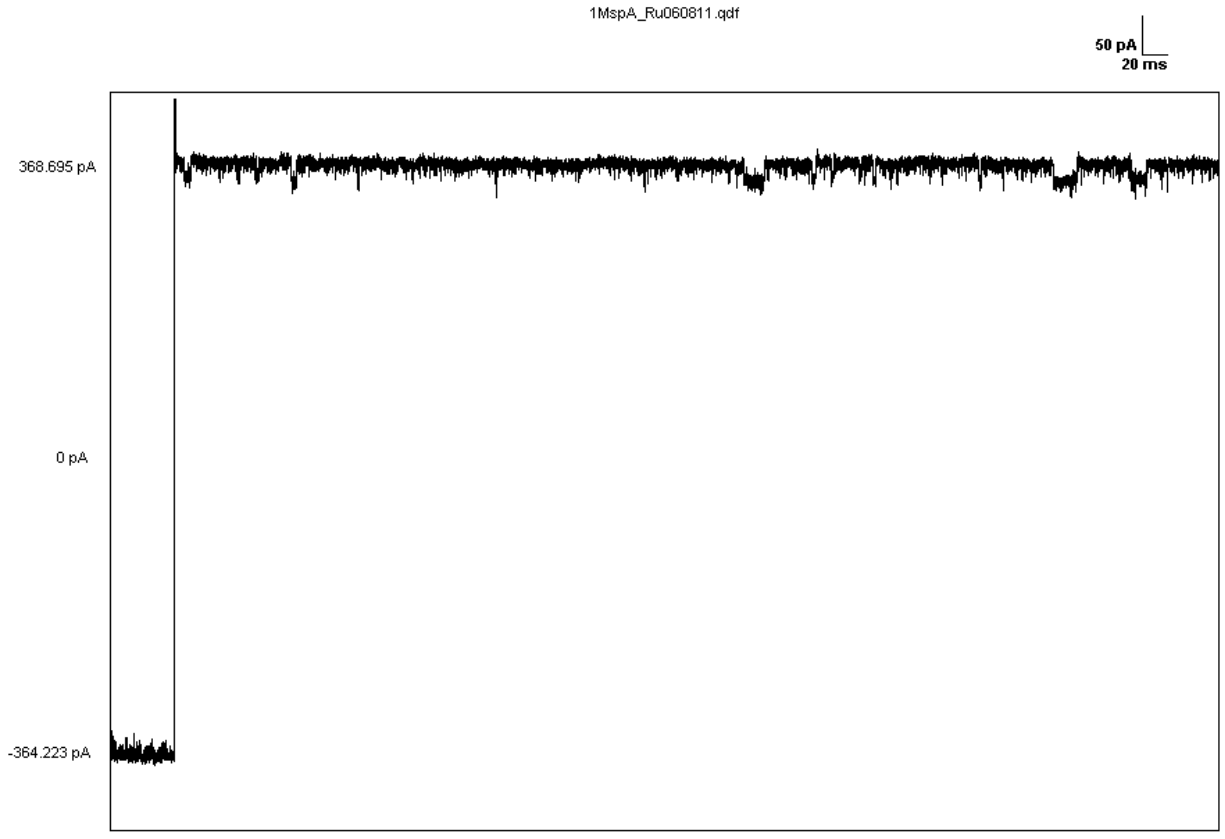


**Figure 3.17: Small current blocking events observed with RuC2 during MspA channel activity experiment (Unpublished, 2011, Perera, A. S. *et al.*)**

To convince ourselves whether these are actual blocking events or experimental artifacts, the experiment was repeated with the newly extracted protein without adding the Ruthenium complex. It was observed that similar pore-blocking events occur consistently, even without the presence of the blocking agent.

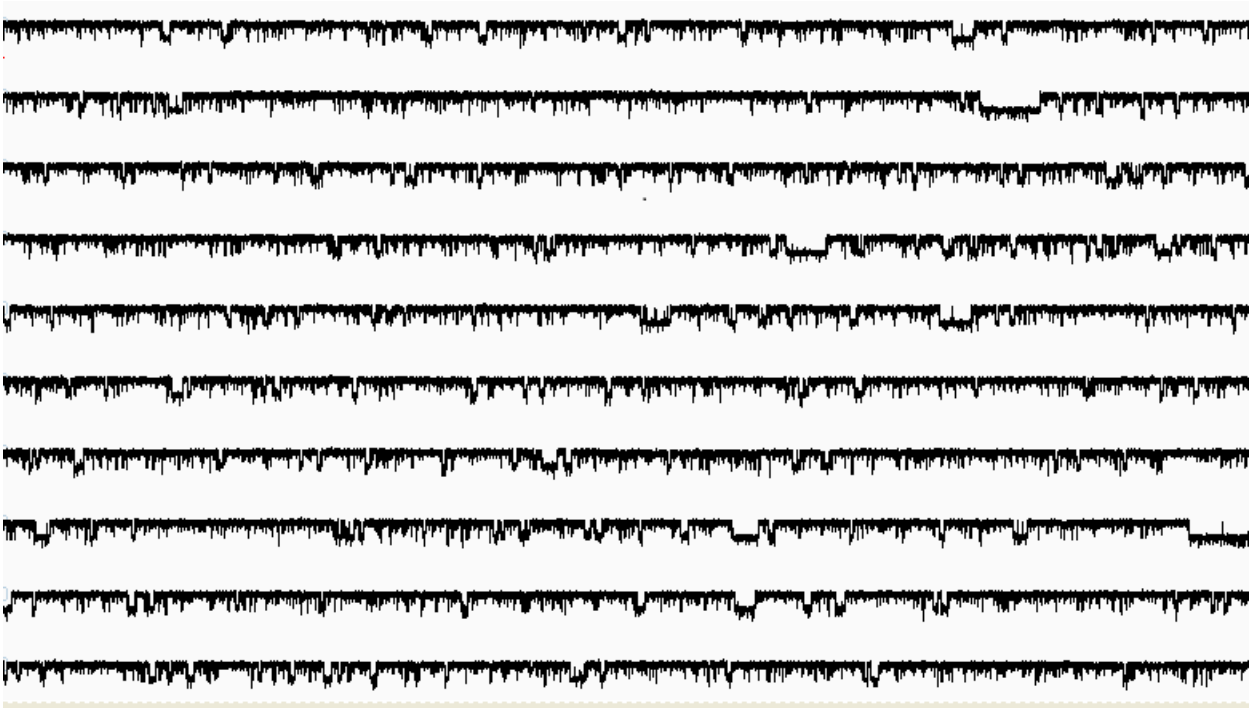

**Figure 3.18: Gating behavior of wild type MspA pore. (Unpublished, 2011, Perera, A. S. *et al.*)**

Hence it was concluded that these events occur due to gating of the protein and not by blocking of the protein pore by the Ruthenium complex. Further evidence for this hypothesis was found by comparing the number of such gating events that occurred with and without the Ruthenium complexes. During one experiment the event rate without RuC2 was recorded to be 1.69 events/s and the event rate with Ru-C2 was observed to be 17.89 events/s. However, in a similar but different experiment, the event rate without RuC2 was 3460 events/s and 4185 events/s with RuC2. The inconsistency of the above values indicate that these “blocking events”

of the MspA pore were in fact caused due to protein gating. After repeated experiments extended over several months yielded very low number of insertions and no visible interaction of blocking agent with MspA, the experiments were not pursued further.

## 3.4 Conclusions

MspA has excellent potential to be developed as a channel active agent due to its high stability and favorable geometry. Channel forming of MspA in lipid bilayers is successfully demonstrated using WT and mutant A96C MspA extracted according to the procedure developed in the Bossmann labs. MspA also has potential to be developed as a biosensor via channel blocking with various analytes. The highly negatively charged pore of MspA provides an ideal binding template for positively charged analytes with the correct dimensions. A series of Ruthenium(II) polypyridyl complexes has been synthesized in the Bossmann labs previously for this particular purpose. Blocking of the MspA pore using these Ruthenium(II) complexes has also been demonstrated. However, these results could not be repeated successfully in order to obtain definite evidence for channel blocking of MspA.

## 3.5 References

[1] Hladky S. B.; Hayden D. A. "Discreteness of Conductance Change in Bimolecular Lipid Membranes in the Presence of Certain Antibiotics", *Nature* **1970**, *225*, 451-453.

[2] Gu L.; Braha O.; Conlan S.; Cheley S.; Bayley H. "Stochastic sensing of organic analytes by a pore-forming protein containing a molecular adapter", *Nature*, **1999**, *398*, 686-690.

[3] Ervin E. N.; White R. J.; White H.; Excerpt from the Proceedings of the COMSOL Users Conference **2006**, Las Vegas.

[4] Schibel A. E.P.; Edwards T.; Kawano R.; Lan W.; White, H.S. "Quartz nanopore membranes for suspended bilayer ion channel recordings", *Analytical Chemistry* **2010**, *82*, 7259-7266.

[5] Deamer D. W.; Branton D. "Characterization of nucleic acids by nanopore analysis", *Acc. Chem. Res.* **2002**, *35*, 817-825.

[6] Bayley, H.; Cremer, P. S. "Stochastic sensors inspired by biology", *Nature*, **2001**, *413*, 226-230.

[7] Kawano R.; Schibel A. E. P.; Cauley C.; White H. S. "Controlling the translocation of single-stranded DNA through α-hemolysin ion channels using viscosity", *Langmuir* **2009,** *25,* 1233-1237.

[8] Ervin E.; Kawano R.; White R.; White H. "Simultaneous alternating and direct current readout of protein ion channel blocking events using glass nanopore membranes", *Anal Chem.***2008**, *80*, 2069-2076.

[9] Mahfoud M.; Sukumaran S.; Hulsmann P.; Grieger K.; Niederweis M. "Topology of the porin MspA in the outer membrane of Mycobacterium smegmatis", *J. Biol. Chem.***2006**, *281*, 5908-5915.

[10] Pokhrel1,M. R.; Gamage, P.; Kalita, M.; Shi, A.; Bossmann, S. H. "Developing new strategies for the treatment of tuberculosis employing Ruthnium(II)quaterpyridylcompexes",*J. Nepal Chem. Soc. 23,***2008/2009**.

[11] Gamage, P. H. S. "Synthesis and applications of ruthenium(II)quaterpyridinium complexes and poly-N-isopropylacrylamide/ acrylic acid copolymers", Department of Chemistry, Kansas State University, **2009.**

[12] Pyle, A. M.; Rehmann, J. P.; Meshoyrer, R.; Kumar, C. V.; Turro, N. J.; Barton, J. K. "Mixed-ligand complexes of ruthenium(II): factors governing binding to DNA"*J. Am. Chem. Soc.*, **1989**, *111*, 3051-3058.

[13] Turro,C.;Bossmann, S. H.; Leroi, G. E.; Barton, J. K. and Turro, N. J. "Ligand specific charge localization in the MLCT excited state of $Ru(bpy)_2(dpphen)^{2+}$ monitored by time-resolved resonance raman spectroscopy" *Inorg. Chem.*, **1994**, *33*, 1344-1347.

[14] Pokhrel M. R.; Dürr H.; Bossmann, S. H. "Synthesis of crown-ester-bipyridines and crown-ester-viologens", *Synthesis,* **2005**, *6*, 907-914.

[15] Dürr H.;Bossmann S. H. "Ruthenium polypyridine complexes. On the route to biomimetic assemblies as models for the photosynthetic reaction center", *Acc. Chem. Res.* **2001,** *34*, 905-917.

[16] Basel, M. T.; Dani, R. K.; Kang, M.; Pavlenok, M.; Chikan, V.; Smith, P. E.; Niederweis, M.; Bossmann, S. H. "Direct Observation of Gold Nanoparticle Assemblies with the Porin MspA on Mica"*ACS Nano***2009**, *3*, 462-6.

[17] Juris A.; Balzani V.; Barigelletti F.; Campagna S.; Belser P.; Von Zelewsky A. "Ru(II) polypyridine complexes: photophysics, photochemistry, eletrochemistry, and chemiluminescence" *Coordination Chemistry Reviews*, **1988**, *84*, 85-277.

# Chapter 4 - 3D Aggregation Behavior of RuC2-MspA Assemblies in Aqueous Media: An Explanation to Lack of Channel Blocking of MspA Pore by RuC2

## 4.1 Introduction

Porins from *M. smegmatis* have been of immense significance in the investigation of alternate treatment options for diseases caused by pathogenic species of mycobacteria such as *M. tuberculosis*. The necessity of such investigations is greater now more than ever. According to the World Health Organization (WHO), tuberculosis (TB) is the second most dangerous infectious disease in the world.[1] Approximately one third of the world's population is infected with *M. tuberculosis* and 10% of the infected human subjects will develop active TB during their lifetime. In 2010, TB incidence and prevalence were estimated at 8.8 and 12 million cases respectively. An astonishing number of 1.1 million HIV-negative and 0.35 million HIV-positive humans have succumbed to the disease in the same year. During the last three decades, multi-resistant strains have appeared due to the discontinuing treatment of tuberculosis in many countries, threatening all countries, which experience immigration.[1]

However, new hope for tuberculosis patients arises from recent massive drug discovery efforts to develop new TB-drugs using either target-based or phenotypic screens.[2] Gatifloxacin, moxifloxacin, metronidazole or linezolid, which are already in use against other bacterial infections, are currently evaluated in clinical phases 2 or 3. Furthermore, there are at least ten compounds in clinical trials and novel strategies for the development of new molecules being discussed.[3] One of these formerly new concepts that will be revisited in this chapter is the blocking of mycobacterial channels.

As discussed in Chapter 1, MspA enhances the permeability of the outer cell envelope in *M. smegmatis* for hydrophilic solutes.[4] Expression of MspA has shown to increase antibiotic susceptibility of *M. bovis* and *M. tuberculosis*.[4] The double ring of eight aspartates (D90 and D91) in the constriction zone of MspA (see figure 4.1) appears to be the most attractive binding site for various cationic substrates, such as cationic resorcin-arenes[5], Ruthenium(II)polypyridyl complexes[6,7] and gold nanoparticles.[8,9]

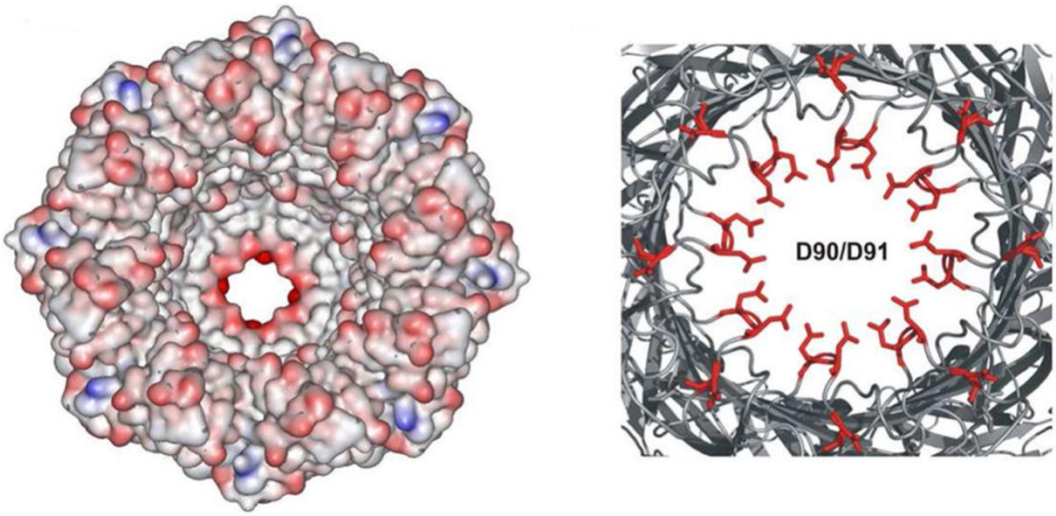


**Figure 4.1: Left – top view of MspA depicting electrostatic potential charges. Red and blue indicates negative and positive charges respectively. Right – close view of constriction zone made up of aspartates 90 and 91. (Taken with permission from reference 9)**

Initially MspA was investigated as a model channel blocking porin to study porins from *M. tuberculosis*. They were thought to have structural similarities at the time, as structural data for porins from *M. tuberculosis* remained elusive. However, in 2008 Niederweis and coworkers identified and characterized the outer membrane proteins of *M. tuberculosis*.[10] Among them, Rv0899 (OmpATb) has been proposed to act as an outer membrane porin and to contribute to the bacterium's adaptation to the acidic environment of the phagosome during infection.[11] However, unlike MspA, Rv0899 does not form a transmembrane β-barrel. Also the core of Rv0899 is

hydrophobic, while the exterior is polar and predominantly acidic, which is opposed to that of MspA.[12] Due to these structural differences, MspA was ruled out as an ideal model protein for development of potential therapeutic channel blockers against TB.

As discussed in Chapter 3, although initial evidence of channel blocking of WT MspA by $Ru(QP\text{-}C_2)_3^{8+}$ (i.e. $RuC_2$) and $Ru(bpy)_3^{2+}$ were observed, the results could not be repeated successfully. The second series of experiments done in this regard failed to provide evidence of any gating events. However, the design of these dyes has been done specifically for blocking of MspA pore.[13] Also channel blocking has been demonstrated successfully with MspA extracted according to previously published procedures.[14] Hence, it was reasonable to assume that the new extraction procedure developed by us renders protein of a different quality. Also extensive analytical assessments performed by us on the MspA extracted by the new procedure (discussed in Chapter 1 in detail), clearly indicates that the protein is of high quality and purity. It is possible that high purity leads to differences in aggregation behavior of protein molecules in a certain medium. This is particularly significant as MspA is highly charged in its surface, leading to numerous possibilities in aggregation behavior. Addition of an external charged molecule such as $RuC_2$ can lead to drastic alterations in the inherent aggregation behavior of MspA.

To test this hypothesis further, we conducted a set of experiments to investigate the 3D aggregation behavior of $RuC_2$-MspA assemblies. Particle sizing and zeta potential experiments have been carried out to obtain a better understanding of the nature of these aggregates. The results obtained shed much needed light into some of the challenges pointed out in the previous chapter. This data also provides insight into the quality, physical properties and solution

dynamics of MspA extracted by our new extraction methodology. We have also compared these results with previous data gathered from time-resolved (ns) absorption and emission spectroscopy. Combination of such results from conceptionally different techniques would ultimately lead to development of a comprehensive paradigm of MspA-channel blocker interactions. The lessons from our studies are applicable to broadening the understanding of virtually all supramolecular systems that are made from proteins and fluorescent nanostructures.

## 4.2 Experimental

Dynamic light scattering and zeta potential measurements were done using ZetaPALS Zeta Potential Analyzer purchased by Brookhaven Instruments Corporation. For all experiments 50 µl of WT MspA (~0.6 mg/ml) was used in 2.0 ml of 1x PBS. The number of moles of MspA in 50 µl is calculated to be $1.875 \times 10^{-10}$ mol. Three mixtures of $RuC_2$ and MspA were prepared with varying concentrations of $RuC_2$:MspA that are 10:1, 100:1 and 1000:1 (i.e. $1.875 \times 10^{-9}$, $1.875 \times 10^{-8}$, $1.875 \times 10^{-7}$ mol's of RuC2 per $1.875 \times 10^{-10}$ mol's of MspA in 2.0 ml of 1x PBS. The 10:1 mixture was prepared to duplicate the concentrations used for the channel blocking experiments conducted previously (refer Chapter 3). Average effective diameter and zeta potential measurements of MspA-$RuC_2$ aggregates were recorded with increasing temperature values of 25, 30, 35, 40, 45, 50, 55, 60, 65 and 70 °C. The $RuC_2$ solutions in each case were added right before the measurement of DLS/zeta potential and were not mixed previously. This was done intentionally to mimic the conditions of typical channel blocking experiments.

## 4.3 Results and discussion

The dimensions of $RuC_2$ are designed to achieve binding at the constriction zone of MspA. This position bears the highest negative charge in the porin due to the presence of aspartates D90 and D91 and would facilitate binding with the positively charged on $RuC_2$ (refer section 4.1 and Chapter 1). A schematic representation on the position of expected binding is given in the figure below.

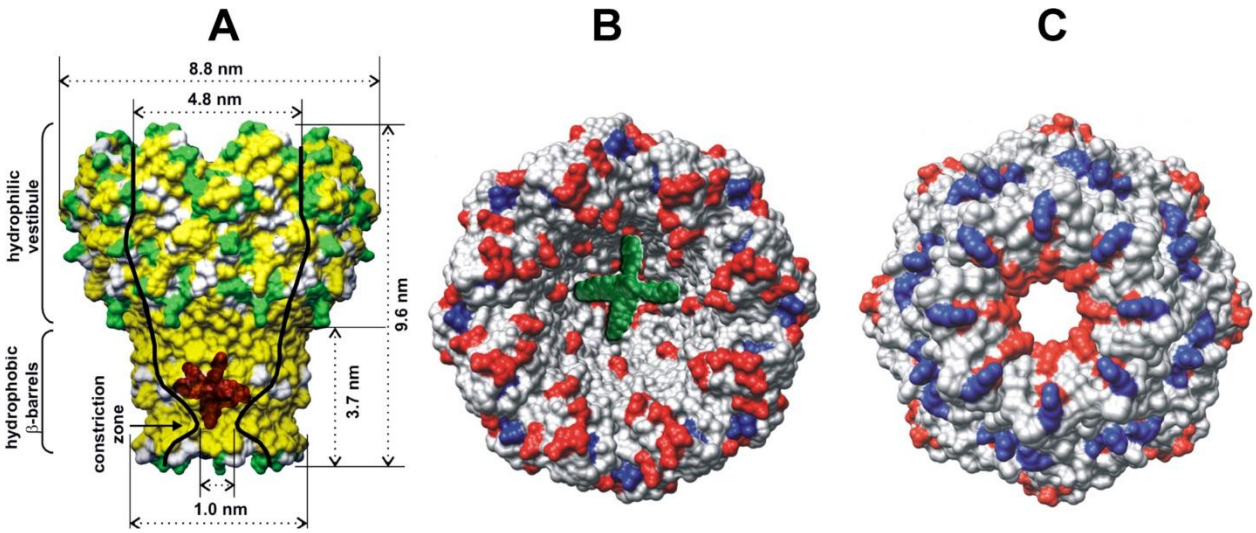


**Figure 4.2: Schematic representation of binding of $RuC_2$ inside MspA. A) Side view B) Top view C) MspA pore viewed from the bottom. (Adapted with permission from reference 16)**

As discussed in Chapter 3, binding of $RuC_2$ (along with other Ru(II) complexes) to MspA has already been established. Calculation of the binding constants in this regard have been done according to an assumed 1:1 stoichiometry of MspA and Ru(II)-complex. However, recent results from dynamic light scattering measurements are not in agreement with 1:1 stoichiometry, as will be discussed in the following sections.

### *4.3.1 Dynamic light scattering studies of MspA-$RuC_2$ aggregates as a function of temperature*

As discussed in Chapter 2, MspA shows a distinct tendency to aggregate with increasing temperature, with a maximum diameter of 180 nm observed at 40 ºC. Although hydrophobic interaction is the major mechanism behind the aggregation behavior of MspA, we have found evidence for contributions from hydrogen bonding and/or ionic interaction in the supramolecular behavior of MspA, as was evident from the discrepancy of theoretical and experimental packing parameter values for MspA (refer Chapter 2, section 2.4).

We conducted a series of DLS experiments with $RuC_2$-MspA aggregates, consisting of three molar ratios; 10:1, 100:1 and 1000:1. Interestingly, MspA forms much larger clusters in the presence of $RuC_2$, as indicated by DLS data. At 25 ºC, all three mixtures of MspA and $RuC_2$ have their maxima in size of approximately $310\pm22$ nm for $RuC_2$:MspA=10:1 and 100:1, and $335\pm10$ nm for $RuC_2$:MspA=1000:1. This is a dramatic size increase, compared with the unbound MspA (refer figure 4.3). At all three ratios of $RuC_2$ to MspA, a steady decrease of the supramolecular aggregates in size was observed with increasing temperature. At 70 ºC, they converge at diameters of $190\pm15$ nm. We also observed that the sizes of aggregates formed in $RuC_2$:MspA=10:1 and 100 are indistinguishable due to experimental errors at every investigated temperature, whereas $RuC_2$:MspA=1000:1 forms significantly bigger aggregates.

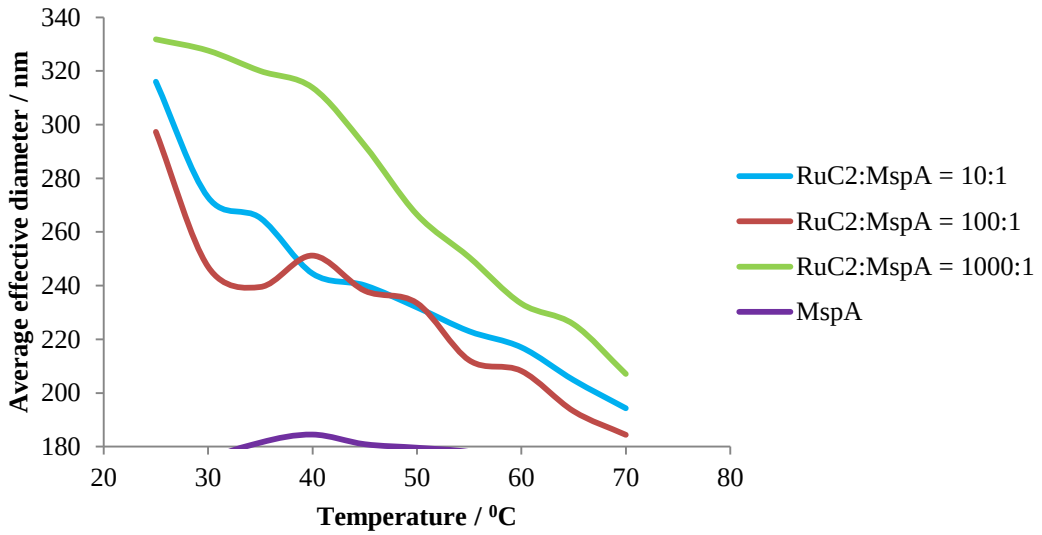


**Figure 4.3: Temperature dependent average effective diameters of $RuC_2$-MspA assemblies**

The data depicted in figure 4.3 provides strong evidence that MspA does not form 1:1 complexes with $RuC_2$. If the aggregates were formed at 1:1 stoichiometry, the hydrodynamic parameter of the $RuC_2$-MspA aggregates should not change, because $RuC_2$ is supposedly bound in the interior of MspA and not attached on the surface, as indicated in figure 4.1. Therefore, the extraordinarily high binding constants for the binding between Ruthenium complexes: RuC1-4 and MspA that have been determined previously by means of HPLC, assuming 1:1 stoichiometry are based on an incorrect hypothesis for interpreting the experimental data.[7] In reality, MspA forms large aggregates of varying stoichiometry with Ru(II)complexes and not 1:1 complexes. It is possible that a fraction of the Ru(II)complexes may be bound in MspA's interior channel, but this is obviously not the sole mode of binding. Consequently, Ru(II)complexes will be far less suitable channel blockers for the treatment of TB, which casts a serious shadow of doubt on their suitability as water-soluble anti-mycobacterial drugs.

### *4.3.2 Zeta potential measurements of MspA and RuC2/MspA aggregates as a function of temperature*

Experiments were also conducted to test the dependability of surface charge on aggregation behavior for the $RuC_2$-MspA aggregates.[15] In this regard, temperature dependent surface charge of $RuC_2$-MspA aggregates was investigated by means of a series of zeta potential measurements by electrophoretic light scattering. The results are shown in the graph below:

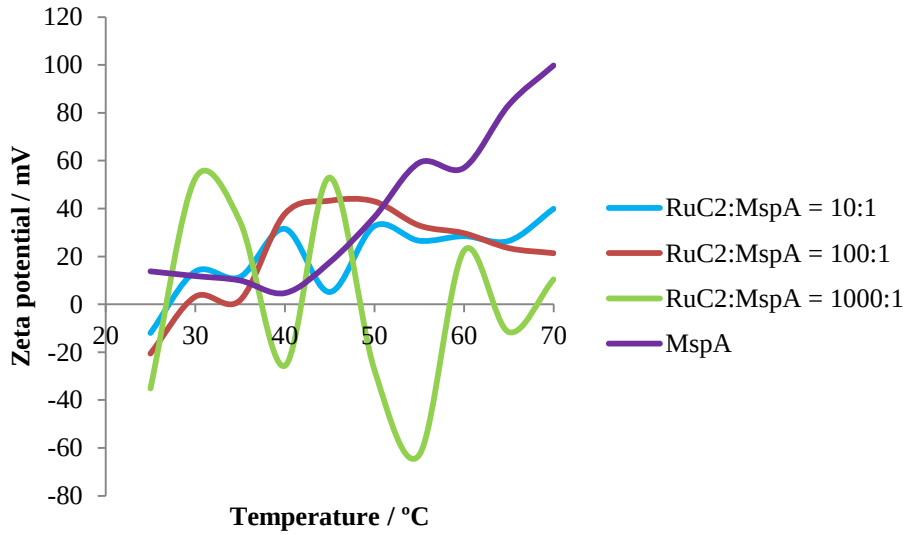


**Figure 4.4: Temperature dependent zeta potential measurements of RuC2-MspA assemblies**

Although the size-temperature relationships are strikingly similar for all three investigated mixtures of $RuC_2$ and MspA, their temperature dependent zeta potentials are extremely different. Again the more diluted ratios of $RuC_2$:MspA (i.e. 10:1 and 100:1) show a similar behavior. There is some similarity in the increase of their zeta potentials as a function of temperature with the curve observed for unbound MspA. It is noteworthy that the zeta potential of all three $RuC_2$-MspA mixtures is negative at low temperatures where the biggest aggregates are found. The temperature dependence of $RuC_2$-MspA=1000:1 is characterized by oscillations

of the zeta potential in the range between +50 and -70 mV. Considering that stable aggregates are formed above +40 mV and below -40 mV, this experimental finding, which is reproducible, is surprising. It is noteworthy that at this mixing ratio, the largest $RuC_2$-MspA aggregates are found at 25 ºC, as indicated by DLS (see Figure 4.3). Furthermore, the size of the $RuC_2$-MspA aggregates decreases continuously with increasing temperature. However, the zeta potentials recorded for the three mixtures do not show a monotonous increase or decrease. The increase of the zeta potential for unbound MspA can be explained with cation adsorption from the PBS buffer, which contains sodium and potassium cations (refer Chapter 2, section 2.4). It is comprehensible that at higher temperatures, the adsorption of cations from 1x PBS is increased, due to the reduced size of the $RuC_2$-MspA aggregates at higher temperature. The enhanced macromolecular motion of MspA with increasing temperature may lead to changing dynamics of forming and breaking of hydrogen bonds as the temperature increases. The observed decrease in size of the MspA vesicles and $RuC_2$-MspA-aggregates provides a higher surface for cation adsorption, resulting in the remarkable increase of the zeta potential observed for MspA in 1 X PBS.

$RuC_2$ competes with $Na^+$ and $K^+$ for adsorption at the outer surface of MspA, as steady-state and time resolved luminescence measurements and time-resolved absorption studies have indicated.[7] $RuC_2$ possesses a higher charge than $Na^+$ or $K^+$. It varies between +2 and +8, depending on the pH. At pH=7.4 (PBS) we can assume that it is fully deprotonated, resulting in an overall charge of +2. At that pH, $RuC_2$ features six negatively charged carboxylate groups. The area covered by $RuC_2$ when adsorbed is 8.6 $nm^2$. $RuC_2$ covers approximately 20 amino-acid residues when bound to MspA's external surface. Consequently, it can block sites at the surface

of MspA, which otherwise would be able to bind $Na^+$ or $K^+$. The oscillation of the zeta potential is most pronounced at the highest concentration of $RuC_2$. It is our hypothesis that the temperature dependence of zeta potential is indicative of two endergonic adsorption processes ($RuC_2$ vs. $Na^+/K^+$) at MspA (similar behavior for unbound MspA was discussed in Chapter 2). The water-accessible surface of MspA in the observed $RuC_2$-MspA aggregates will be predominantly covered with $RuC_2$ when the zeta potential is negative (below 25 ºC, between 37 to 42 ºC, 49 to 61 ºC, and 64 to 69 ºC). The positive charges from arginine and protonated lysine residues of MspA, together with $Na^+$ and/or $K^+$ adsorbed from PBS, causes positive zeta potentials between 25 and 37 ºC, 42 and 49 ºC, 61 to 64 ºC, and beyond 69 ºC. Apparently, changes in temperature are able to tip the balance of the competing adsorption of $RuC_2$ and/or $Na^+/K^+$ to MspA. In addition to both adsorption processes, deprotonation of the carboxylate side-chains of MspA and protonation of amine side chains are temperature dependent, resulting in the observed (reversible) oscillation of the zeta potentials as a function of temperature.

## 4.4 Conclusions

The ability of mycobacterial porin MspA to act as a model system for the development of channel blockers as novel anti-TB drugs have been investigated. The concept that Ruthenium(II)quaterpyridinium complexes have the capability to act as efficient channel blockers for MspA and related porins, which feature a funnel-like structure and a high density of negative charges at their interior, as well as a pronounced constriction zone (bottleneck), emerged after very high binding constants ($1.1 \times 10^9$ $M^{-1}$ (RuC4) to $7.5 \times 10^9$ $M^{-1}$ (RuC1)) have been measured by HPLC and steady-state luminescence measurements.[7] Here, we have revisited this approach using DLS and zeta potential studies of RuC2-MspA aggregates. Three molar

ratios of $RuC_2$:MspA, which are 10:1, 100:1 and 1000:1 were chosen for these experiments. The 10:1 mixture in particular, was chosen to mimic the concentrations of analyte-protein mixtures used in channel blocking experiments.

Temperature dependent dynamic light scattering studies have confirmed that $RuC_2$ and MspA form large clusters with interesting surface characteristics in PBS. Therefore, it has been confirmed that the binding of prospective channel blockers to porins that are not firmly immersed in membranes, cannot be investigated without the occurrence of large errors that arise from the formation of large supramolecular aggregates between porins and channel blockers. Temperature dependent zeta potential measurements show similar behavior of surface charge fluctuations for the two most diluted mixtures. However, for the more concentrated 1000:1 mixture, large oscillations of zeta potential values are seen throughout the study. It is our hypothesis that this is evidence of a two component endergonic adsorption process, which occurs from the adsorption of $RuC_2$ and $Na^+/K^+$ on MspA surface. The values of zeta potentials obtained are markedly different from those of unbound MspA, confirming that $RuC_2$ adsorption is significant. These oscillations are also influenced by the deprotonation and protonation of the carboxylate and amine side-chains of MspA, which are known to be temperature dependent. The overall results from DLS and zeta potential studies give undeniable evidence that $RuC_2$ and MspA do not interact in a 1:1 stoichiometry, but form large aggregates even at dilute concentrations and at various temperatures. These observations provide clear explanations to the lack of channel blocking of MspA by $RuC_2$ and $Ru(bpy)_3^{2+}$, which we have previously observed. Hence we conclude that Ruthenium(II)quarterpyridine complexes are not suitable channel blocking agents for MspA.

## 4.5 References


[1] World Health Organization, Global Tuberculosis Control **2011**, ISBN 978 92 4 156438 0.

[2] Villemagne, B.; Crauste, C.; Flipo, M.; Baulard, A. R.; Deprez, B.; Willand, N. "Tuberculosis: The drug development pipeline at a glance", *Eur J Med Chem* **2012**, *51*, 1-16.

[3] Lamichhane, G. "Novel targets in M. tuberculosis: search for new drugs", *Trends Mol Med* **2011**, *17*, 25-33.

[4] Mailaender, C.; Reiling, N.; Engelhardt, H.; Bossmann, S.; Ehlers, S.; Niederweis, M. "The MspA porin promotes growth and increases antibiotic susceptibility of both Mycobacterium bovis BCG and Mycobacterium tuberculosis", *Microbiology (Reading, U. K.)* **2004**, *150*, 853-64.

[5] Leaym, X.; Kraft, S.; Bossmann, S. H. "Synthesis of water-soluble highly charged and methylene-bridged resorcin[4]arenes", *Synthesis* **2008**, 932-42.

[6] Shi, A.; Pokhrel, M. R.; Bossmann, S. H. "Synthesis of highly charged ruthenium(II)-quaterpyridinium complexes: a bottom-up approach to monodisperse nanostructures", *Synthesis* **2007**, 505-14.

[7] Pokhrel, M. R.; Gamage, P.; Kalita, M.; Shi, A.; Bossmann, S. H. "Developing new strategies for the treatment of tuberculosis employing ruthenium(II)quaterpyridyl complexes", *J. Nepal Chem. Soc.* **2009**, *23*, 2-10.

[8] Dani, R. K.; Kang, M.; Kalita, M.; Smith, P. E.; Bossmann, S. H.; Chikan, V. "MspA Porin-Gold Nanoparticle Assemblies: Enhanced Binding through a Controlled Cysteine Mutation", *Nano Lett.***2008**, *8*, 1229-36.

[9] Basel, M. T.; Dani, R. K.; Kang, M.; Pavlenok, M.; Chikan, V.; Smith, P. E.; Niederweis, M.; Bossmann, S. H. "Direct Observation of Gold Nanoparticle Assemblies with the Porin MspA on Mica", *ACS Nano* **2009**, *3*, 462-6.

[10] Song, H.; Sandie, R.; Wang, Y.; Andrade-Navarro, M. A.; Niederweis, M. "Identification of outer membrane proteins of Mycobacterium tuberculosis", *Tuberculosis* **2008**, *88*, 526-44.

[11] Song, H. H.; Huff, J.; Janik, K.; Walter, K.; Keller, C.; Ehlers, S.; Bossmann, S. H.; Niederweis, M. "Expression of the ompATb operon accelerates ammonia secretion and adaptation of Mycobacterium tuberculosis to acidic environments", *Mol Microbiol* **2011**, *80*, 900-18.

[12] Teriete, P.; Yao, Y.; Kolodzik, A.; Yu, J.; Song, H.; Niederweis, M.; Marassi, F. M. "Mycobacterium tuberculosis Rv0899 adopts a mixed alpha/beta-structure and does not form a transmembrane beta-barrel", *Biochemistry* **2010**, *49*, 2768-77.

[13] Pokhrel, M. R.; Gamage, P.; Kalita, M.; Shi, A.; Bossmann, S. H. "Developing new strategies for the treatment of tuberculosis employing ruthenium(II)quaterpyridyl complexes", *J. Nepal Chem. Soc.***2009**, *23*, 2.

[14] Niederwise M.; Danilchanka O.; Huff J.; Christian Hoffmann C.; Engelhardt, H. "Mycobacterial outer membranes: in search of proteins", *Mol. Microbiol.***1999**, *33*, 933.

[15] Doane, T. L.; Chuang, C.-H.; Hill, R. J.; Burda, C. "Nanoparticle zeta-Potentials", *Acc. Chem. Res.* **2012**, *45*, 317.

# Chapter 5 - Fabrication of MspA Incorporated Dye Sensitized Solar Cell Prototypes

## 5.1 Introduction

### *5.1.1 Dye sensitized solar cells*

Alternate, sustainable energy sources are gaining increased attention from chemists, physicists and engineers, as mankind realizes the limited availability and adverse environmental impacts of burning fossil fuels. Most of the world's fossil fuel sources are expected to be exhausted within the next 300 years; hence investigation of alternate sustainable energy sources is of paramount importance in sustaining human life. Solar energy is a highly renewable source of energy, which has no match in abundance and availability in most places on earth. Solar cells have been in existence since as long ago as 1887[1,2] and they have great potential to be used as the world's leading sustainable energy source for the future. Photovoltaic cells have been developed and improved throughout history and have evolved into many different types.[3,4,5]

The introduction of dye sensitized solar cells (DSSC's) by Michael Grätzel and Brian O'Regan in 1991, have revolutionized the scope and efficiency of solar cell applications.[6] This remarkable invention won the "Millennium Technology Prize" in 2010.[7] A dye sensitized solar cell essentially consists of a thin layer of (~ 10 μm) of $TiO_2$ nanoparticles coated with a sensitizer which is adsorbed onto a base of conducting glass. The sensitizer is a light absorbing dye which is usually a Ruthenium(II) based organic compound. The fundamental difference between these cells and the conventional p-n junction photovoltaic cells that existed at the time was that dye sensitized cells had separate components to carry out light harvesting and charge transport. In

the latter, both of these functions were carried out by the semiconducting material. The counter electrode is also conducting glass and the two electrodes are connected by an Iodolyte electrolyte ($I^-/I_3$) immersed in between.

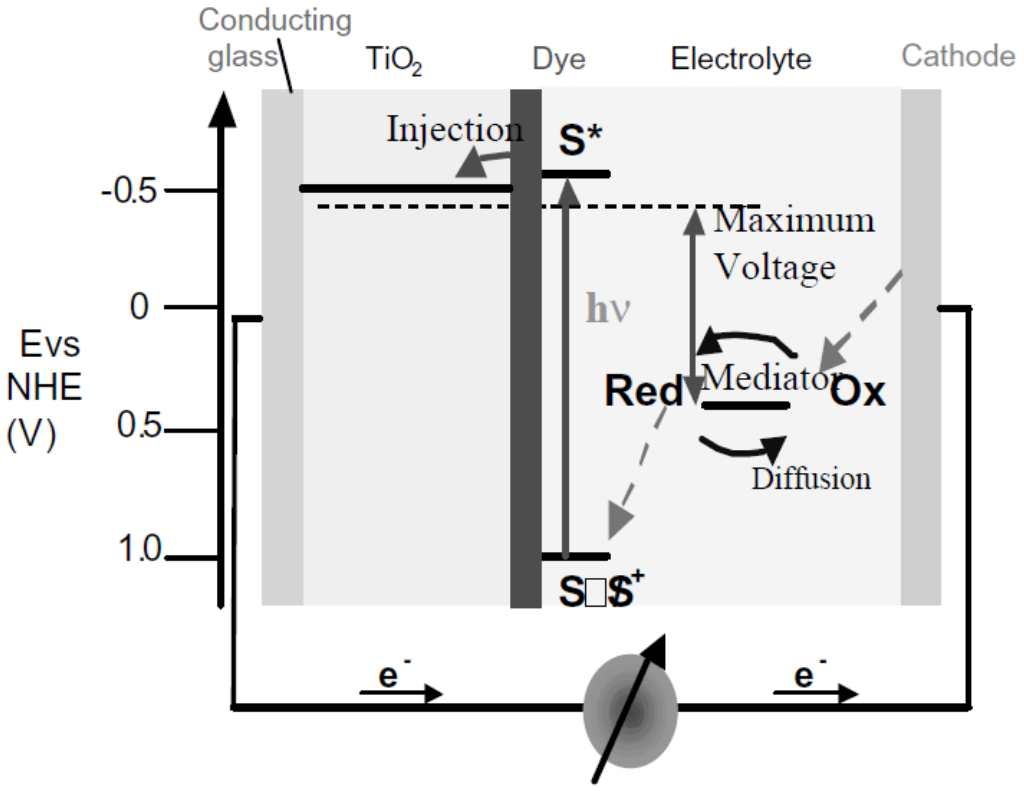


**Figure 5.1: Basic components and principle operations of a dye sensitized solar cell (Taken with permission from reference 13)**

When the system is exposed to light, the dye absorbs a photon and releases an electron, which gets injected into the conduction band of $TiO_2$. The dye is regenerated by electrons that are transferred from the electrolyte containing a redox couple, which gets reduced at the counter electrode. The circuit is thus complete and a current is generated across the system.

The presence of a thin layer of nanocrystalline $TiO_2$ significantly increases the surface area available for dye adsorption. This amounts to approximately 20-30% increase in surface

area as opposed to a flat surface. The technology at the time had potential to be cost effective as low/medium pure semiconductor material could be employed for cell fabrication. The conversion of incident photons into current had an efficiency of >80% which was a highly attractive feature. The overall yield for converting light to current was 7.1-7.9% and the device was proven to be stable up to five million cycles. Together with the above desirable features these cells had enormous potential to be a highly practical energy source for the future.

Over the years dye sensitized solar cell technology has been developed and improved significantly. The high efficiency of electron transport by the $TiO_2$ layer was one of the key features that contributed to the initial success of dye sensitized solar cells.[8] However, one feature, which was a disadvantage in this area was that there was a high degree of disorder in this layer, so one could not effectively control the amount, orientation and binding efficiency of dye sensitizer deposited onto it. A possible improvement on this regard would be to incorporate nanorods or channel-forming materials that are oriented vertically from the conducting glass base. This would provide order and render more control over formation of dye-semiconductor interface. Accordingly, techniques were developed to fabricate $TiO_2$ nanotubes[9] and nano-polymer hybrid incorporated cells,[10] which proved to be far more efficient than cells with randomly deposited $TiO_2$.

Methods were also developed to improve the overall photon-current conversion efficiency of DSSC's. This was primarily achieved by the development of computational techniques that simulate the geometry of adsorbed sensitizer on $TiO_2$[11] and surface interactions between semiconductor-sensitizer as well as rearrangement of surface properties as a result of

this interaction.[12] These lead to far better understanding of interface chemistry and physical properties which consequently lead to better control of assembly of Ruthenium dyes onto $TiO_2$.[8] An improved overall conversion efficiency of 10.6% was achieved using N3 dye and marks the highest efficiency achieved by DSSC's so far.[13]

Another area of growing developmental interest is the incorporation of solid state materials to replace electrolytes in DSSC's. Liquid electrolytes tend to decompose and fail under long-term exposure to light. This result in loss of sealing in the cell and the continuous contact between the electrodes is lost.[8] This drawback can be overcome by using a p-type solid semiconducting material as a continuous contact between $TiO_2$-sensitizer side and the counter electrode, instead of the conventional liquid electrolytes. Although it is not obvious how two solids can achieve the close contact that is achieved by a liquid that can penetrate through a porous material, positive results have been obtained by using solid contacts. "Spirobifluorene" is the most prominent solid employed for this purpose and has given a current conversion efficiency of 3.2%.[14]

### *5.1.2 Ruthenium(II) polypyridyl complexes*

Since their introduction in 1991, much research has been done to enhance and upgrade the efficiency of DSSC's including introduction of new dyes. An ideal sensitizer dye would have several characteristic features to optimize light absorption and electron transfer inside a solar cell.[8] These include the ability to absorb electromagnetic radiation efficiently in the entire visible region, ability to inject electrons into the conduction band of the semiconductor in unit quantum yield, have a high redox potential to allow efficient regeneration via electron transfer from the electrolyte, contain charged ligands such as carboxylate groups that allow adsorption onto the

$TiO_2$ surface and have high stability to withstand many turn over cycles over a long period of time. In this regard, $Ru(dcbpy)_2(NCS)_2$ (i.e. cis-di(thiocyanato)-bis(2,2'-bipyridyl-4,4'-dicarboxylate) ruthenium(II)), which is also known as N3 dye has been recognized as a highly efficient dye for DSSC's.[15] This dye is superior to others not only because of its fast electron transfer due to its ability to absorb visible light over a broad wavelength range, but also because of its efficient binding with $TiO_2$ nanoparticles. In 2002, Sundstorm *et al.* conducted further investigations on mechanism of electron transfer between the ruthenium dye and $TiO_2$ interface.[16] It was found that the N3 dye has a characteristic metal-to-ligand charge transfer (MLCT) that involves electron transfer from the Ruthenium center to the p* orbital of the carboxylated bipyridyl ligand. The carboxyl groups attach the dye to the $TiO_2$ surface and the electron is then injected into the $TiO_2$ conduction band. The quantum yield of this process is unity.

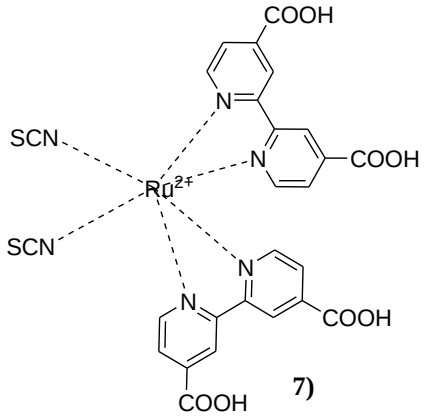


**7)**

**Figure 5.2: Cis-di(thiocyanato)-bis(2,2'-bipyridyl-4,4'-dicarboxylate) (Taken from references 15, 16)**

In 2001, another efficient dye called the "black dye" was introduced.[17] This was the only other sensitizer capable of matching the conversion efficiency of the N3 dye (i.e. 10.4%) when

used in a DSSC. The main advantage of the black dye over N3 dye is that it absorbs 100 nm further in the red region, which is close to the optimal absorption limit for a sensitizer.

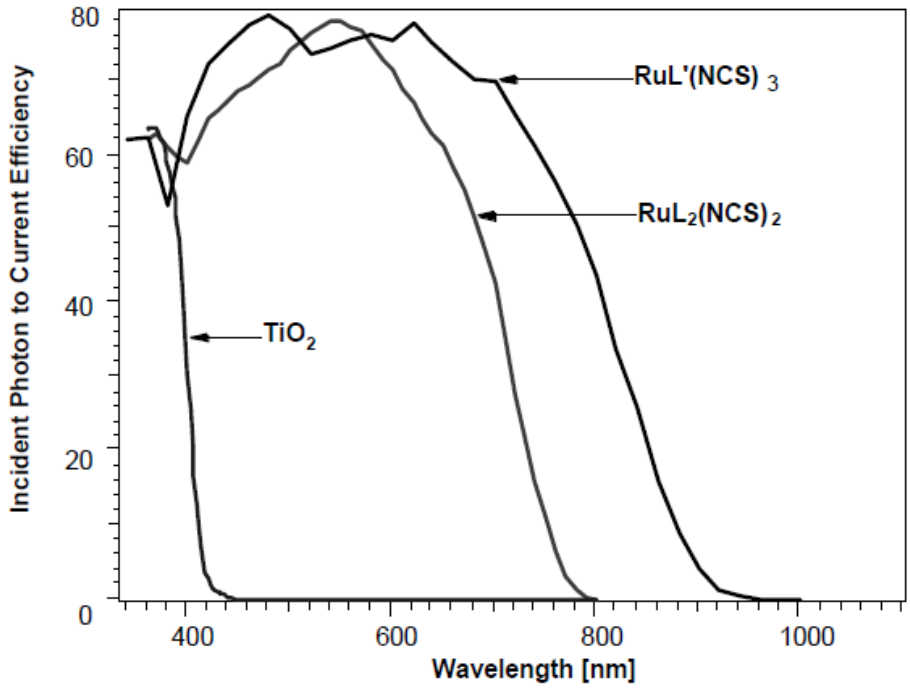


**Figure 5.3: Current conversion efficiency of N3 dye (ligand L = 4, 4'-COOH-2,2'-bipyridine) and black dye (ligand L' = 4,4',4" -COOH-2,2':6',2"-terpyridine) (Taken with permission from reference 15)**

Continuous research has been done throughout the years to optimize the absorption ability of dye sensitizers in the near IR region. Metal complexes containing 2,2'-bipyridine subunits have been vastly investigated in this regard. They are known to act as efficient electron transfer systems as well as be useful in electrochemical and photochemical applications.[18,19,20] Ruthenium(II) complexes consisting of 2,2'-bipyridine units have proven to be significant as potential applicators in artificial photosynthetic systems.[21] Among these compounds Ruthenium(II)polypyridyl-based diads and triads have shown promising results as an artificial model for the photosynthetic reaction center, due to their high efficiency in electron transfer and

increased charge separation lifetimes. Synthesis of the following compound has been established by Seiler and Dürr in 1994.[17]

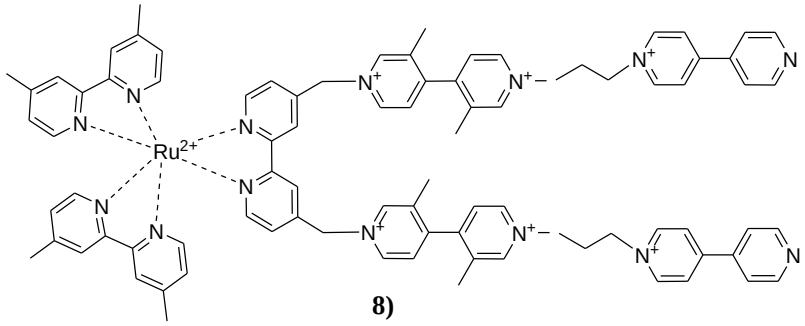

**8)**

**Figure 5.4: $[Ru(dmbpy)_2(di\text{-}(dmV^{2+}\text{-}V^{2+}\text{-}bpy))]^{10+}$ as an efficient artificial model for the photosynthetic reaction center (Taken with permission from reference 17)**

The success of the above compound as a biomimetic supramolecular unit is largely due to the presence of two combined 3,3'-dimethyl-4,4'-dialkyl viologen-4,4'-dialkyl viologens. This system mimics the dual electron transfer (ET) systems found in the natural photosynthetic reaction center, which interestingly utilizes only one of the ET pathways, out of the two.[22] It consists of a donor (D) linked to two identical acceptors (A) to form a bifurcated electron transfer pathway. In case of the photosynthetic system, these are two quinone units and in the ruthenium complex, this is represented by two bisviologen arms.

In order to achieve longer life times for charge separated species, the terminal 4,4'-bisviologen was attached to three different large crown ethers.[16] It has been observed that the Ruthenium complex exclusively binds 1:1 with the crown ethers, hence, only one branch is employed for ET reactions. The crown ether complexed species has shown a remarkable 5500 times increment for the lifetime of charge separated states, compared to the non-complexed

species. It was assumed that the crown ether greatly decreases the "reorganization energy λ" at the bisviologen acceptor, leading to increased charge separation lifetime.[19]

Ruthenium(II)-phenanthroline based dyes have been known to be promising candidates for light harvesting.[23] In order to further investigate their scope and applicability as light harvesting systems a novel series of Ruthenium(II)-phenanthroline dyes have been synthesized. These would be discussed in detail in the following sections. Our major objective was to produce highly charged dyes, which are less toxic to living organisms than the existing ones that are commercially available at present.

### *5.1.3 Concept of a 'greener' solar cell*

As discussed previously, a tremendous amount of research has been conducted to optimize the efficiency of DSSC's. However, after more than two decades since their discovery, the maximum conversion efficiency has not been increased beyond 11%. This is a major drawback that limits the application of DSSC's compared to other types of photovoltaic devices such as silicone-based cells that have proven to be efficient up to 80%.

Therefore, our research approach was to develop a more environmentally friendly or 'greener' DSSC rather than to focus on increasing its efficiency. The existing DSSC technology utilizes sensitizers that are rather toxic and an electrolyte component that is equally undesirable for living organisms. Hence our major objectives were to produce less toxic dyes and to replace the electrolyte with an alternate medium that is eco-friendly. This has been achieved by synthesis of highly charged Ruthenium dyes and by incorporating MspA as a matrix for electron

transportation between the dye and the counter electrode. A schematic representation of the concept is given below:

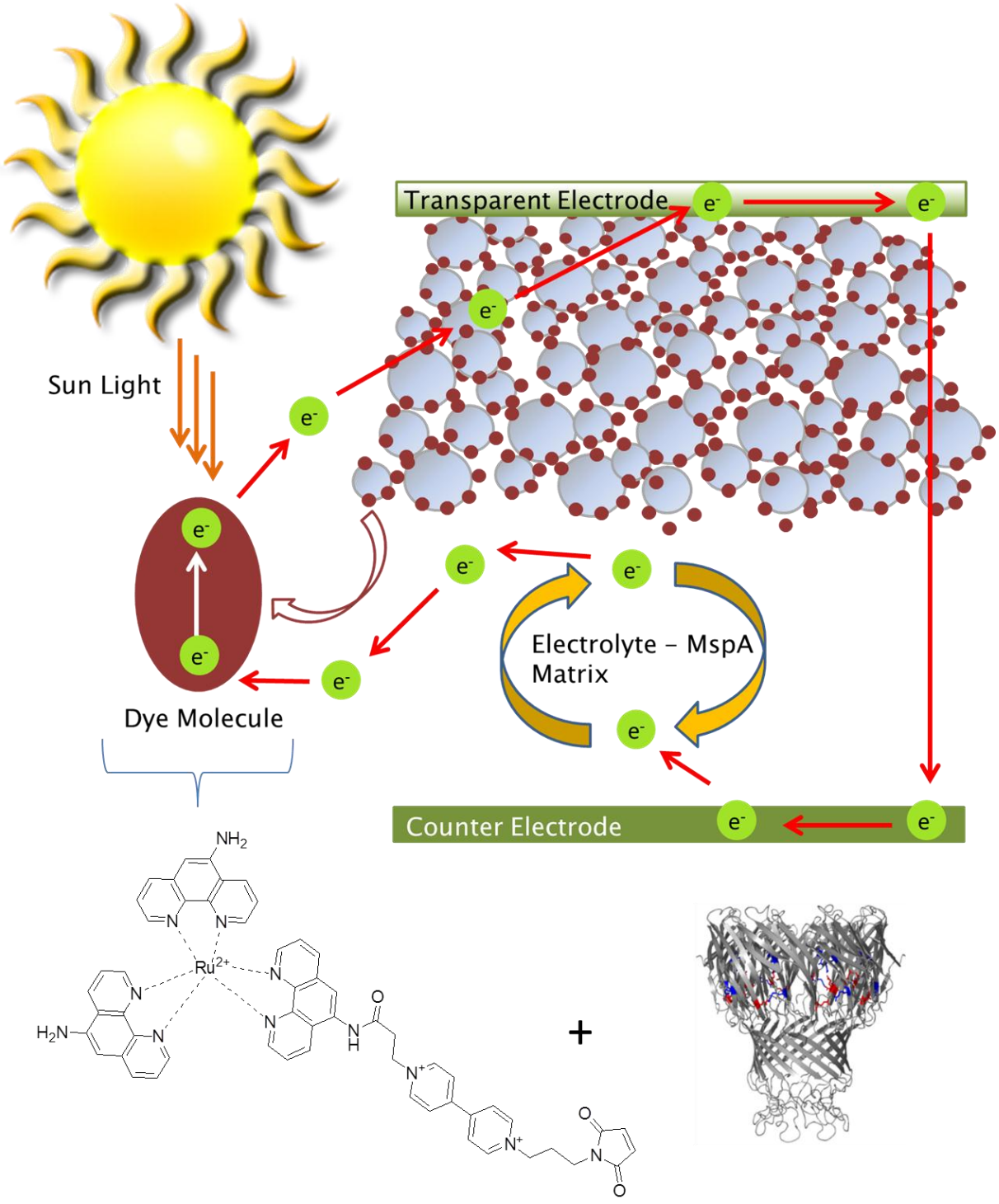


**Figure 5.5: Diagram showing components of an MspA incorporated dye sensitized solar cell prototype**

As depicted in the diagram, the protein incorporated cell consists of a transparent electrode, onto which a nanocrystalline $TiO_2$ layer is deposited. The semiconductor is coated with a Ruthenium(II)-phenanthroline dye sensitizer that is chemically bound to MspA. The initial reasoning behind incorporation of MspA in a solar cell was to probe the limits of its stability and applicability in a highly stressful environment. The specific contact between dye and protein can be altered depending on the nature of dye and use of wild type or mutant protein. A platinum electrode is used as the counter electrode and a commercial iodolyte solution was initially used as the contact electrolyte, which was later on replaced with an aqueous buffer medium. A solar simulator is used to simulate sunlight inside the laboratory. We have demonstrated that the protein incorporated nano DSSC prototype is functional under laboratory conditions. This marks the first evidence of incorporation of a biological macromolecule component inside a photovoltaic device and has the potential to be developed as a new class of solar cells. For this reason we classify the cell as a "hybrid soft cell".

Initially, the cell prototype was designed as a typical Grätzel-type DSSC, as discussed above. Significant results were obtained by these experiments as is discussed in the following sections. However, as the experiments progressed, we realized that in order to optimize the efficiency of the new hybrid soft cell, a novel approach to surface design and use of a different electrolyte, which is more compatible with the protein, is necessary. Therefore, a second set of experiments were carried out to investigate a smoother surface by employing polished Fluorine doped Tin Oxide (FTO) plates, coated with a very thin layer of $TiO_2$. A novel electrolyte solution was also investigated and gave surprisingly better results than the commercial iodide electrolyte, which was used for the initial experiments. An increased efficiency and a deeper mechanistic

understanding of this novel solar cell concept was achieved after completion of the study. The experiments and results are discussed below.

## 5.2 Experimental

### *5.2.1 Synthesis of Novel Ruthenium(II) dyes*

#### *5.2.1.1 Ru-phenanthroline-linker-maleimide dyes*

Synthesis of 4,4'-dipyridinium-*N*-propanoic acid was achieved as follows: 1 g of 4,4'-dipyridine (6.53 mmol) was reacted with 5 equivalents of 3-bromopropionic acid (32.65 mmol) in 15 ml of dry DMF at 80 ºC for 48 hrs. The precipitated product was filtered and dried under vacuum. TLC and $^1$H NMR revealed that the crude product obtained was a mixture of bipyridine mono salt and double salt. To separate the two compounds, alumina column chromatography was performed, using MeOH:$H_2O$ solvent systems of 1:1, 1:4 and 0:1 respectively. The combined fractions were dried using a rotary evaporator and characterized by TLC and $^1$H NMR.

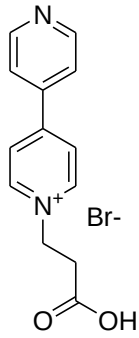


**9)**

**Figure 5.6: 4,4'-Dipyridinium-*N*-propanoic acid**

Synthesis of *N*-propylbromomaleimide was achieved by means of a Mitsunobu reaction that has been modified by Walker.[24] $PPh_3$ (1.35 g, 5.15 mmol) was dissolved in 20 ml dry THF

and the temperature of the mixture was brought down to -78 $^0$C by using dry ice/acetone. Diisopropylazodicarboxylate (DIAD) (1.01 ml, 5.15 mmol) was added dropwise to the reaction mixture over 2 minutes resulting in a yellow solution. The reaction was stirred for 10 minutes followed by addition of 3-bromo propanol (0.77 ml, 8.5 mmol) for over 2 min. After 5 minutes of stirring, maleimide (0.5 g, 5.15 mmol) was added in solid form at –78 $^0$C, which dissolved in another 10 min. The reaction was then, brought to room temperature and allowed to stir at room temperature for 10 hours. A dark grey solution was resulted and TLC at 2:1 hexane:EtOAc showed formation of product. The reaction mixture was concentrated under rotary evaporator and applied to silica gel column with an eluent of 2:1 hexane:EtOAc. After removing solvent, 0.78 g (69.64 %) of pale yellow crystal of *N*-propylbromomaleimide was obtained. The compound was characterized by $^1$H NMR. Melting point of the compound was found to be 45 $^0$C.$^1$H- NMR ($CDCl_3$, 400 MHz) δ (ppm): 6.72 (singlet, 2H), 3.68 (triplet, J= 6.8 Hz, 2H), 3.37 (triplet, J=6.6 Hz, 2H), 2.18 (quintet, J=6.6 Hz, 2H). $^{13}$C-NMR ($CDCl_3$, 400 MHz) δ (ppm): 170.82, 134.43, 36.82, 31.69, and 29.82.IR data (cm $^{-1}$, dropcast on KBr):3088.48, 2960.46, 2924.61, 1700.71, 1408.82, 1234.71:

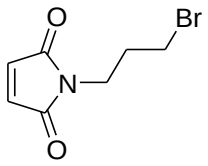


**10)**

**Figure 5.7: *N*-propylbromomaleimide**

Next 0.1 g (0.323 mmol) of 4,4'-dipyridinium-*N*-propanoic acid was reacted with 0.084 g (0.39 mmol) of *N*-propylbromomaleimide in 5 ml of dry DMF and refluxed at 120 ºC for 72 hrs. This resulted in di-quaternization of 4,4'-bipyridinium salt. DMF was removed under high vacuum at 50 $^{\circ}$C. The product was characterized by $^1$H NMR.

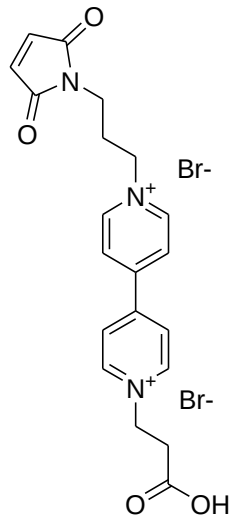


**11)**

**Figure 5.8: 1-(2-carboxyethyl)-1'-(3-(2,5-dioxo-2,5-dihydro-1*H*-pyrrol-1-yl)propyl)-[4,4'-bipyridine]-1,1'-diium**

EDC coupling between the carboxylic acid of above compound with 1,10-phenanthroline-5-amine was achieved as follows: 0.82 mmol of *N*-propylmaleimide-4,4'-dipyridinium salt was mixed with 0.385 mmol of 1,10-phenanthroline-5-amine along with 1.23 mmol of EDC and 0.82 mmol of HOBt. The reagents were dissolved in 5 ml of DMF and 2 ml of ethanol was needed to achieve complete solvation. The mixture was stirred for 24 hours, which resulted in a yellowish liquid.

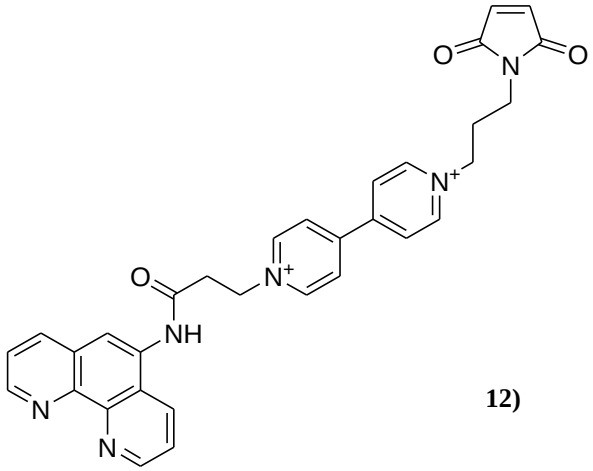


**12)**

**Figure 5.9: 1-(3-((1,10-phenanthrolin-5-yl)amino)-3-oxopropyl)-1'-(3-(2,5-dioxo-2,5-dihydro-1*H*-pyrrol-1-yl)propyl)-[4,4'-bipyridine]-1,1'-diium**

Next, $RuCl_3.H_2O$ (0.38 mmol) was dissolved in 4 ml of DMSO and refluxed for 30 minutes, after which the reddish brown solution turned to pale yellow. This was cooled to room temperature then 25 ml of distilled water was added, followed by heating to 100 ºC for 2 hours. Next the mixture was cooled to 60 ºC and compound **12**, at 40 ºC was added drop wise over 1 hour. Afterwards the temperature of the mixture was kept at 60 ºC for another hour, followed by cooling to room temperature. The excess solvent was evaporated using rotor vapor and air. The obtained crude product was separated using an alumina column, starting with 1:1 MeOH/water solvent system. The polarity of the solvent was increased as 2:1, 4:1, 8:1 and 1:0 MeOH/water mixtures. Fifteen fractions were collected and were checked with thin layer chromatography, after which the following two compounds were isolated and analyzed via $^1H$ NMR, mass, UV and fluorescence spectrometry.

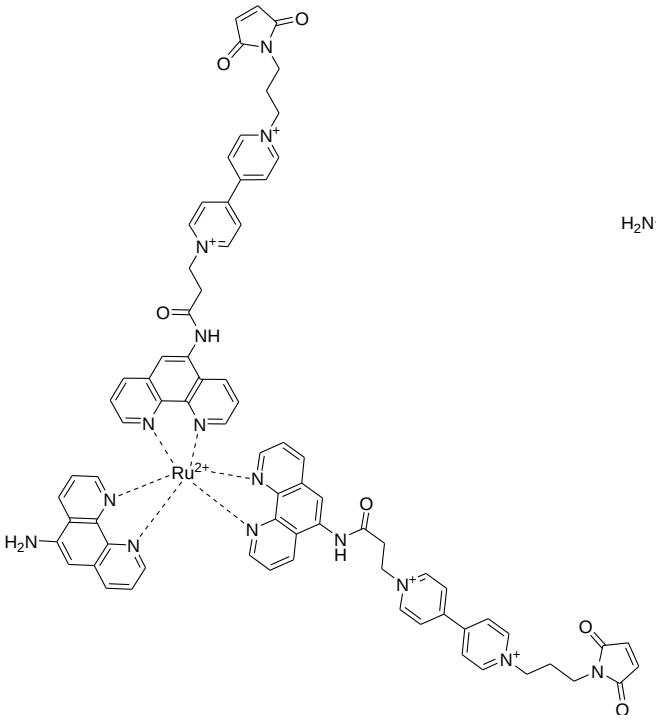

Fractions 1-2 = Ru2 **13)**

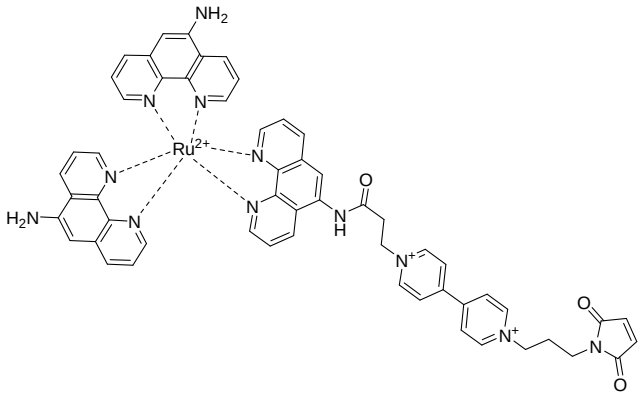

Fractions 12-15 = Ru1 **14)**

**Figure 5.10: Structures of dyes Ru1 and Ru2.**
**Ru1: Ruthenium(2+), (1-(3-((1,10-phenanthrolin-5-yl)amino)-3-oxopropyl)-1'-(3-(2,5-dioxo-2,5-dihydro-1*H*-pyrrol-1-yl)propyl)-[4,4'-bipyridine]-1,1'-diium-κ$N^1$,κ$N^{10}$)bis( 1,10-phenanthrolin-5-amine-κ$N^1$,κ$N^{10}$)- (4CI)**
**Ru2: Ruthenium(2+), (1,10-phenanthrolin-5-amine-κ$N^1$,κ$N^{10}$)bis(1-(3-((1,10-phenanthrolin-5-yl)amino)-3-oxopropyl)-1'-(3-(2,5-dioxo-2,5-dihydro-1*H*-pyrrol-1-yl)propyl)-[4,4'-bipyridine]-1,1'-diium-κ$N^1$,κ$N^{10}$)- (6CI)**

Out of the fractions that were collected, fractions 1-2 and 12-15 contained one compound each and were pooled. These were dried using a rotary evaporator and TLC was performed and checked under UV light. Fractions 1-2 contained a compound, which appeared purple under UV light and was labeled as Ru2. Similarly 12-15 fractions contained a compound that appeared in a highly fluorescent pink and was labeled as Ru1. These were characterized by mass spectroscopy and $^1$H NMR. Fractions 3-11 contained mixtures of varying concentrations of Ru1 and Ru2.

### *5.2.1.2 Ru-phenanthroline-linker-carboxylate dyes*

In addition to the dyes Ru1 and Ru2, synthesis of another Ruthenium(II)-phenanthroline based dye Ru3 was also achieved. This dye is similar to Ru2 but does not contain the maleimide component but has a propanoic acid group in its place. The synthesis is analogous to that that of Ru2 except the viologen is reacted with equivalent amount of 3-bromopropanoic acid instead of *N*-propylbromomaleimide. Also 1,10-phenanthroline was used instead of its analogues amine for initial complexation with $Ru^{2+}$.

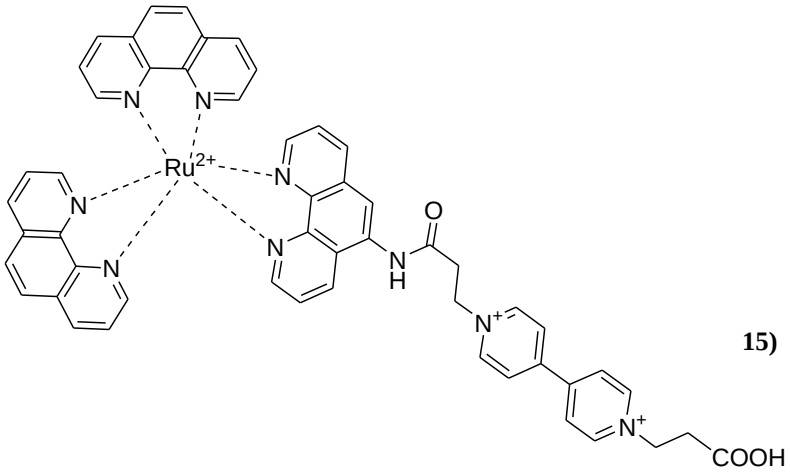


**15)**

**Figure 5.11: Structure of Ru3: Ruthenium(2+), 1' -(1-(3-(1,10-phenanthroline)amino)-3-oxopropyl)-1'-(3-(2,5-dioxo-2,5-dihydro-1*H*-pyrrol-1-yl)propyl)-[4,4'-bipyridine]-1,1'-diium-κN1,κN10)bis( 1,10-phenanthrolin-κN1,κN10)- (4CI)**

## *5.2.2 Binding Ruthenium-phenanthroline dyes with MspA*

Ru1 and Ru2 dyes were subject to chemical binding with MspA mutant A96C via formation of the cysteine-maleimide bond. First the following mixtures were prepared in 10 ml beakers:

1) A96C MspA(1.0 ml) (extracted on 02/02/11) + Fraction 12-15 (5mg) + AOPOE (2.0 ml)
2) A96C MspA(1.0 ml) (extracted on 02/02/11) + Fraction 1-2 (5mg) + AOPOE (2.0 ml)

3) A96C MspA(1.0 ml) (extracted on 06/07/10) + Fraction 12-15 (5mg) + AOPOE (2.0 ml)
4) A96C MspA(1.0 ml) (extracted on 06/07/10) + Fraction 1-2 (5mg) + AOPOE (2.0 ml)

The overall volume of each mixture was adjusted to 5.0 ml by addition of distilled water. The beakers were then sealed with parafilm and the mixtures were stirred at room temperature for 36 hrs. Next mixtures 1 and 3, 2 and 4 were combined and dialysis were performed (Fisherbrand, regenerated cellulose tubing, nominal 3500 MWCO), first using 1x AOPOE next with distilled water for one day each. The dialyzed fractions were collected and gel electrophoresis was performed using an acrylamide gel as follows:

1) Fraction 12-15 with A96C MspA (10µl) + loading buffer (8µl)
2) A96C MspA (extracted on 02/02/11) (10µl) + loading buffer (8µl)
3) Molecular marker + loading buffer (8µl)
4) Fraction 1-2 with A96C MspA (10µl) + loading buffer (8µl)
5) A96C MspA (extracted on 06/07/10) (10µl) + loading buffer (8µl)

From each of these mixtures 10 µl were taken to load the wells of the gel. Electrophoresis performed with Fisher Scientific FB300 elecrophoretic apparatus at 100 V, 400 mA for 90 minutes.

Similarly purified Ru3 dye was reacted with wild type (WT) MspA by amide formation via EDC coupling reaction. Approximately 5 mg of Ru3 dye was dissolved in 2.0 ml of 1x PBS buffer and 1.0 ml of WT MspA was added to the mixture. EDC was added in approximately 1000x moles compared to MspA and 0.5 molar equivalents of HOBt was added into the mixture and the volume was brought to 5 ml in total by adding distilled water. The mixture was then stirred at room temperature for 48 hours and dialysis was performed as described above. Gel

electrophoresis was performed using 10 µl of the dialysis mixture and 5 µl of loading buffer and 10 µl of this mixture was used to load the wells. Unbound WT MspA was used as a control.

### *5.2.3 Fabrication and operation of Grätzel-type MspA incorporated nano solar cell prototype*

Experiments discussed herein were done in collaboration with Dr. Francis D'Souza and Navaneetha K. Subbaiyan, Department of Chemistry, University of North Texas.

The semiconductor electrodes were prepared as follows: Commercial FTO glass plates were used for the base of the prototype cells. These were cut into 1.5' x 1' pieces and cleaned using detergent by gently rubbing over the microcloth pads (BAS). The soap was washed off with deionized water and the plates were further cleaned using 0.1 M HCl in ethanol, acetone and 2-proapanol solutions in an ultrasonic bath for 15 min sequentially. Finally, the plates were treated with plasma cleaning to remove all the organic impurities

Thin films of $TiO_2$ were deposited on the cleaned FTO plates according to procedures given in literature[25]: The electrodes were heated at 450 $^oC$ to remove organic impurities. Then, a layer of $TiO_2$ (18NR AO) paste was coated on the FTO glass plates using the Doctor Blade technique. The plates were kept for 10 minutes to reduce surface irregularity and then they were heated gradually from 120 $^oC$ to 550 $^oC$. After annealing, the $TiO_2$ films were treated with 40 mM $TiCl_4$ solution at 70 $^oC$ for 30 minutes, rinsed with water and ethanol, followed by annealing again at 520 $^oC$. Then the $TiO_2$ electrodes were allowed to cool to 80 $^oC$. Next the plates were immersed in diluted MspA-dye solutions (180 µl in 2.0 ml of MeOH) in methanol for 24 hours.

The counter electrode was formed by depositing the Pt catalyst on the FTO glass (Tec 8, Pilkington) using a drop $H_2PtCl_6$ solution (5 mg Pt in 1 ml of ethanol) and heating at 400 $^0$C for 15 minutes.

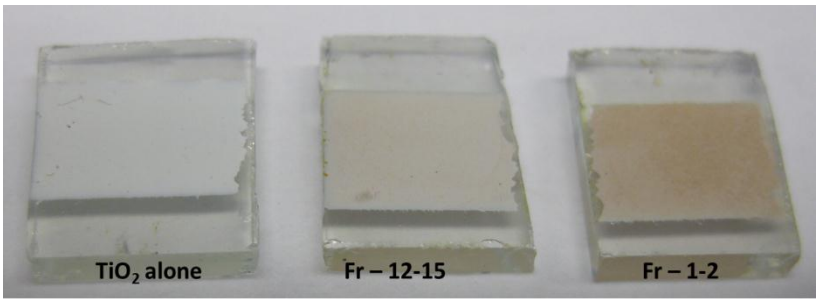


**Figure 5.12: Photograph of Grätzel-type solar cell prototypes. From left to right: glass plates coated with $TiO_2$, $TiO_2$ adsorbed with MspA-Ru1 dye and $TiO_2$ adsorbed with MspA-Ru2 dye**

The photocurrent-photovoltage (I/V) characteristics of the solar cells were measured using a Model 2400 Current/Voltage Source Meter of Keithley Instruments, Inc. (Cleveland, OH) under illumination with an AM 1.5 simulated light source using a Model 9600 of 150W Solar Simulator of Newport Corp. (Irvine, CA). A 340 nm filter was introduced in the light path to eliminate UV radiation. The light intensity was monitored by using an Optical Model 1916-C Power Meter of Newport. Incident photon-to-current efficiency (IPCE) measurements were performed under ~2.5 $mWcm^2$ monochromatic light illumination conditions using a setup comprised of a 150 W Xe lamp with a Cornerstone 260 monochromator (Newport Corp., Irvine, CA).

### *5.2.4 Fabrication and operation of FTO based MspA solar cells*

Experiments discussed herein were done in collaboration with Dr. Jun Li and Steven Klankowski at the Department of Chemistry, Kansas State University.

Fabrication of fluorine doped tin oxide (FTO) solar cells were adapted from procedure given by J. Essner.[26] Commercially available FTO plates (TEC8, Dyesol, Queanbeyan, NSW, Australia & Pilkington, Toledo, Ohio, USA) were cut into 2 cm x 2.5 cm pieces. Holes were drilled into few pieces, which were intended to be used as Platinum electrodes. Next, these were dipped in hexane for 24 hours and then sonicated 10 minutes to remove wax from cutting. This was followed by washing with 0.1M HCl in Ethanol and acetone respectively and then oven dried at 75 ºC. The resistance of the dried plates has an average of 12-15 Ω's. Next the plates were polished to obtain a completely flat FTO surface.

Polishing of FTO plates were done by hand using 0.05 μm $Al_2O_3$ slurry. Various different polishing times were used until a >100 Ω resistance were obtained consistently. Times were varied from 2, 4, 6 minutes etc. up to 16 minutes followed by 26 and 30 minutes as well. Then they were washed with deionized water and sonicated for 5 minutes to remove excess Alumina. Plates were then observed under UV-Vis (Beckman DU 640 Spectrophotometer) for characterization SEM (Hitachi S-3400 N) to determine surface homogeneity. The plates polished for 26 minutes demonstrated the most even surface. Similarly plates polished with 1 μm Alumina slurry for 10-15 minutes followed by 5 min sonication also produced sufficiently flat surfaced cells. All experiments reported below were performed with plates polished using either one of the two optimal techniques. Deposition of $TiO_2$ onto polished FTO plates were achieved by first taping off three side edges with double sided tape and the remaining edge with Scotch® Magic Tape (thickness of 50-60 μm). Onto the remaining open FTO surface $TiO_2$ paste was applied using 'doctor blade' technique. Fixing and annealing of $TiO_2$ was done according to procedure given by Vesce et al.[27] using a thermo oven purchased by Thermo Electron Corporation, model

Lindberg/Blue M. Thickness of the $TiO_2$ layer was controlled to achieve an even deposition of 10 nm. Characterization was done with SEM. Preparation of the Platinum counter electrode was achieved by polishing 2 x 2.5 cm FTO plate for 10 minutes using 0.3 μm $Al_2O_3$ slurry. Pt coating was achieved using a high resolution ion beam coater from Gatan, model 681.

MspA extracts (WT or A96C) were deposited onto flat FTO plates by adding 50 μl of protein extract (in 1x PBS medium) onto the open window of taped plate and spread evenly by a plastic micro pipette tip. On $TiO_2$ deposited FTO plates, protein deposition was achieved by dipping the plates at a 45º angle in a diluted protein extract (1.0 ml extract + 1.0 ml 1x PBS) for 24 hours. In both techniques, after deposition, the plates were dried under laminar flow at room temperature for 24 hours. Unbound dye and dye-protein bound samples were adsorbed onto $TiO_2$/FTO plates by using a similar dipping technique (500 μl dye-MspA extract + 1.5 ml 1x PBS) followed by drying under laminar flow.

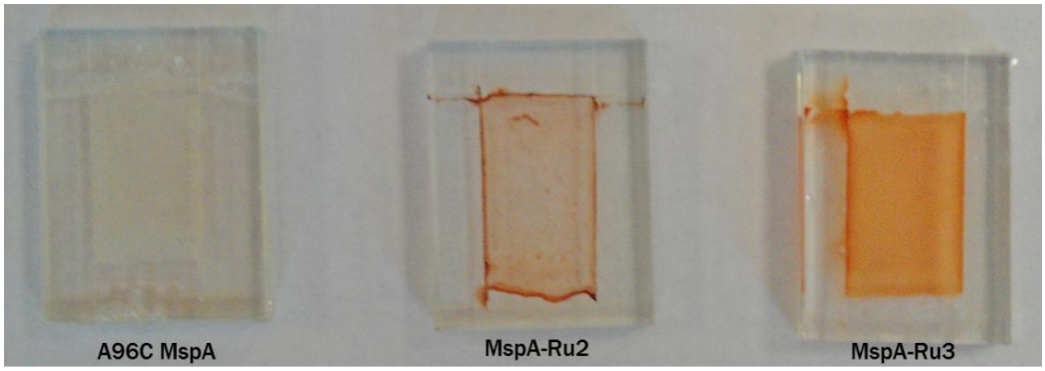


**Figure 5.13: FTO-based MspA electrodes. Left - A96C MspA, middle - MspA-Ru2, right - MspA-Ru3**

Once dried, the Magic Tape was removed from the prepared plates and the Pt deposited counter electrode was fixed to the plates by adhesion with the remaining double-sided taped edges. An electrolyte which was either Iodide (Solaronix, Iodolye AN-50) or 1x PBS (pH = 7.4)

was added in 2 x 9 µl fractions between the two electrodes via the hole drilled in the Pt electrode. The assembled electrodes were mounted onto a stage and connected to a solar simulator apparatus (from Newport Corporation). Solar simulator irradiance was used as either 1 sun or 0.5 sun (i.e. full intensity and half intensity of simulated sunlight respectively). The latter was achieved by using neutral density filter (Newport #FSQ-ND03). All I/V and IPCE measurements were collected by a source measurement unit (SMU) from Agilent (SMU #U2722A).

## 5.3 Results and Discussion

### *5.3.1 Ruthenium(II) dyes*

The synthesis of 4,4'-dipyridinium-*N*-propanoic acid rendered a mixture of two products as identified by TLC. To separate the compounds, alumina column chromatography was performed. Since both products are highly polar, silica column chromatography would not be an effective separation technique. The positively charged salts would be adsorbed onto silica hence a neutral medium such as alumina is more desirable. Fractions 2-11 contained the mono salt and 17-25 contained the double salt. Fractions 12-16 contained a salt mixture. The combined pure fractions were dried to obtain 0.7208 g of mono salt (w/w 34.3% yield) and 0.3705 g of double salt (w/w 17.63% yield). $^{1}$HNMR was performed to reveal that the combined fractions 2-11 contained 4,4'-dipyridinium-*N*-propanoic acid and fractions 17-25 contained 4,4'-dipyridinium-bis-(*N*-propanoic acid).

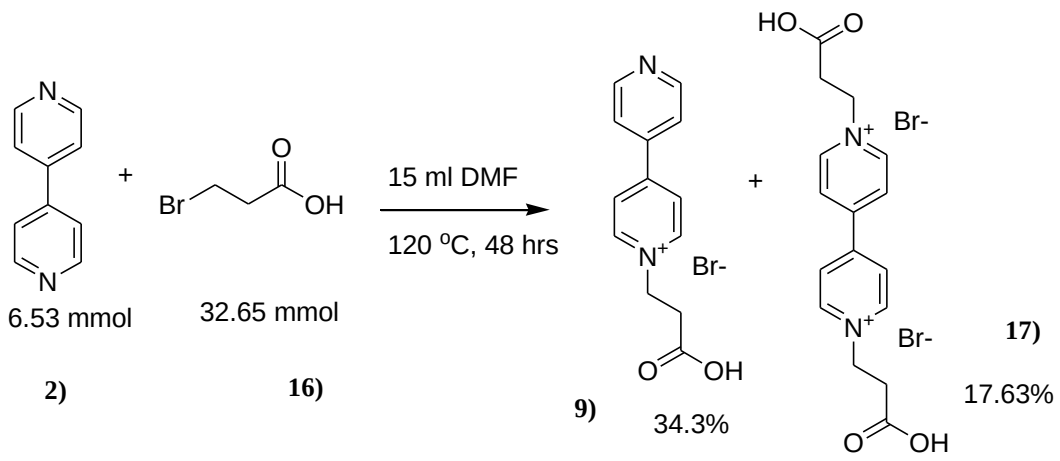


**Scheme 5.1: Synthesis of 4,4'-dipyridinium-*N*-propanoic acid and bis-(4,4'-dipyridinium-*N*-propanoic acid)**

*N*-propyl-3-bromomaleimide was synthesized by reaction of maleimide with 3-bromopropanol via a modified Mitsunobu reaction as shown below. The product was obtained in 69.64% yield.

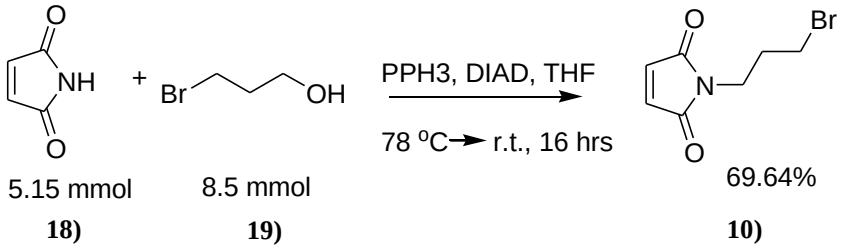


**Scheme 5.2: Synthesis of *N*-propylbromomaleimide**

Synthesis of 4,4'-dipyridinium-*N*-propylmaleimide-*N*-propanoic acid was achieved by reacting a 1:1 mixture of *N*-propylbromomaleimide with 4,4'-dipyridinium-*N*-propanoic acid by refluxing in anhydrous DMF for 72 hours. The product precipitated out as a white solid and was filtered and washed several times with dry DMF and dried under vacuum. Yield of the dry product was 59.78%.

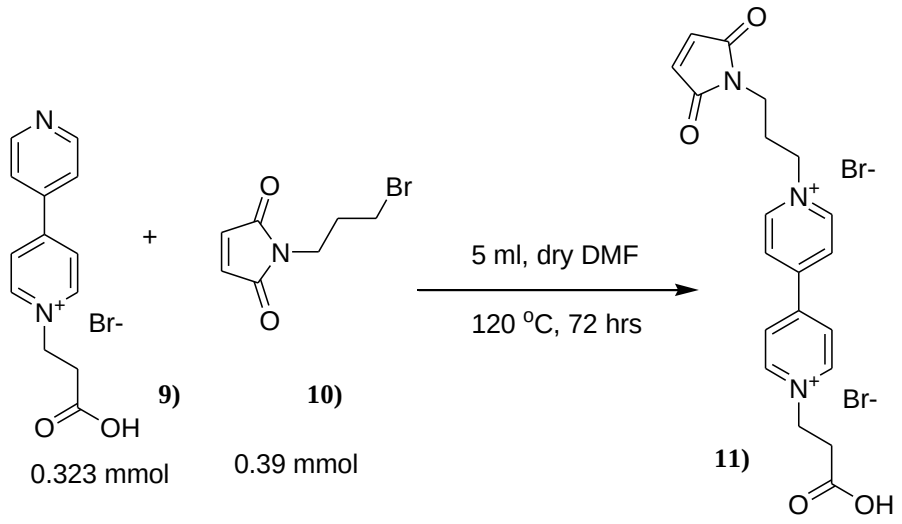


**Scheme 5.3: Synthesis of 4,4'-dipyridinium-*N*-propylmaleimide-*N*-propanoic acid**

Synthesis of the phenanthroline-viologen-maleimide linker component **(12)** was achieved by performing EDC coupling reaction between 1,10-phenanthroline-5-amine and 4,4'-dipyridinium-*N*-propylmaleimide-*N*-propanoic acid. The complex $[Ru(DMSO)_4\text{-}n(H_2O)_n]^{2+}$ was generated as shown in scheme 5.4 and reacted with 1,10-phenanthroline-5-amine (2:1 mol) to achieve Ru(II)-bis-(1,10-phenanthroline-5-amine). The latter was reacted with compound **12**, which resulted in a mixture of the dyes Ru1 and Ru2. (Refer scheme 5.4) the products were separated using alumina column chromatography. Fractions 1-2 contained Ru2 and fractions 12-15 contained Ru1 as was detected by TLC. Fractions 3-11 contained a mixture of products. After drying, weight of Ru1 collected was 0.2889 g and weight of Ru2 obtained was 0.4343 g. However, after isolation the dyes could not be dried completely due to high amounts of adsorbed water, even after excessive vacuum drying. Therefore, yields of pure Ru1 and Ru2 could not be calculated accurately. Under the assumption that each sample contained 50% adsorbed water by weight, approximate yields were calculated to be 27.25% for Ru1 and 40.97% for Ru2. Similarly yield of Ru3 was found to be ~ 34.65%.

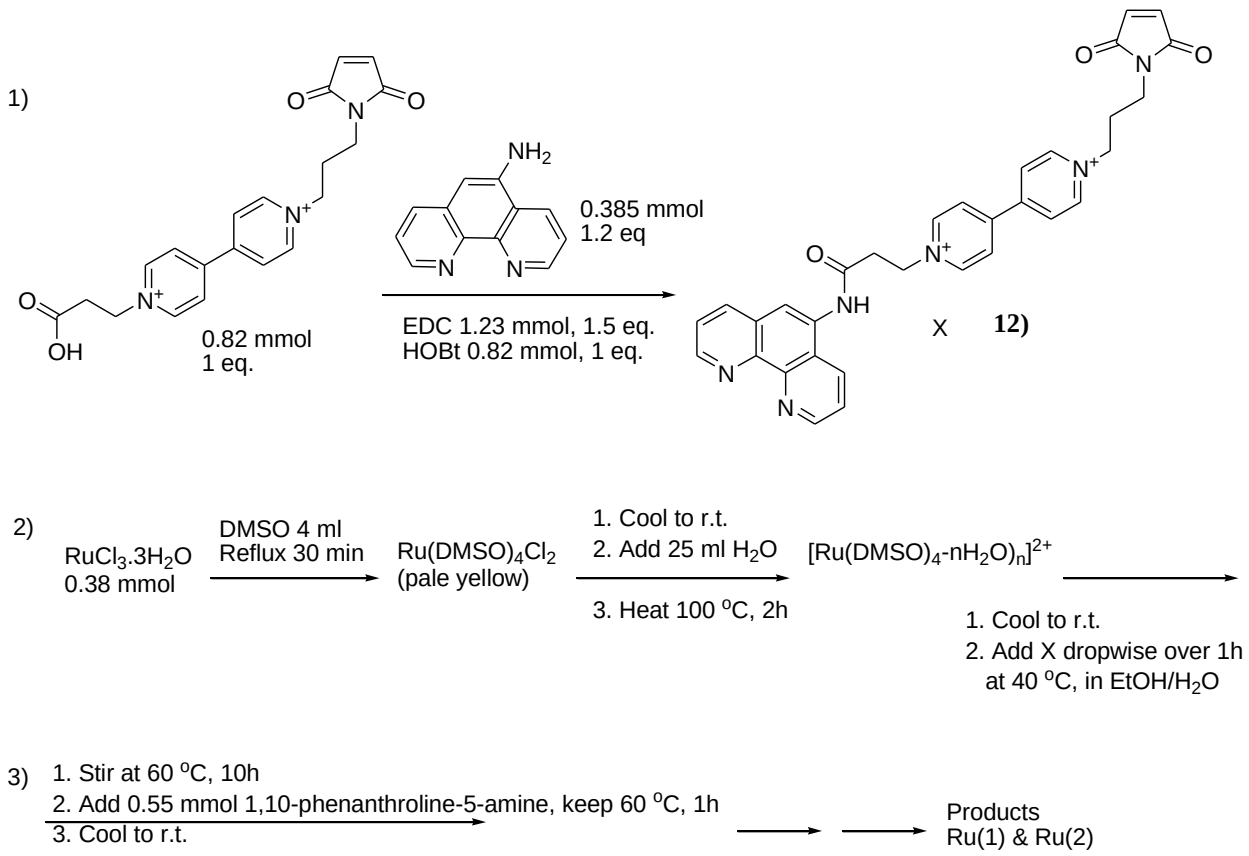


**Scheme 5.4: Synthesis of Ru1 and Ru2**

Initial characterization of the Ruthenium dyes Ru1, Ru2 and Ru3 were done using UV/Vis and fluorescence spectra.

Ru1 dye had a UV maxima of 268 nm and a fluorescence maxima of 389 nm. This is a much more blue-shifted value from the typical fluorescence maxima for Ruthenium dyes, which usually falls on the 400-600 nm range. The shoulders to the left of the fluorescence maxima indicate $\pi$ to $\pi^*$ and MLCT transitions. The overall fluorescence intensity was rather low and could very well be the reason behind lack of solar activity from unbound and MspA bound Ru1 dye.

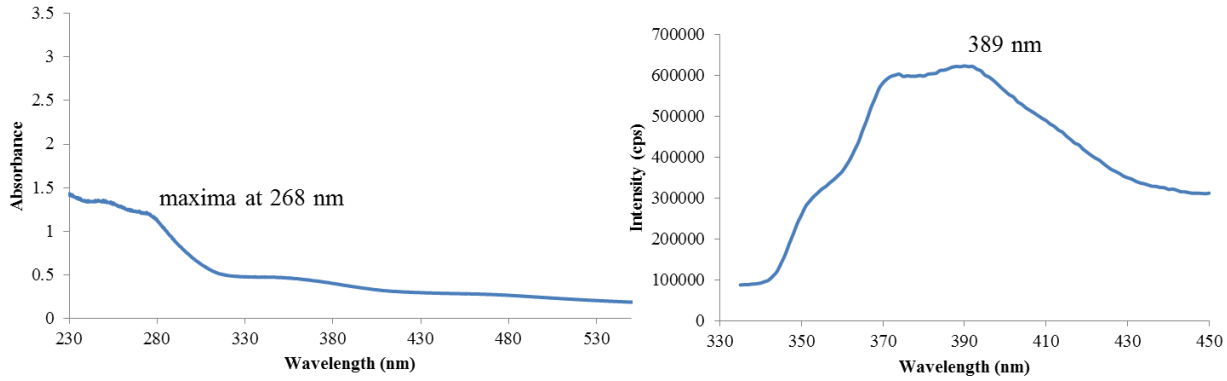


**Figure 5.14: UV spectrum (left) and fluorescence emission acquisition spectrum (right) of Ru1 dye**

The Ru2 dye had a more red-shifted UV maxima of 346 nm. Fluorescence spectrum had two prominent peaks, one at 395 nm and a maxima of 610 nm. Although UV absorbance and fluorescence intensity was low for this dye, it gave significant results in solar cell experiments as discussed in section 5.3.3.

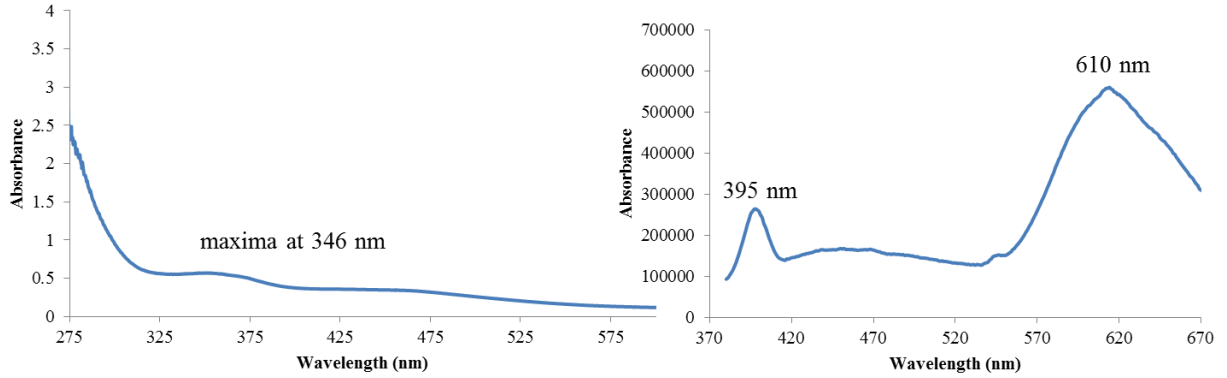


**Figure 5.15: UV spectrum (left) and fluorescence emission acquisition spectrum (right) of Ru2 dye**

Interestingly the UV/Vis maxima for Ru3 dye was even more red-shifted and included in the visible region, at 412 nm. The overall fluorescence for this dye was significantly higher than

that of Ru1 and Ru2 dyes. The fluorescence spectrum had two prominent peaks, at 427.33 nm and 599.9 nm.

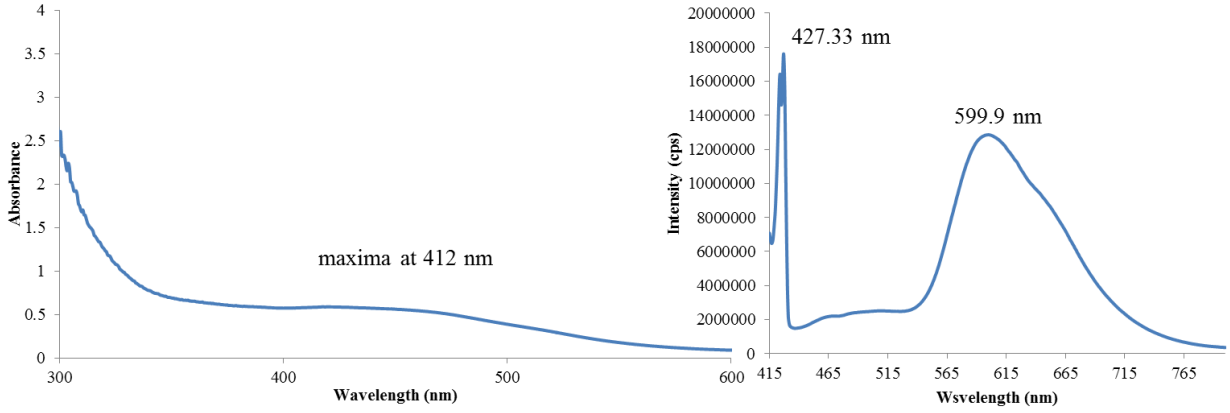


**Figure 5.16: UV spectrum (left) and fluorescence emission acquisition spectrum (right) of Ru3 dye**

### *5.3.2 Characterization of MspA bound Ru1, Ru2 and Ru3 assemblies with gel electrophoresis*

Ru1 and Ru2 dyes contain maleimide groups linked to the viologen. The reason behind this molecular design is to ultimately achieve chemical binding between MspA and the dyes via formation of the cysteine-maleimide bond. This form of bonding is a well-known method to link proteins with other reagents. MspA mutant A96C contains eight cysteine groups at the terminal end of the goblet. The thiol groups of these are intended to react with the double bond of maleimide. Therefore it theoretically becomes possible to engineer eight dye molecules per each MspA unit.

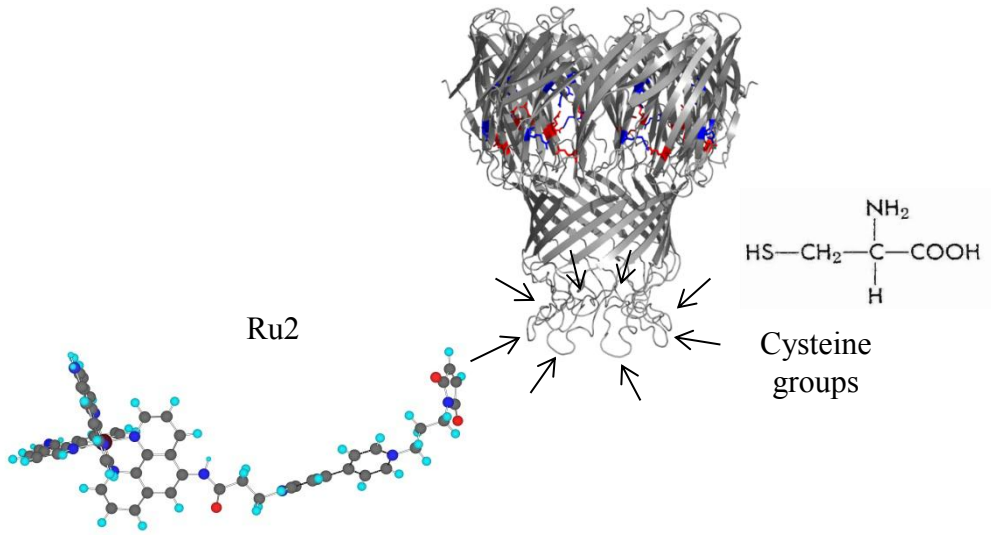


**Figure 5.17: Diagram showing binding of Ru2 dye with A96C MspA via the cysteine-maleimide bond**

Similarly, eight Ru3 dye molecules can be bound to each WT MspA unit. In this case the binding site is the upper-mid region of the protein, where it contains eight free amine groups. These are intended to react with the carboxyl group of the Ru3 dye. An EDC coupling reaction is necessary to achieve amide formation.

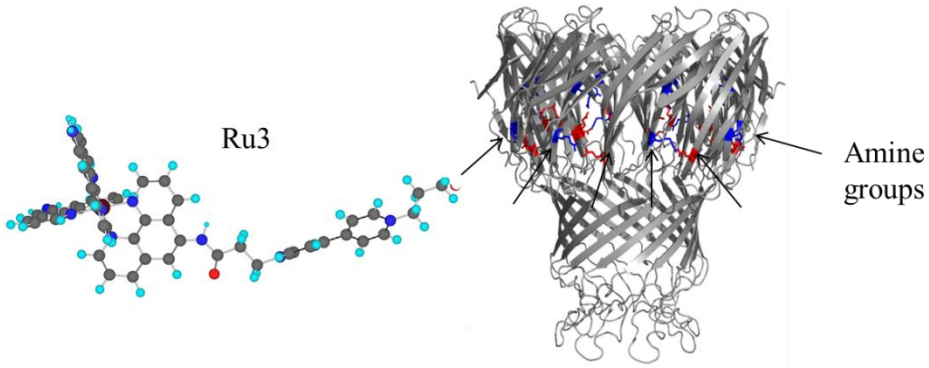


**Figure 5.18: Diagram showing binding of Ru3 dye with WT MspA via amide formation**

Gel electrophoresis was employed as the characterization technique for this study. The MspA samples, which were bound to the Ruthenium complexes Ru1 and Ru2, appeared

approximately 50 kDa higher than the unbound A96C MspA, indicating that the dyes were bound to the protein. Given below is the gel obtained for binding of Ru1 and Ru2 with MspA mutant A96C. Extensive streaking of bands is evident in the dye-bound samples.

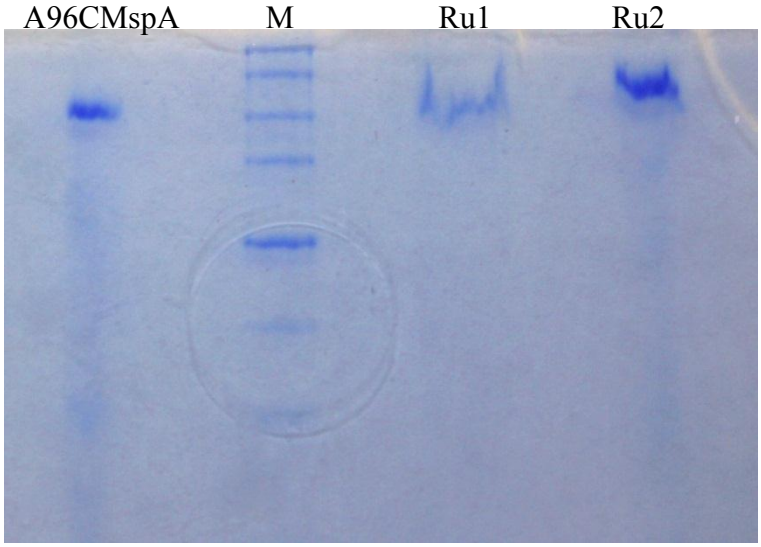


**Figure 5.19: Gel showing unbound A96C, molecular marker (M), MspA bound Ru1 and Ru2**

Similarly WT MspA bound R3 dye assembly was characterized. In this case the bound sample appeared ~50 kDa below the unbound sample. Streaking was evident in the dye-bound sample as indicated in the figure below. In this case the unbound protein also shows streaking due to the protein extract being highly concentrated. This phenomenon has been observed before for highly concentrated MspA extracts.

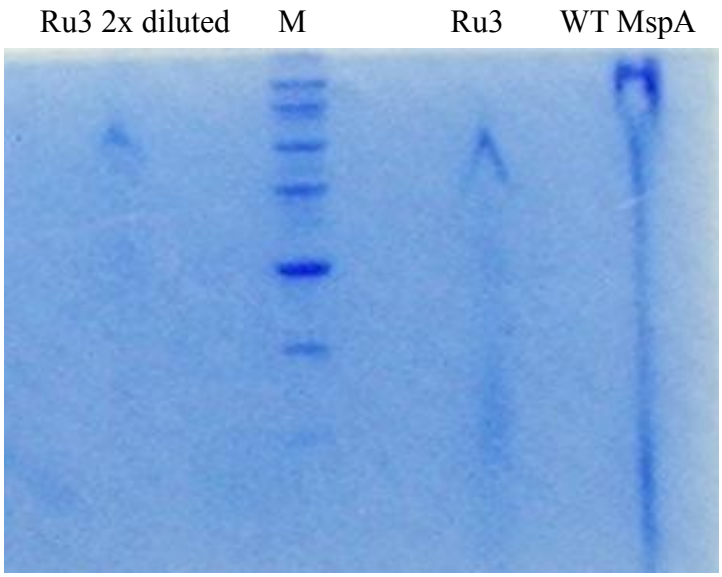


**Figure 5.20: Gel showing from left to right: MspA+R3 extract diluted 2x, molecular marker, undiluted R3+MspA extract and unbound WT MspA**

As explained in Chapter 2, MspA molecules exist as aggregates in solution and are rarely found as single molecules or dimers. This aggregation is largely a result of the interaction between the highly charged surface of MspA molecules with the surrounding water molecules. Addition of a highly charged secondary species, such as a Ruthenium dye, would significantly alter the molecular aggregation behavior in the protein solution (refer Chapter 4). This behavior could lead to either higher aggregation or dis-aggregation depending on the particular secondary species involved and is often difficult to predict. Hence, we have considered a deviation of approximately 50 kDa from the free protein in each case as evidence for chemical binding between dye molecules and MspA.

### *5.3.3 Grätzel-Type MspA solar cells*

The current switching behavior of $TiO_2$ and MspA bound Ru1 and Ru2 dyes were tested initially to determine whether the protein-dye assemblies are stable under the employed voltaic

conditions. As expected, $TiO_2$ alone did not show any evidence of current conductance. The MspA-Ru1 complex showed very clear evidence of conductance under the applied current and the effect was reproducible throughout the experimental time. However, the MspA-Ru2 complex did not show any ability to conduct current. (Refer to figure below)

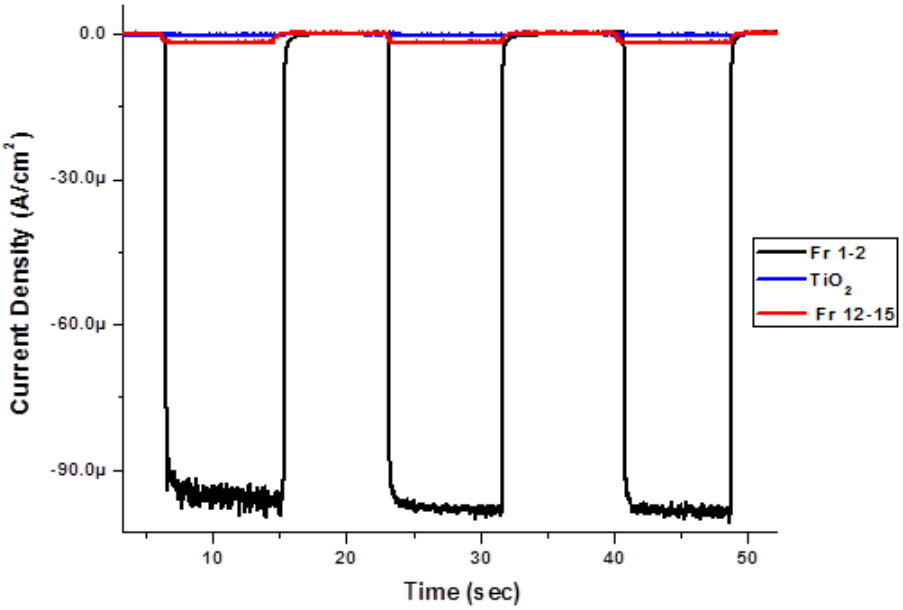


**Figure 5.21: Current switching behavior of $TiO_2$, MspA-Ru1 dye (Fr 1-2) and MspA-Ru2 dye (Fr 12-15)**

Next, the conductance of the complexes was tested with varying voltages (I/V curve). In accordance with results obtained above, only MspA-Ru2 complex showed substantial and stable current under the applied voltage range. In the dark, observed current was close to zero but under simulated solar light, a steady current of 100 $\mu A/cm^2$ was observed from -0.1 V to 0.2 V range. After 0.2 V, the current starts to increase exponentially and by 0.4 V we observe open current. (Refer to figure below)

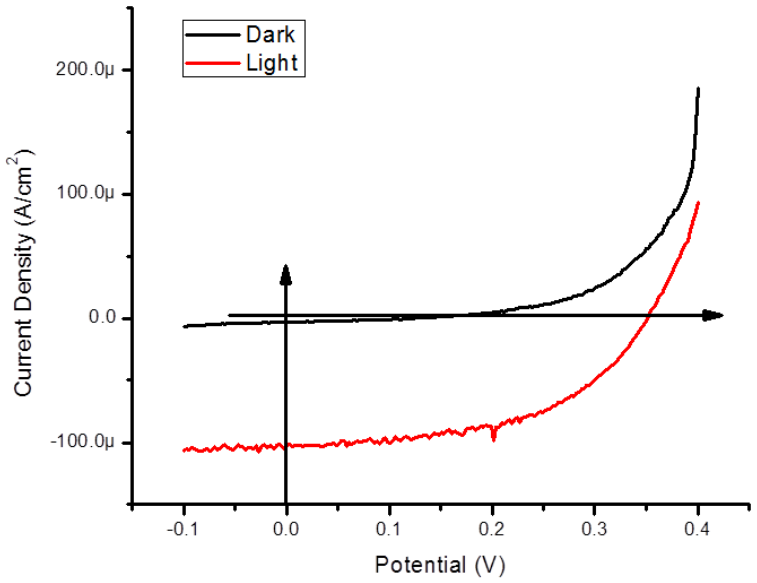


**Figure 5.22: Current vs. potential graph for MspA-Ru2 dye solar cell prototype**

In order to calculate the overall efficiency of the MspA-dye solar cell prototypes, the percentage of incident photon efficiency (i.e. IPCE%) was calculated. The current generated in the visible region, i.e. 400 – 700 nm was tested for this purpose. For the MspA-Ru1 cell, a maximum efficiency of ~ 0.35% was achieved at 420 nm. A higher efficiency of 1% was achieved for MspA-Ru2 cell at 400 nm. (Refer to figure below)

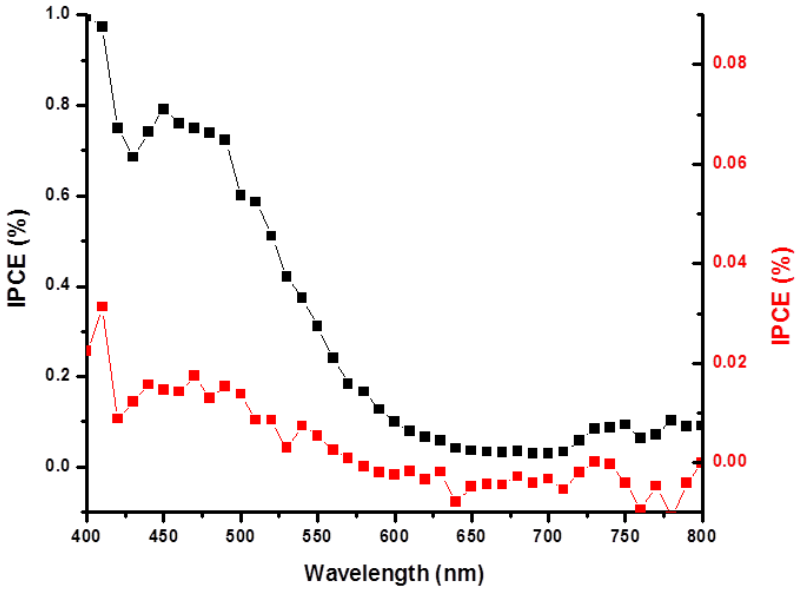


**Figure 5.23: IPCE% vs. wavelength graph for MspA-Ru1 dye (red line) and MspA-Ru2 dye (black line)**

The data obtained above, marks the first ever evidence of a protein incorporated dye sensitized solar cell prototype.

### *5.3.4 FTO based MspA solar cells*

The polished plates were observed under SEM in order to determine the optimum polishing and sonicating time to generate flat surfaced cells. Polishing under optimum time would result in an uneven surface and over-polishing would lead to breakage of the oxide film altogether. Both the above factors would result in failure of optimum current conductance in the finished cell.

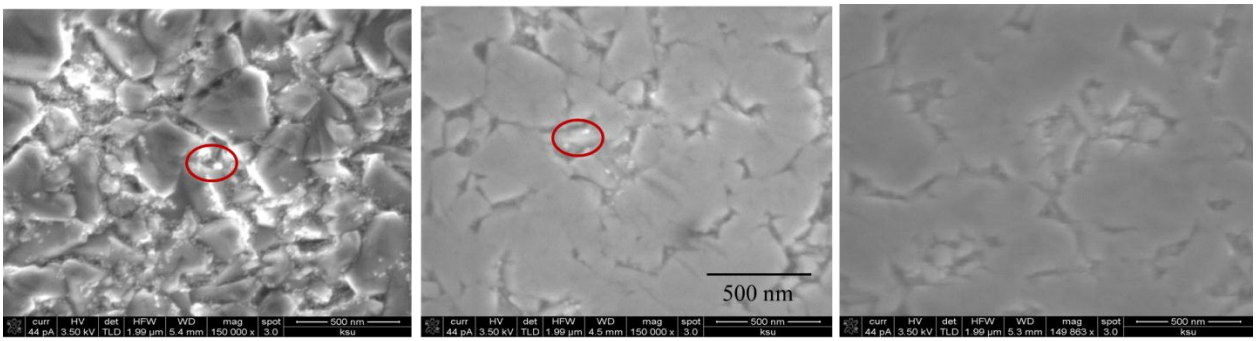


**Figure 5.24: SEM images of polished FTO plates: (a) polished 6 mins w/o sonication (b) polished 16 mins w/o sonication (c) polished 26 mins, sonicated 5 mins. Red circle indicates residual $Al_2O_3$**

A cell was constructed by deposition of a thin layer of MspA alone, on the polished FTO surface, without addition of any external electrolyte. The initial MspA extract added was a diluted PBS buffer solution, which was allowed to dry overnight, forming a dry protein layer. The objective here was to obtain basic knowledge on how a completely flat surface would accommodate the protein. It was clearly evident that MspA alone can conduct a small current under simulated solar light, as shown in the figure below.

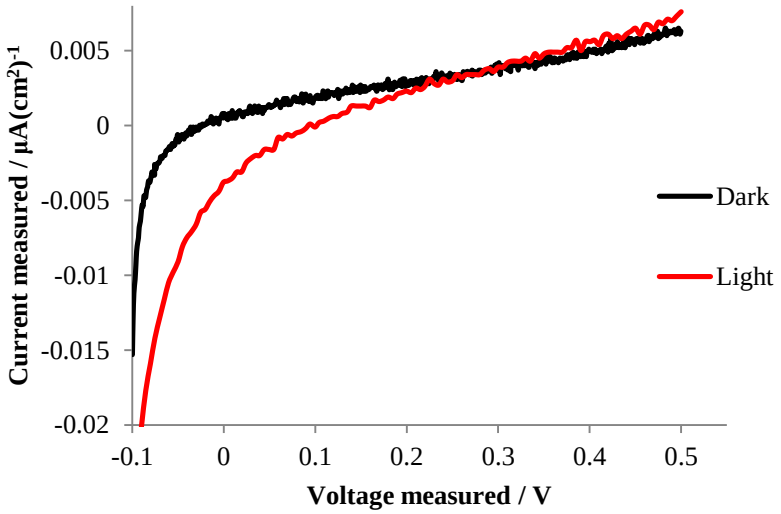


**Figure 5.25: Current vs. voltage graph for FTO based MspA cell without electrolyte**

Similar results were successfully repeated several times, employing the same protein sample and no evidence of protein decomposition were evident. Although the current generated is in nano Ampere range, it is still significant as it is accomplished from a biomolecule without the use of a sensitizer or a commercial electrolyte. This marks the first evidence of photovoltaic ability of a protein, in an aqueous environment, without the use of any sensitizer.

Since to our knowledge, 1x PBS buffer is the best medium that is most suited to accommodate MspA, this was added as an electrolyte to an MspA cell and the I/V experiments were repeated. Indeed a significant increase (although still in nA range) was observed as shown in the figure below.

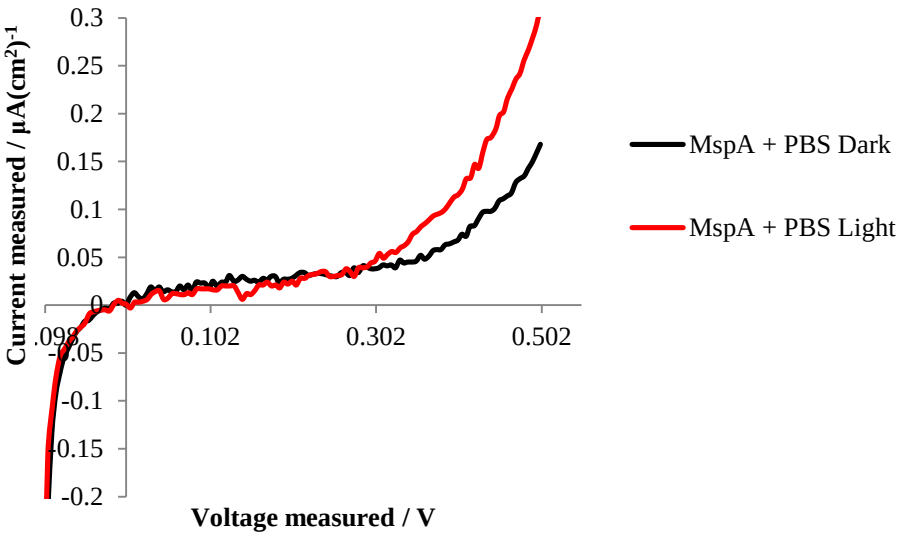


**Figure 5.26: Current vs. voltage graph for FTO based MspA cell with 1x PBS as electrolyte**

In order to compare the buffer environment to that of the commercially available electrolyte, another set of experiments was conducted. A commercial Iodolyte solution was used

as medium of electron transfer for MspA and the I/V experiments were repeated. To our surprise almost no current was generated consistently by the protein in this environment. (Refer to figure below)

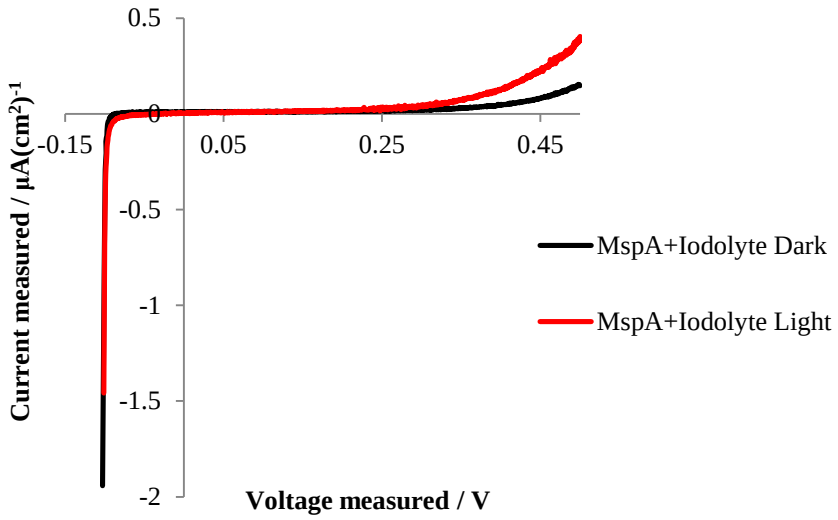


**Figure 5.27: Current vs. voltage graph for FTO based MspA cell with commercial Iodolyte as electrolyte**

The absence of current in Iodolyte brings into consideration whether the protein undergoes decomposition or loss of octameric structure in this medium. Hence a gel experiment was conducted employing WT and A96C extracts that were mixed with the Iodolyte solution, along with the complimentary unreacted extracts. There was no evidence of decomposition detected in the gel. However, excessive streaking in the MspA band was observed compared to the control, indicating a certain degree of chemical or physical modification.

To test whether or not the favorable results obtained above for MspA in PBS medium was just an artifact caused by the charges generated within the medium itself, we conducted an I/V experiment with 1x PBS alone as an electrolyte between FTO/Pt electrodes. It was evident

that by itself, PBS is not capable of conducting any current under dark or light conditions. (Refer to figure below) Hence it can be concluded that in the former instance, MspA alone is actually responsible for the observed current conductance.

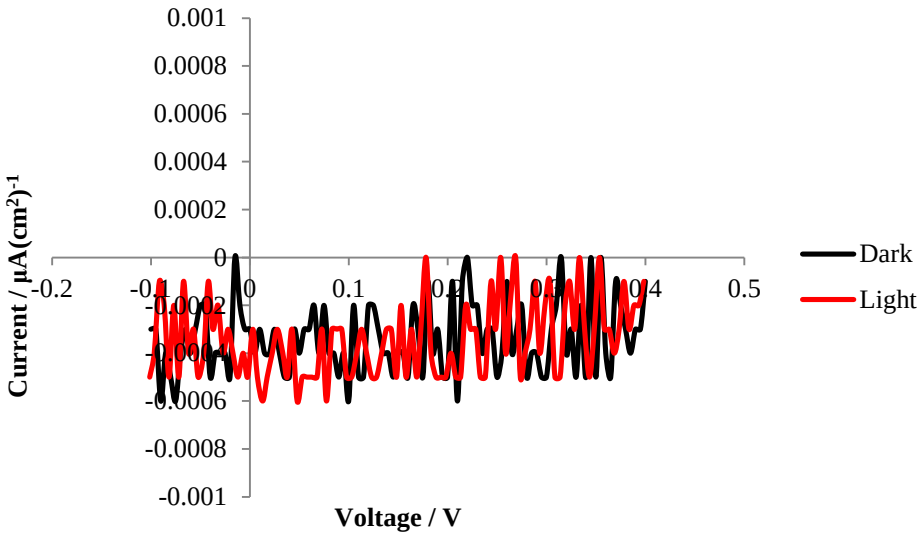


**Figure 5.28: Current vs. voltage graph for 1x PBS solution**

A comparison of I/V behavior for MspA cell prototypes in all three media is given in figure 5.29. It is apparent that a 1x PBS buffer solution is the most suited environment to accommodate an MspA photovoltaic cell. It is interesting to note that even without any added electrolyte, MspA conducts more current than in a commercially optimized Iodolyte solution.

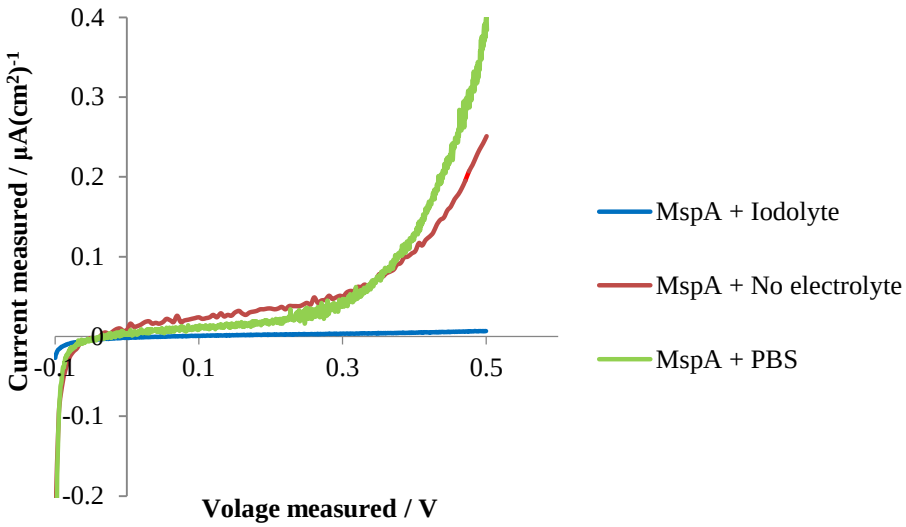


**Figure 5.29: Comparison of current conductance of MspA in different media under light**

In order to optimize the efficiency of the protein-incorporated cell, we also investigated MspA incorporated cells based on FTO electrodes deposited with a thin layer of $TiO_2$ (~10 nm). The objective of this study was to create a surface that would be better suited for the protein than a completely flat FTO surface. The experiment using the Grätzel-type cell, which was used for the initial MspA-Ru2 dye solar cell (section 5.3.3) was repeated using this new, optimized surface. i.e. a thin layer of MspA bound Ru2 dye was adsorbed onto FTO/$TiO_2$ surface to build the electrode. However, since it was found that commercial Iodolyte is not a favorable medium for MspA, the new experiments were conducted in 1x PBS electrolyte medium. (Refer to figure below)

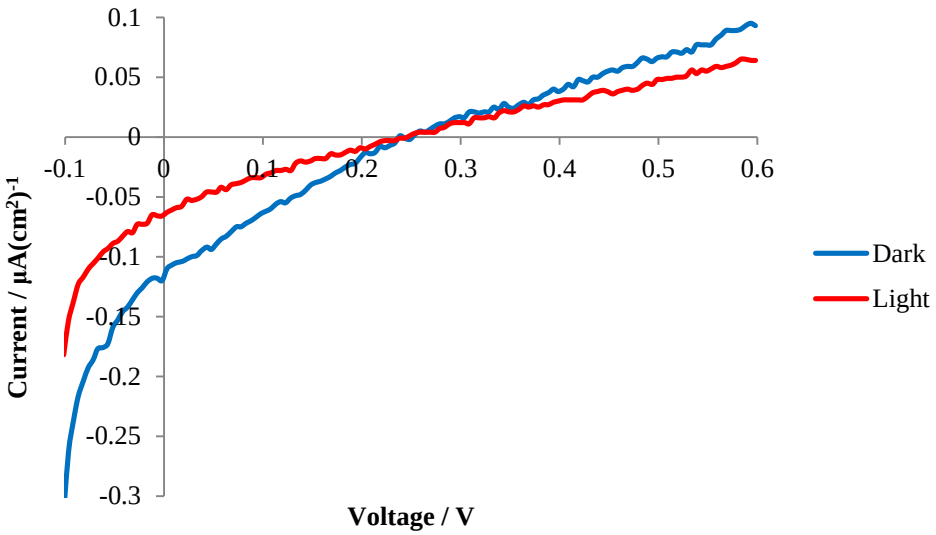


**Figure 5.30: Current vs. voltage graph for FTO/$TiO_2$ cell with MspA bound Ru2 dye in 1x PBS**

As is evident above, the overall value of current generated is much lower than that observed for the Grätzel type cell. However, when observing the dark and light currents it is apparent that they are generated in opposite direction compared to the former Grätzel type cell. It is our hypothesis that in this cell, the current generated from the protein is opposed to that of the current generated from the dye. This results in an overall current that is low in value. To test this theory we conducted an experiment using a cell constructed with Ru2 alone on FTO/$TiO_2$ surface. (Refer to figure below)

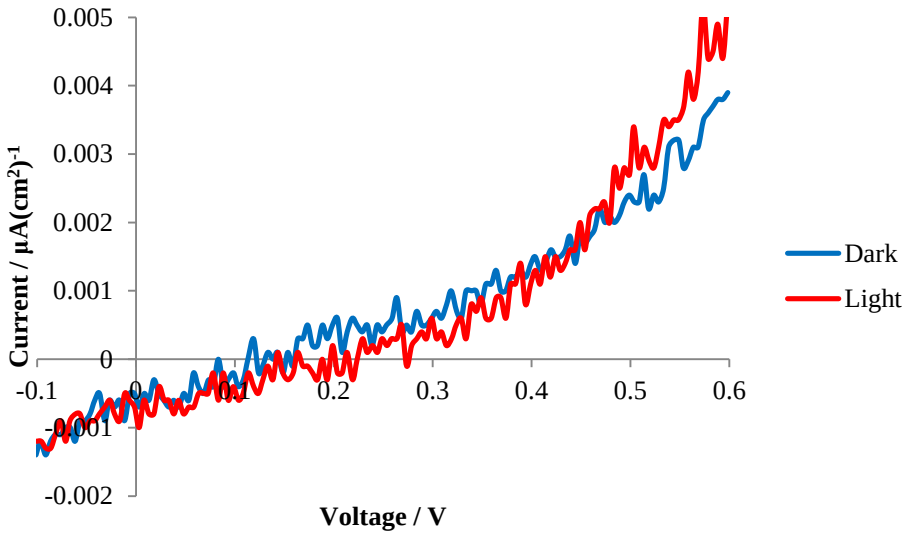


**Figure 5.31: Current vs. voltage graph for FTO/$TiO_2$ with Ru2 dye in Iodolyte**

In accordance with our hypothesis, it was observed that the direction of current generated by the Ru2 dye alone is opposed to that of the MspA-dye cell. This phenomenon provides a possible explanation for the generation of lower current and also could be a factor why the initial experiments gave an IPCE value of only 1%. No significant current was observed for MspA-Ru1 cell as was seen for the Grätzel type cell experiments.

A comparison of results from the FTO-based MspA and MspA-Ru2 cells with PBS is given in the figure below. The characteristic shape observed for the MspA I/V curve is changed when MspA is bound to Ru2 dye.

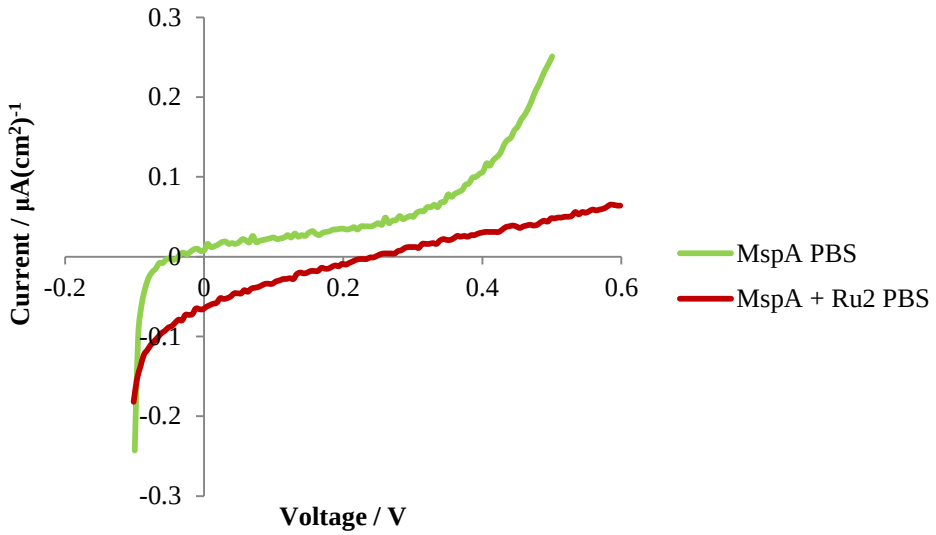


**Figure 5.32: Comparison of I/V data for MspA on PBS and MspA-Ru2 cells**

The onset of 'open current' generation observed in the positive region of the voltage (starting ~0.3 V in above graph) for the MspA cell is not observed for the MspA-Ru2 cell. In fact, the latter curve is reminiscent of the unbound Ru2 curve depicted in figure 5.29. This observation provides further evidence to our earlier analysis in that MspA and Ruthenium dyes conduct current in opposite directions. Since part of the currents from both MspA and the dye, cancels each other out, the overall current observed for MspA-dye cells is less than that observed for unbound MspA cells. This is clearly evident in figure 5.30.

Incident Photon Conversion Efficiency % (IPCE %) measurements were performed for FTO/$TiO_2$ based MspA, MspA-Ru2 and MspA-Ru3 cells. A broader wavelength range (200-800 nm) as opposed to the previous experiments (400-700 nm) was used in order to include UV and near-IR absorption regions. The results are summarized in the figure below:

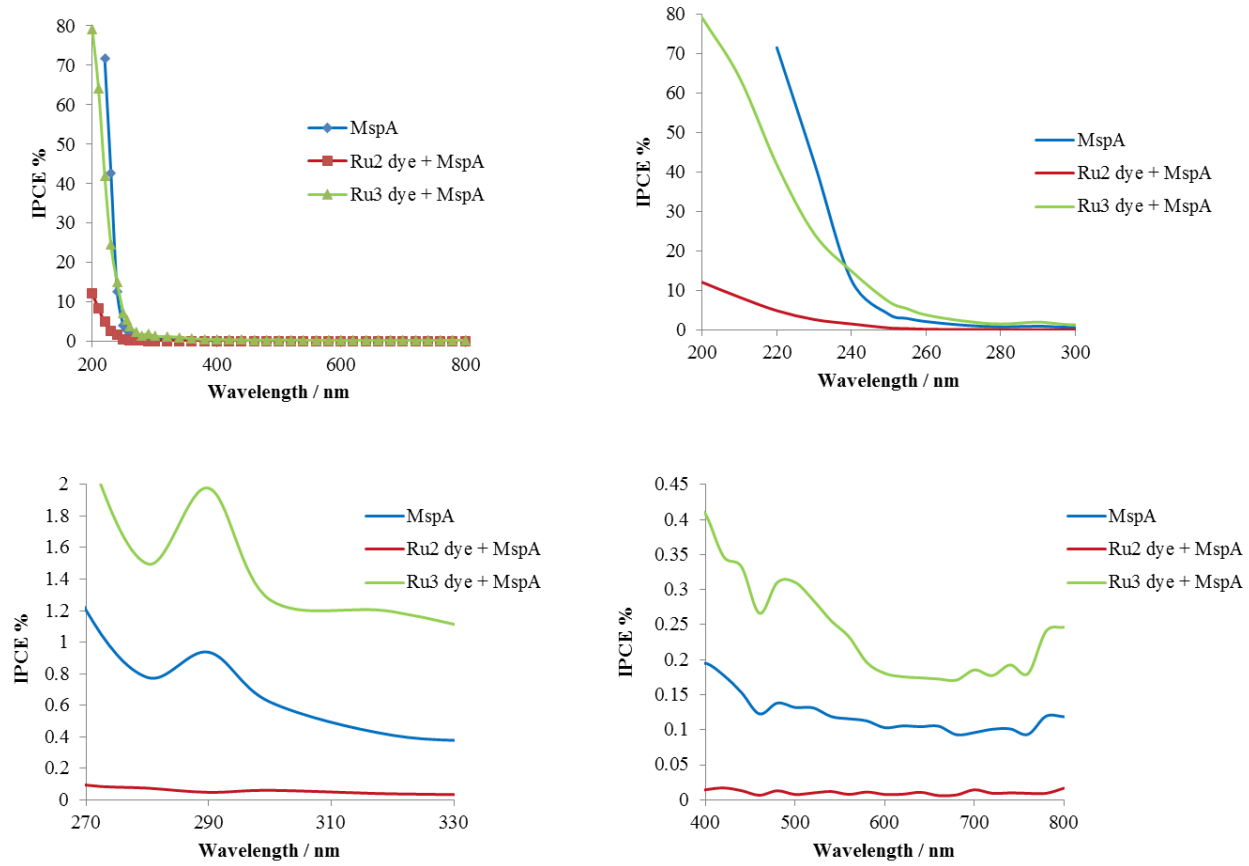


**Figure 5.33: IPCE% measurements for the FTO/$TiO_2$ based MspA and MspA-dye solar cells. Graphs depict the following wavelengths: top left – 200-800nm, top right – 200-300 nm, bottom left – 270-330 nm, bottom right – 400-800 nm**

It is evident from the above data that all three cells absorb maximum light in the UV region. This is in accordance with the absorption maxima of MspA, which is at 258 nm. There is no significant increase in IPCE% near the absorption maxima of Ru2 or Ru3, hence, it can be concluded that most of the current is generated from the protein itself and not from the dyes. This is in accordance with the I/V measurements discussed earlier.

The top right graph shows that the most intense absorption is seen in 200-240 nm region. An interesting observation was that the current kept decreasing and then fluctuating at one

wavelength over a considerable amount of time. At lower wavelengths, it took several minutes to reach a stable current to record a measurement. As the wavelength increased, the stabilization time decreased and recording of stable measurements was easier. The highest efficiency was observed for the MspA-Ru3 cell, which was 79.18% at 200 nm. The second highest efficiency of 71.63% was observed for the unbound MspA cell at 220 nm. The first couple of data points for this cell were discarded due to unstable current. The MspA-Ru2 cell gave an efficiency of 12.08% at 200 nm. These results mark the highest efficiency obtained by any of the protein incorporated DSSC's so far.

The bottom-left graph depicts absorption in 270-330 nm region. For the MspA and MspA-Ru3 cells, a very characteristic tryptophan singlet state absorption is observed at 290 nm. This is not seen for the MspA-Ru2 cell, probably due to dilution. The tryptophan absorption accounts for 1.98% conversion in the MspA-Ru3 cell. This in itself is twice the maximum efficiency observed for the Grätzel type MspA-Ru2 cell, which was 1% at 400 nm. This tryptophan absorption is solely from the transfer of singlet state energy and not from tryptophan excimers or from triplet state absorption. There is no evidence of electron back donation, so it is favorable energy transfer for current generation. This provides further evidence that the protein plays a key role in current generation as opposed to the sensitizer.

We also took a closer look at the visible region of 400-800 nm, which is the most significant region of absorption for a photovoltaic devise. This is depicted in the bottom-right graph. Even though overall absorption recorded was rather low, characteristic absorption patterns were detected in this region. The highest efficiency was given by MspA-Ru3 cell, which was

0.44% at 380 nm and 0.41% at 400 nm. The unbound MspA cell gave an efficiency of 0.2% at 400 nm and the efficiency of MspA-Ru2 cell was rather low in this region. All three cells had a characteristic minima at 460 nm accompanied by a maxima at 480 nm, which was clearly discernible. Another common peak was also present at 780 nm.

The overall conversion efficiencies of the FTO/$TiO_2$ based cells were calculated with respect to the solar irradiation spectrum. The results are depicted in the graphs below:

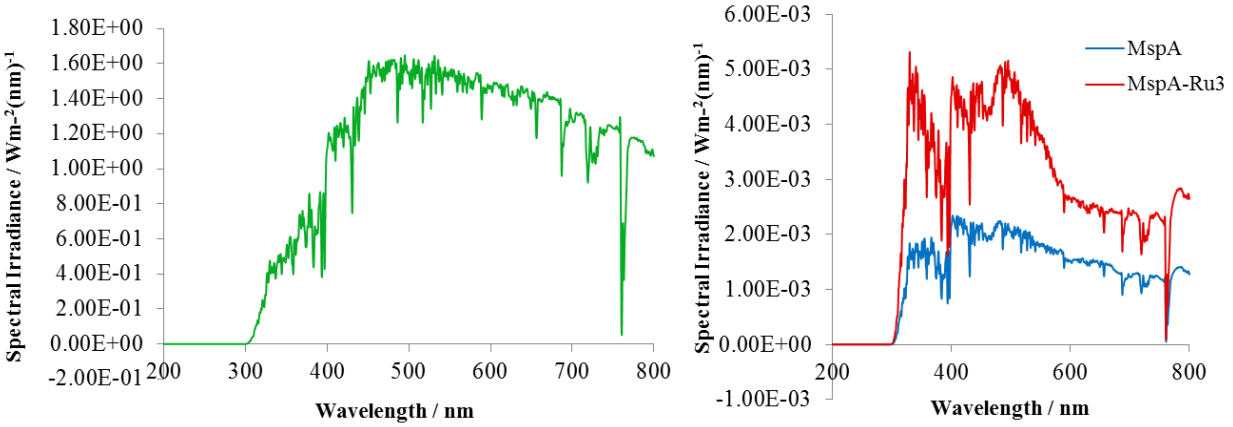


**Figure 5.34: Left - solar irradiation spectrum, right - irradiation spectra of FTO/$TiO_2$ based MspA and MspA-Ru3 cells**

The overall conversion efficiency of the unbound MspA cell was calculated to be 0.13%, with respect to the entire solar radiation spectrum at sea level. Since we observe significant difference in IPCE values for the UV and visible regions, conversion values for these regions were calculated separately. It was found that the MspA cell has an overall conversion of 0.31% at 200-380 nm and 0.12% at 381-800 nm. Hence, the cell converts three times more sunlight in the UV region, compared to the visible region. The overall conversion of the MspA-Ru3 cell, which gave the highest values of IPCE was 0.27%, which is twice as that of the MspA cell. In

the UV region however, this cell has a markedly higher conversion of 0.79%. For the visible region, conversion is found to be 0.24%, which is again twice the value of the unbound MspA cell.

### *5.3.5 Discussion*

The initial MspA-based solar cells were designed in accordance with the typical Grätzel DSSC's given in literature. Therefore the light wavelength tested for the cells was only in the visible region and a UV filter was used to cut-off light above 340 nm wavelengths. These experiments did not take into account the fact that the maximum absorbance of MspA occurs at the UV region in the electromagnetic spectrum (i.e. 258 nm). The second series of experiments were directed towards addressing the drawbacks of the preliminary studies hence a broader light range from 200 to 800 nm was employed. Indeed it was observed that the cells tested gave the maximum IPCE efficiency in the UV region.

Experiments done on polished FTO surfaces alone were intended to establish a fundamental understanding of how MspA would function in a completely flat surface, devoid of any physical or chemical support. Since these do indeed generate current, it is a testament first to the stability and second to the purity of the protein. If MspA were unstable, there would be no current at all or the results would not be repeatable. It is reasonable to assume that the free carboxylates found on its surface help to anchor the molecule onto the oxide surface and if the protein had impurities or was not in the form of an octamer, it would not adsorb so effectively onto a flat surface. This would result in lack of current or inconsistent results, which was not the case.

Initial use of a nanocrystalline $TiO_2$ layer on Grätzel cells was intended to increase surface area of the adsorbed sensitizer, thereby leading to a higher efficiency per unit area. However, for the MspA cell this is not entirely favorable. MspA tends to form vesicles in aqueous media and rarely exist as individual molecules (Refer to Chapter 2). These aggregates may clog on the particulate $TiO_2$ surface and may not expose the maximum number of protein molecules to the light source. This is even more complicated by addition of a dye to the protein as this increases the size and polydispersity of MspA aggregates (Refer to Chapter 4). Therefore it is crucial that a monolayer of protein or protein-dye complex is evenly deposited onto a monolayer of nanocyrstalline $TiO_2$. Hence a $TiO_2$ layer of 10 nm was deposited on a polished, flat FTO surface and a minimum amount of protein/protein dye solution was added and spread on the semiconductor surface as a thin layer. Schematic representation of an ideally constructed surface is given below:

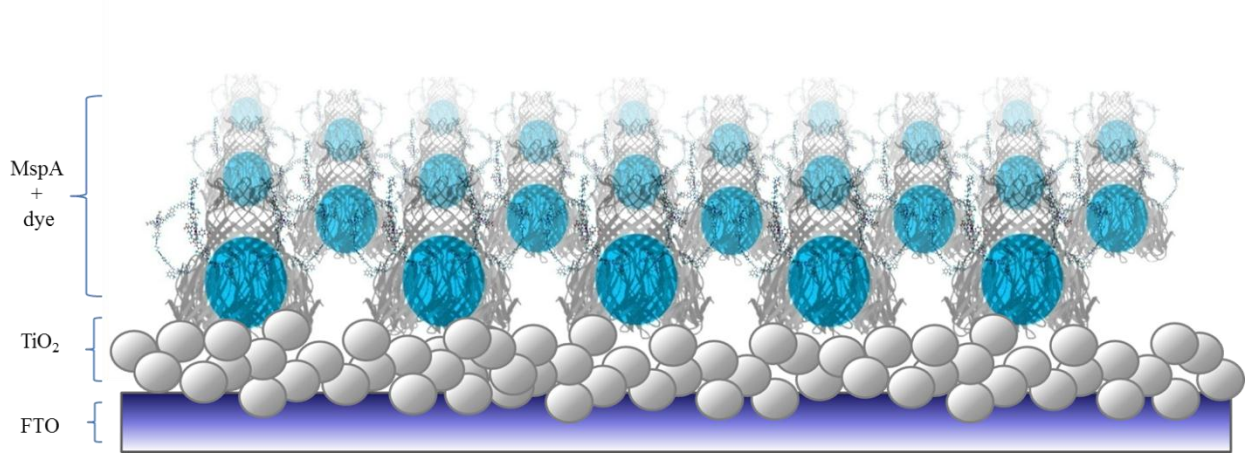


**Figure 5.35: Schematic representation of an ideally constructed surface for the MspA-dye solar cell**

In all the MspA and MspA-dye incorporated cells, a rapid increase in the current generated is observed close to -0.1 V. However, this is not observed in the Grätzel type cells or on FTO based cells, which contained the unbound dyes but did not contain MspA. This is a

rather unique feature of the protein solar cells and if analyzed correctly would provide insight into the electrochemical mechanisms of these cells. It is our hypothesis that this phenomenon is an effect created by the surface charge on MspA. It was shown earlier that zeta potential of MspA vesicles formed in 1x PBS, increases gradually with increasing temperature (refer to section 2.3.1.2). Increase in zeta potential is due to the buildup of positive charge on the surface of protein vesicles and could get as high as ~100 mV at higher temperatures for MspA. This is a result of accumulation of $Na^+$ and $K^+$ ions from the buffer, on the vesicle surface. A similar effect is predicted to occur when a voltage is applied to the MspA solar cell, causing a sudden jump in current across the system. In this regard, the MspA cell can be viewed as a capacitor, where positive charge is built up on the FTO electrode (containing MspA) and negative charge is built up on the Pt counter electrode. Hence the 'breakdown voltage' of the MspA electrode can be assumed to be around -0.1 V.

In order to prove the above theory, an MspA cell was constructed, completely devoid of the 1x PBS buffer. This was achieved by drying an MspA incorporated FTO/$TiO_2$ electrode under high vacuum for 24 hours. Prior to vacuuming, the cell was constructed by applying a thin film of MspA extract onto the electrode and drying it under laminar flow at room temperature for 24 hours (refer section 5.2.4). If the capacitance effect is true, then the current jump at -0.1 V should not be visible anymore in the I/V curve of the vacuum-dried cell. The I/V measurement for the dry cell was recorded first and afterwards, 50 µl of 1x PBS was added to the cell and the measurement was repeated. The latter was done to observe whether addition of the electrolyte would bring about any changes in current conductance of the dried cell. The results are given in the figure below:

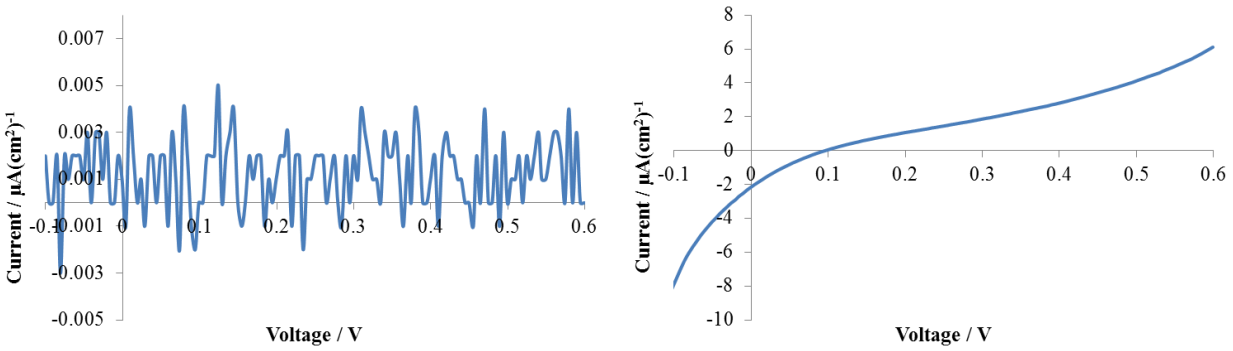


**Figure 5.36: I/V curves for FTO/$TiO_2$ based MspA cells; Left - vacuum dried MspA cell, Right – 1x PBS added MspA cell**

As can be seen on the left curve, the vacuum dried cell does not conduct any current. A similar curve was obtained earlier for FTO/$TiO_2$ based cell containing 1x PBS alone (refer to figure 5.28). Hence it is evident that the PBS electrolyte is necessary for the overall function of MspA based cells. The curve on the right shows the I/V data obtained for the same cell after addition of PBS. This curve is very much similar to the characteristic curves obtained earlier for MspA and MspA-dye cells (refer figures 5.26, 5.29). It provides further evidence to the crucial role played by the PBS buffer as an electron transport medium for MspA. However, the reproducibility of the above results was questionable. For example, when the experiment was repeated after few minutes, the shape of the I/V curve changed significantly. The repeated measurements consistently gave a curve with an almost straight line, much like a characteristic curve of a resistor. (Refer figure 5.37) We are unable to provide a definite explanation to this phenomenon at present.

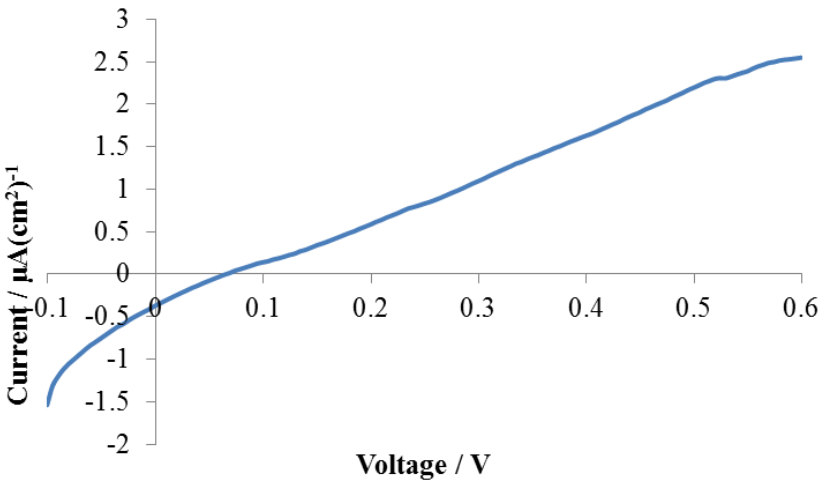


**Figure 5.37: Repeated I/V measurement for vacuum dried MspA cell after addition of 1x PBS**

The results depicted in the right curve of figure 5.35 provide evidence to support our theory on the influence of positive ions from the buffer in creating a characteristic curve for the MspA based cells. However, we did not expect to see complete lack of current but rather the absence of the current jump at -0.1V. This was simply because the earlier experiments conducted on MspA cells without PBS also showed similar current conductance behavior (refer to figure 5.25). It is now clear that the current is brought about by interaction of MspA with the remaining buffer medium, after drying in room temperature. It is also evident that the combination of MspA and PBS is both complementary and necessary to conduct a current across the electrodes.

### *5.3.6 Future prospects*

It was our hypothesis from the beginning that the free carboxylate groups that are mostly concentrated close to the wider rim of MspA would anchor the molecule onto the oxide surface of the semiconductor. However, in the initial experiments there was no way of controlling the orientation of MspA molecules hence, no way of controlling the homogeneity of the protein-dye

layer on the oxide surface. During the FTO-based cell experiments, a very thin layer of MspA or MspA-dye solution was spread onto the oxide surface. Here the assumption is made that the free polar ends of MspA would rearrange themselves in the thin film to be oriented towards FTO/$TiO_2$ surface. However, careful construction of a protein monolayer and proper deposition of that monolayer onto a $TiO_2$ monolayer would give us more control over formation of a homogeneous surface, which would eventually lead to higher efficiency of the cell. Formation of a surfactant bilayer on water and injecting an MspA solution onto it would result in spontaneous rearrangement so that the hydrophobic terminal ends of MspA molecules would insert into the bilayer while the hydrophilic rims would face towards the water. (Refer to figure below) A Langmuir trough can be employed to facilitate the formation of monolayers.[28,29]

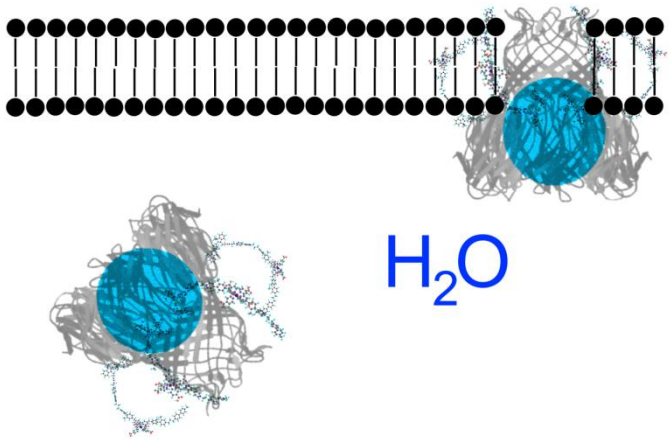


**Figure 5.38: Schematic representation of monolayer formation of MspA in surfactant bilayers**

A significant finding on the FTO/$TiO_2$ based cells was that the protein and dyes conduct current in opposite directions, thereby cancelling out part of the overall current. Since this is

obviously a drawback, which leads to reduced current, it is necessary to plan future endeavors to design alternate dyes that contribute to current generation in the correct direction.

It is apparent that one of the major drawbacks of the MspA solar cell is that is does not absorb significant amount of light in the visible region. One possibility of addressing this issue would be to express the Green Fluorescent Protein[30,31] (GFP) gene in *M. smegmatis,* resulting in MspA capable of actively absorbing light in the green region of the visible spectrum.[32] The GFP gene is commonly used for biosensing and as a reporter of expression. It also has been known to be successfully expressed in bacteria. Since *M. smegmatis* is known to conveniently express engineered genetic mutations, the above method provides a viable means of introducing an enhanced feature to our mycobacterial porin based solar cells. This is in effect similar to the use of multiple dyes, which absorb in different visible light ranges in DSSC's.

It was apparent that the electrode surface that provides optimum protein-dye accommodation leads to enhanced current generation and efficiency. Therefore it is necessary to carry out further investigations in search of an ideal surface for MspA-based cells. One such possible prospect is the use of organic polymer based surfaces, which are also known as Organic Photovoltaics (OPVs). These are gradually becoming significant in the field of photovoltaics as alternate materials, which are cost effective and easy to process.[33] We propose the use of poly-pyrrole and poly-thiophene compounds in this regard. The Nitrogen and Sulfur atoms in these compounds would provide sufficient electro-chemical attachment sites to anchor the cysteine groups in A96C MspA.

## 5.4 Conclusions

Development of the first ever protein-based nano solar cell prototypes has been achieved, as a new class of sustainable and 'greener' alternate energy source. Two categories of cells have been fabricated and tested in this regard. Initially, Grätzel type (i.e. nanocystalline $TiO_2$ based, dye sensitized) cells were developed using chemically bound MspA-dye assemblies. Synthesis of two novel Ruthenium(II)-polypyridine dyes, Ru1 and Ru2 have been achieved for this purpose. All dyes and MspA-dye assemblies have been successfully characterized. The MspA-Ru2 cells conduct a steady, reproducible current with a maximum IPCE of 1% at 400 nm.

A second class of MspA cells based on FTO and FTO/$TiO_2$ was developed as an attempt to enhance and improve overall efficiency and performance. Another novel dye, Ru3 has also been developed and tested along with the previous dyes in this regard. The FTO based cells containing only MspA and MspA-dye assemblies show conductance of a nano Ampere range, steady current with and without 1x PBS buffer as electrolyte. The commercial Iodolyte electrolyte medium is shown to be unfavorable for these cells.

FTO/$TiO_2$ based MspA and MspA-dye cells of a similar nature have also been developed and show promising results. These have a slightly higher overall current than the former. 1x PBS buffer is recognized as the optimum electrolyte medium for the MspA-based cells. Important mechanistic insight into the direction of electron transfer of MspA and the Ruthenium dyes have been achieved and are shown to be in opposite directions. This is emphasized as a cause of reduction of current. IPCE% of these cells shows a remarkable improvement from the Grätzel type cells. While all cells have maximum efficiencies in the UV region, the highest was obtained

from MspA-Ru3 cells. These cells were active in both UV and visible regions and gave efficiencies at ~80% at 220 nm and ~2% at 400 nm. The MspA and MspA-Ru2 cells also show promising results.

These results mark the first evidence of a photovoltaic device, which is based on a protein. We propose this technology as a new class of solar cells classified as "hybrid soft cells".

## 5.5 References


[1] Moser, J. Monatsh. *Chem.***1887**, *8*, 373.

[2] Peter Gevorkian (1 August 2007). "Sustainable energy systems engineering: the complete green building design resource". McGraw-Hill Professional.pp.498, ISBN 978-0-07-147359-0. http://books.google.com/books?id=i8rcHsOfPScC&pg=PA498. Retrieved 29 February 2012.

[3] Honda, K.; Fujishima, A. "Electrochemical photolysis of water at a semiconductor electrode", *Nature,* **1972**, *238*, 37-39.

[4] Wrighton, M. S. "Photoelectrochemical conversion of optical energy to electricity and fuels", *Acc. Chem. Res.***1979**, *12*, 303-310.

[5] http://en.wikipedia.org/wiki/Solar_cell#cite_ref-Gevorkian2007_1-0

[6] O'Regan, B.; Gra¨tzel, M. "A low-cost, high-efficiency solar cell based on dye-sensitized colloidal $TiO_2$films", *Nature* **1991**, *353*, 737-739.

[7]http://www.millenniumprize.fi/news/165/111/PROFESSOR-GRaeTZEL-WINS-THE-2010-MILLENNIUM-TECHNOLOGY-GRAND-PRIZE-FOR-DYE-SENSITIZED-SOLAR-CELLS/d,news_en/

[8] Grätzel, M. "Dye-sensitized solar cells", *Journal of Photochemistry and Photobiology C: Photochemistry Reviews* **2003**, *4,* 145–153.

[9] Adachi, M.; Murata, Y.; Okada, I.; Yoshikawa, S. "Formation of Titania Nanotubes and Applications for Dye-Sensitized Solar Cells",*J. Electrochem.Soc.***2003**, *150*, G488.

[10] Huynh, W. U.; Dittmer, J. J.; Alivisatos, A. P. "Hybrid nanorod-polymer solar cells", *Science* **2002**, *295*, 242.

[11] Shklover, V.; Ovchinnikov, Yu.E.; Braginsky, L. S.; Zakeeruddin, S. M.; Gratzel, M. "Structure of organic/inorganic interface in assembled materials comprising molecular components. Crystal structure of the sensitizer bis[(4,4'-carboxy-2,2'-bipyridine)(thiocyanato)]ruthenium(II)" *Chem. Mater.***1998**, *10*, 2533.

[12] Vittadini, A.; Seloni, A.; Rotzinger, F. P.; Gratzel, M. "Structure and energetics of water adsorbed at TiO2 anatase \(101\) and \(001\) surfaces", *Phys. Rev. Lett.***1998**, *81*, 2954.

[13] Gao, F; Wang, Y; Zhang, J; Shi, D; Wang, M; Humphry-Baker, R; Wang, P; Zakeeruddin, S. M.; Grätzel, M. "A new heteroleptic ruthenium sensitizer enhances the absorptivity of mesoporoustitania film for a high efficiency dye-sensitized solar cell", *Chemical communications* **2008**, *23*, 2635–7.

[14] Kruger, J.; Plass, R.; Gratzel, M. "Improvement of the photovoltaic performance of solid-state dye-sensitized device by silver complexation of the sensitizer cis-bis(4,4′-dicarboxy-2,2′bipyridine)-bis(isothiocyanato) ruthenium(II)", *Appl. Phys. Lett.***2002**, *81*, 367-369.

[15] Nazeeruddin, M. K.; KayA.;Rodicio I.;Humpbry-Baker R.; MiillerE.;LiskaP.; VlachopoulosN.; GratzelM. "Conversion of light to electricity bycis-$X_2$bis( 2,2'-bipyridyl-4,4'-dicarboxylate)ruthenium(II) charge-transfer sensitizers (X = C1-, Br-, I-, CN-, and SCN-) on nanocrystalline $TiO_2$ electrodes", *J. Am. Chem. Soc.* **1993**, *115*, 6382-6390.

[16] Benko G.; Kallioinen J.; Korppi-Tommola J. E. I.; Yartsev A. P.;Sundstrom V. "Photoinduced ultrafast dye-to-semiconductor electron injection from nonthermalized and thermalized donor states", *J. Am. Chem. Soc.124*, **2002**, 489.

[17] Nazeeruddin,M.K.;Pechy, P.; Renouard, T.; Zakeeruddin, S.M.; Humphry-Baker, R.; Comte, P.; Liska, P.; Cevey, L.; Costa, E.; Shklover,V.; Spiccia, L.; Deacon, G.B.; Bignozzi, C.A.; Grätzel, M. "Engineering of efficient panchromatic sensitizers for nanocrystalline TiO2-based solar cells", *J. Am. Chem. Soc.* **2001**, *123*, 1613–1624.

[18] Hu Y.; Bossmann S. H.; van Loyen D.; Schwarz O.; Durr H. "A novel 2,2′-bipyridine[2]catenane and its ruthenium complex: synthesis, structure, and intramolecular electron transfer— A model for the photosynthetic reaction center",*Chem. Eur. J* .**1999**, No. 4, 1267-1277.

[19] Casper J. V.; Meyer T. J. *J. Am. Chem. Soc.***1983**, *105*, 558.

[20] Seiler M.; Durr H.; Willner I.; Joselevich E.; Doron A.; Stoddart J. F. "Photoinduced electron transfer in supramolecular assemblies composed of dialkoxybenzene-tethered Ruthenium(II) trisbipyridine and bipyridinium Salts", *J. Am. Chem. Soc.***1994**, *116*, 3399.

[21] Schild V.; van Loyen D.;Durr H.; Bouas-Laurent H.; Turro C.; Worner M.; Pokhrel M. R.; Bossmann S. H. "Tuning the charge-separated life times of Ruthenium(II)polypyridyl-viologen dyads and Ruthenium(II)polypyridyl-viologen triads by the formation of supramolecular assemblies with crown ethers", *J. Phy. Chem. A* **2002**, *106*, 9149-9158.

[22] Butler T. Z.; Pavlenok M.; Derrington I. M.; Niederweis M.; Gundlach J. H. "Single-molecule DNA detection with an engineered MspA protein nanopore", *PNAS*, **2008**, *105*, 20647-20652.

[23] Bossmann, S. H.; Ghatlia, N. D.; Ottaviani, M. F.; Turro, C.; Durr, H.; Turro, N. J. "Synthesis and characterization of nitroxide-linked ruthenium complexes as molecular probes for microheterogeneous environments", *Synthesis*, (November) **1996**, 1313-1319.

[24] Walker, M. A."A High Yielding Synthesis of N-Alkyl Maleimides Using a Novel Modification of the Mitsunobu Reaction", *J. Org. Chem.* **1986**, *60*, 5352-5355.

[25] Xia, J.; Masaki, N.; Jiang, K.; Yanagida, S. "Deposition of a thin film of TiO*x* from a titanium metal target as novel blocking layers at conducting glass/$TiO_2$ interfaces in ionic liquid mesoscopic $TiO_2$ dye-sensitized solar cells", *J. Phy. Chem. B* **2006**, *110*, 25222-25228.

[26] Essner, J. "Dye sensitized solar cells: optimization of Gratzel solar cells towards plasmonic enhanced photovoltaics", Department of Chemistry, Kansas State University, **2011**.

[27] Vesce, L.; Riccitelli, R.; Soscia, G.; Brown, T. M.; Di Carlo, A.; Reale, A., "Optimization of nanostructured titaniaphotoanodes for dye sensitized solar cells: Study and experimentation of TiCl4 treatment", *Journal of Non-Crystalline Solids*, **2010**, *356*, (37-40), 1958-1961.

[28] Langmuir I. "The constitution and fundamental properties of solids and liquids" *J. Am. Chem. Soc*. **1917**, *9*, 1848.

[29] Langmuir I.; Schaefer V. J. "Properties and structure of protein monolayers" *Research Laboratory, General Electric Company, Schenectady, New York* **1939**.

[30] Prendergast, F.: Mann, K. "Chemical and physical properties of aequorin and the green fluorescent protein isolated from Aequoreaforskålea",*Biochemistry***1978**, *17*, 3448–53.

[31] Tsien, R."The green fluorescent protein", *Annu Rev Biochem* **1998**, *67*, 509–44.

[32] Phillips, G. "Green fluorescent protein--a bright idea for the study of bacterial protein localization", *FEMS MicrobiolLett* **2001**, *204*, 9–18.

[33] Gunes, S.; Neugebauer, H.; Sariciftci, N. S.; "Conjugated Polymer-Based Organic Solar Cells", *Chem. Rev.* **2007**, *107*, 1324-1338.

# Appendix A - Analytical Assessment of MspA

| Detergent | Class (anionic = A, cationic = C, neutral = N) | Buffer |
|---|---|---|
| Dodecyl sulfate, sodium salt (SDS) | A | PS05 |
| Cholate, sodium salt | A | PCH09 |
| Cetyltrimethylammonium bromide (CTAB) | C | PCT01 |
| 3-Dodecyldimethylammoniopropane-1-sulfonate (Zwittergent 3-12) | Z | PZ01 |
| *n*-Dodecyldimethylamine oxide (LDAO) | Z | PLD005 |
| *n*-Octylpolyethylene oxide (OPOE) | N | POP05 |
| *n*-Octyl-b-D-thioglucoside (OSG) | N | POT06 |
| Isotridecylpolyethyleneglycolether (Genapol X-80) | N | PG001, PG05 |

**Table A. 1: Names of detergents tested for solubilizing of MspA, their class and abbreviations (Taken with permission from reference 15)**

# HPLC data for wild type MspA

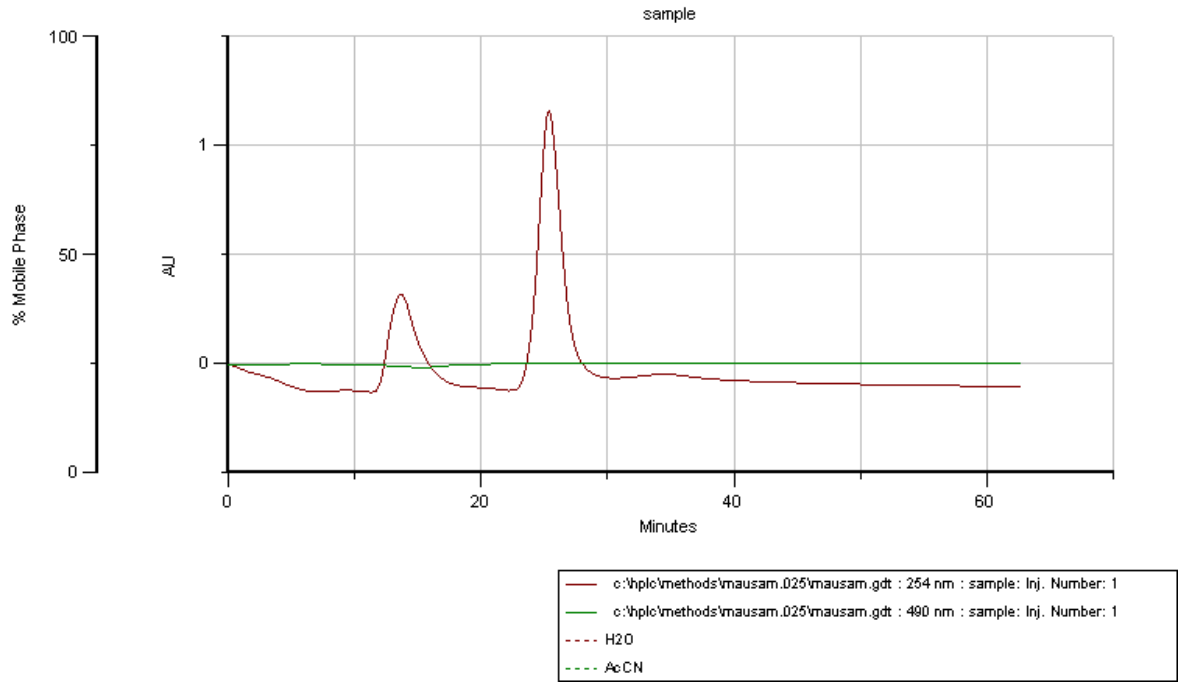


**Figure A. 1: Preparative HPLC of mc$^2$ 155 MspA extracted on 05/21/10**

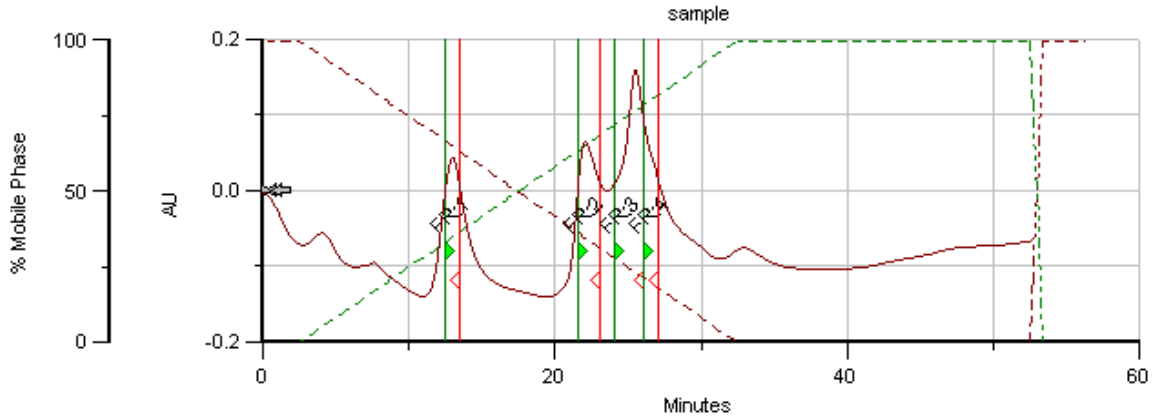


**Figure A. 2: Quantitative HPLC of mc2 155 MspA extracted on 05/21/10**

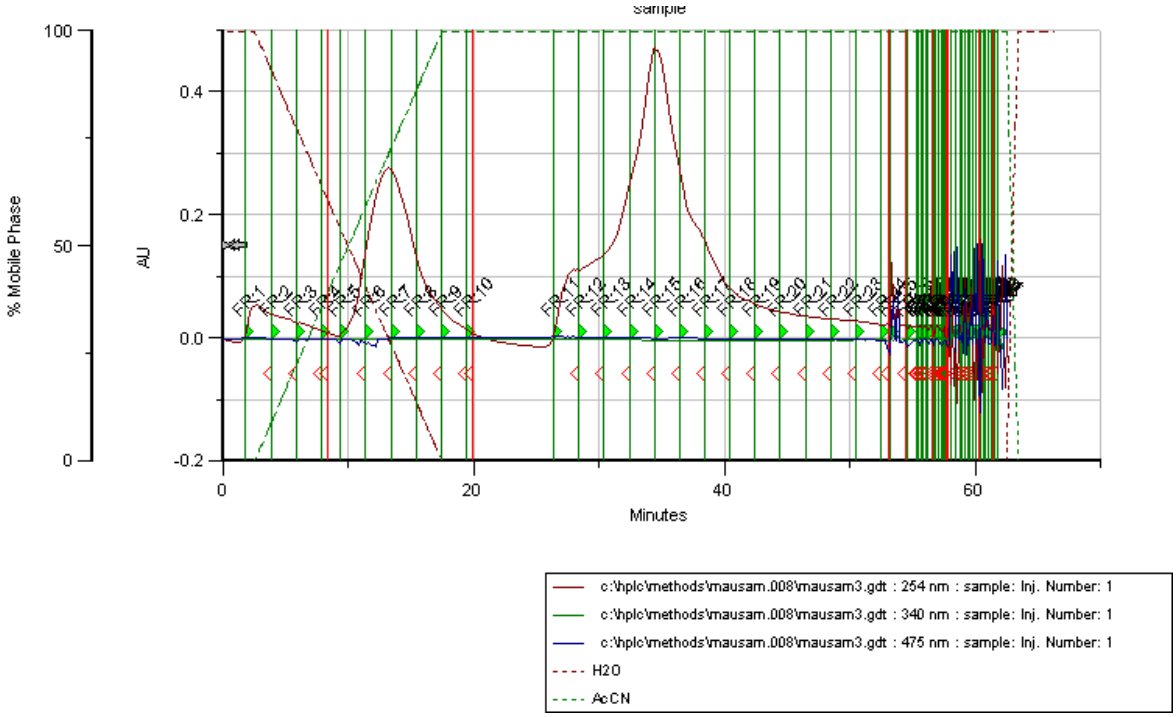


**Figure A. 3: Quantitative HPLC of mc2 155 MspA extracted on 10/03/10**

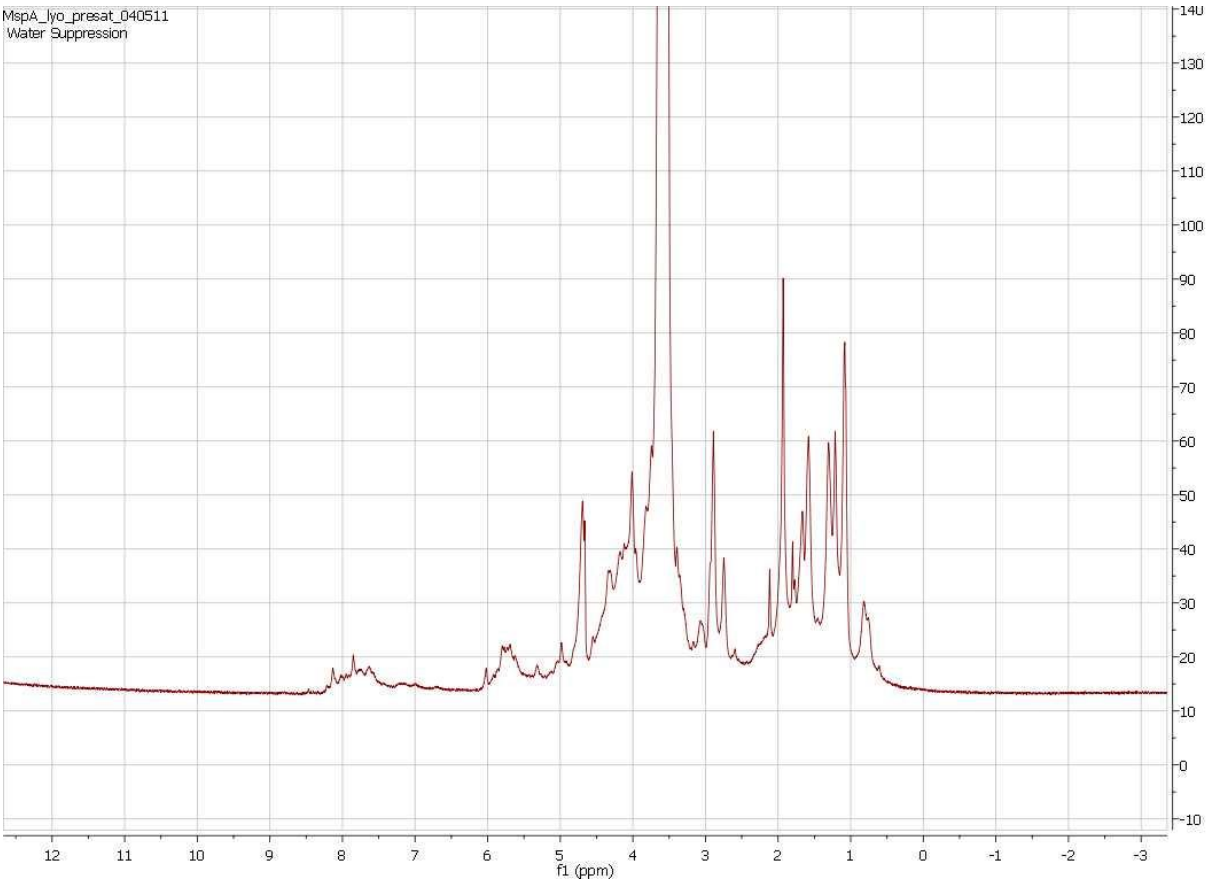


**Figure A. 4: $^{1}$H NMR of wild type MspA**

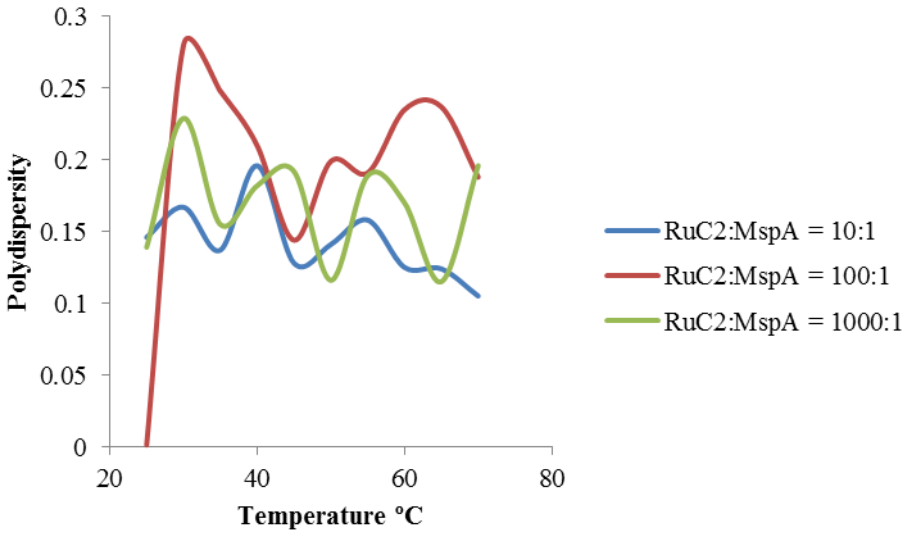


**Figure A. 5: Polydispersity vs. temperature of RuC2-MspA assemblies**

# Appendix B - Characterization of Ruthenium(II)-Phenanthroline Complexes

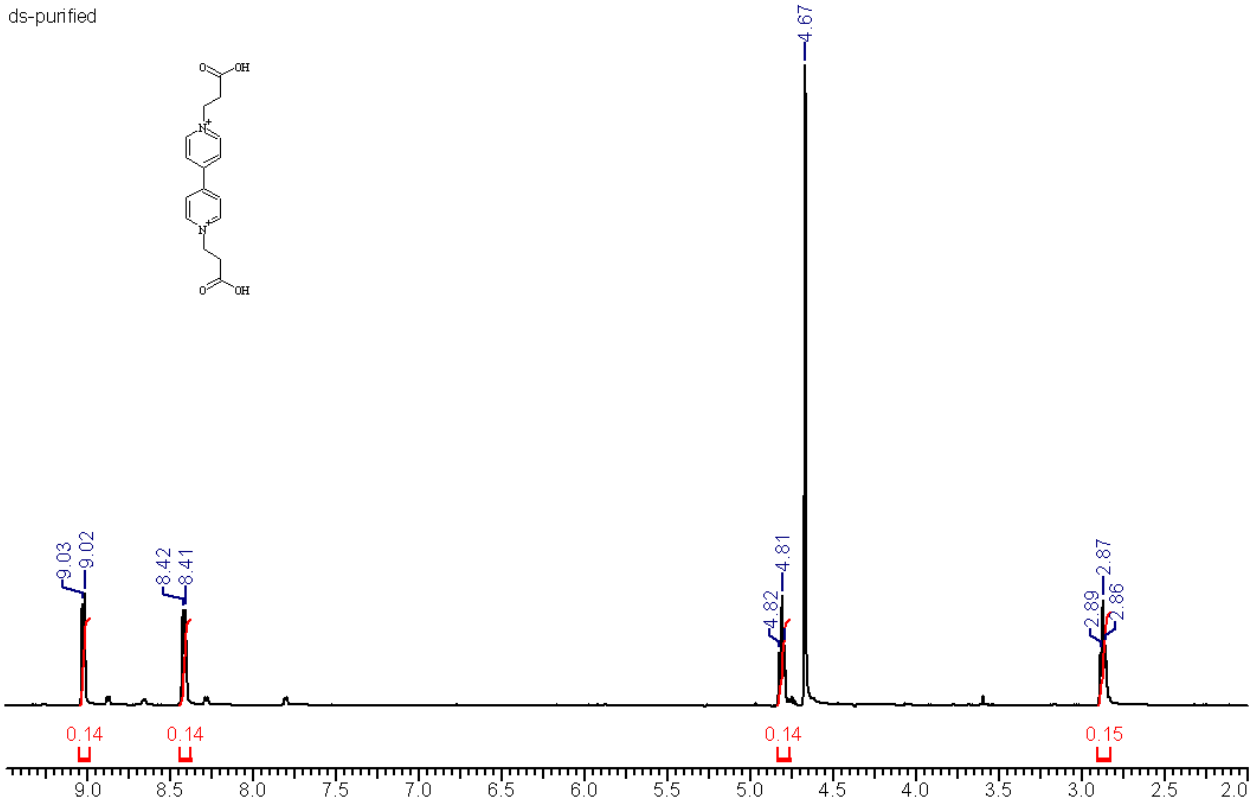


**Figure B. 1: $^{1}$H NMR of4,4'-Dipyridinium-bis-(*N*-propanoic acid)**

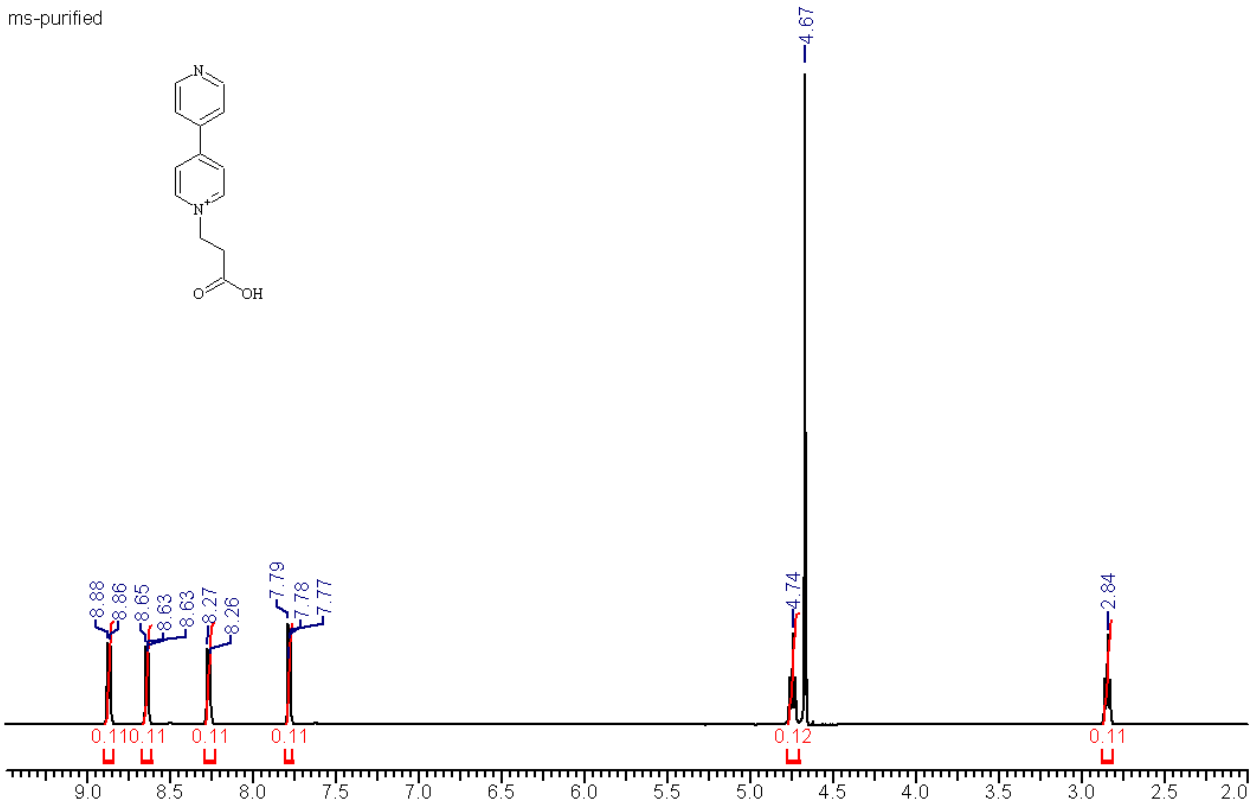


**Figure B. 2: $^{1}$H NMR of4,4'-Dipyridinium-*N*-propanoic acid**

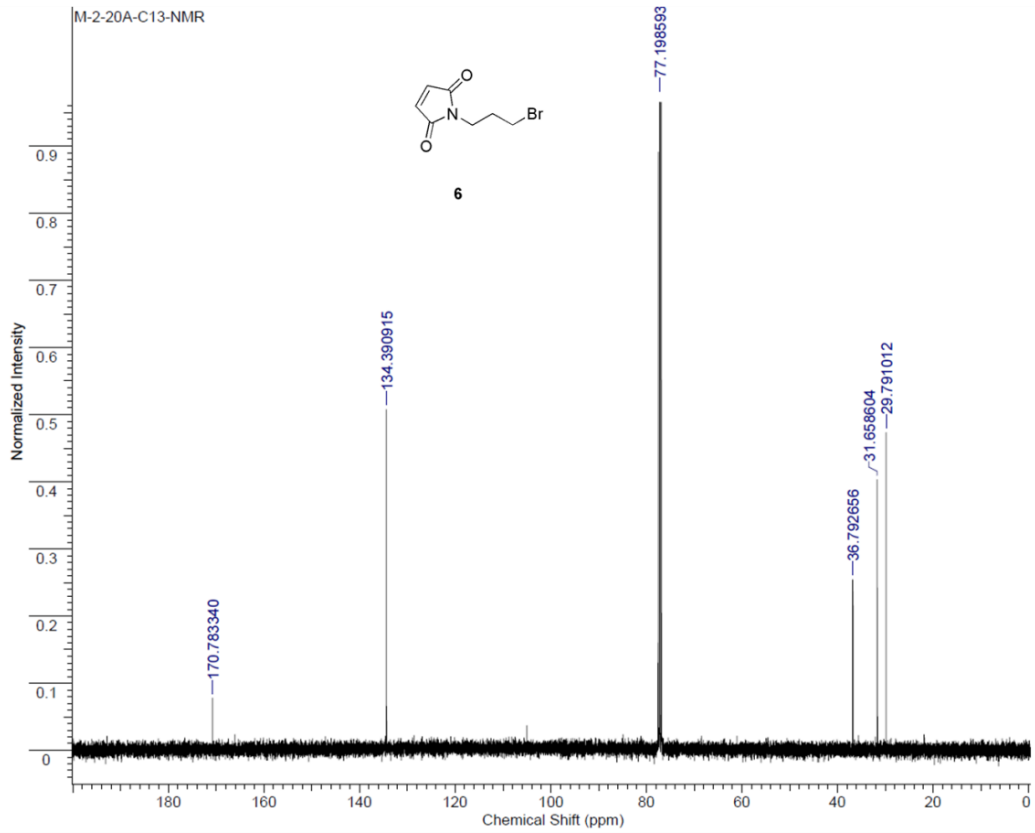


**Figure B. 3: $^{1}$H NMR of *N*-propylbromomaleimide**

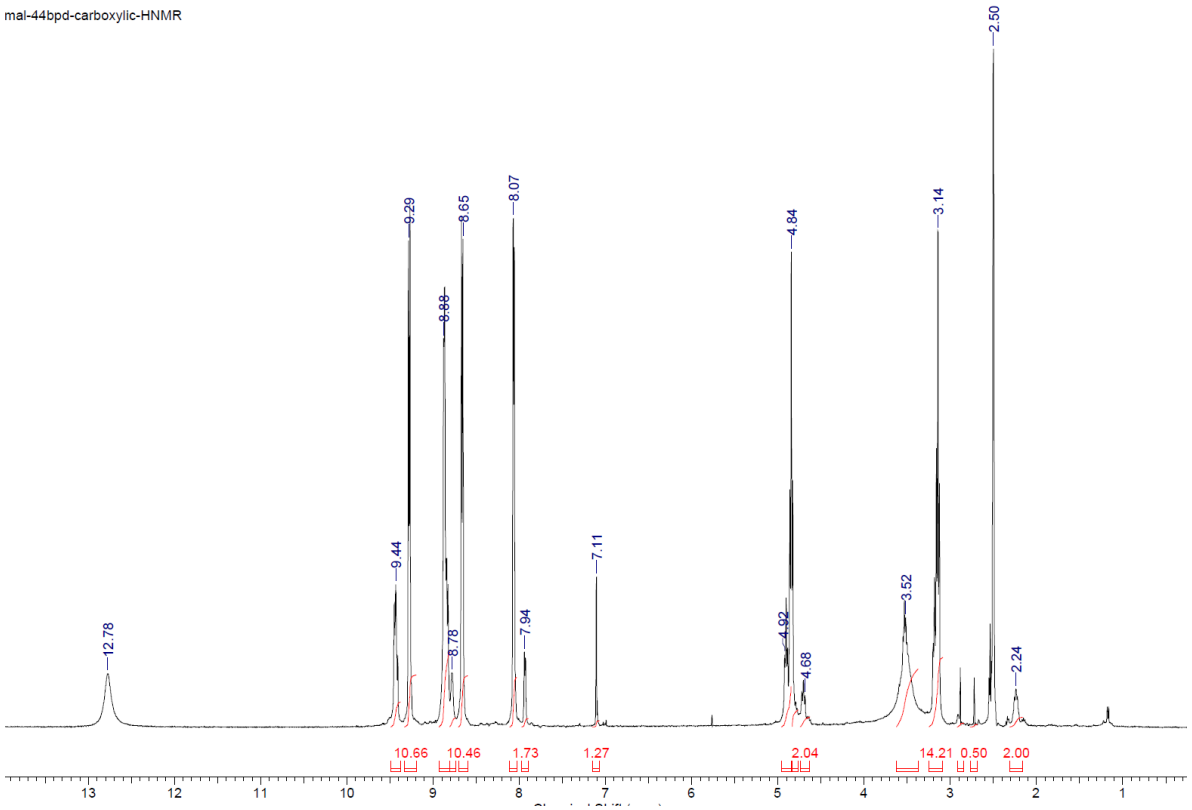


**Figure B. 4: $^{1}$H NMR of1-(2-carboxyethyl)-1'-(3-(2,5-dioxo-2,5-dihydro-1H-pyrrol-1-yl)propyl)-[4,4'-bipyridine]-1,1'-diium**

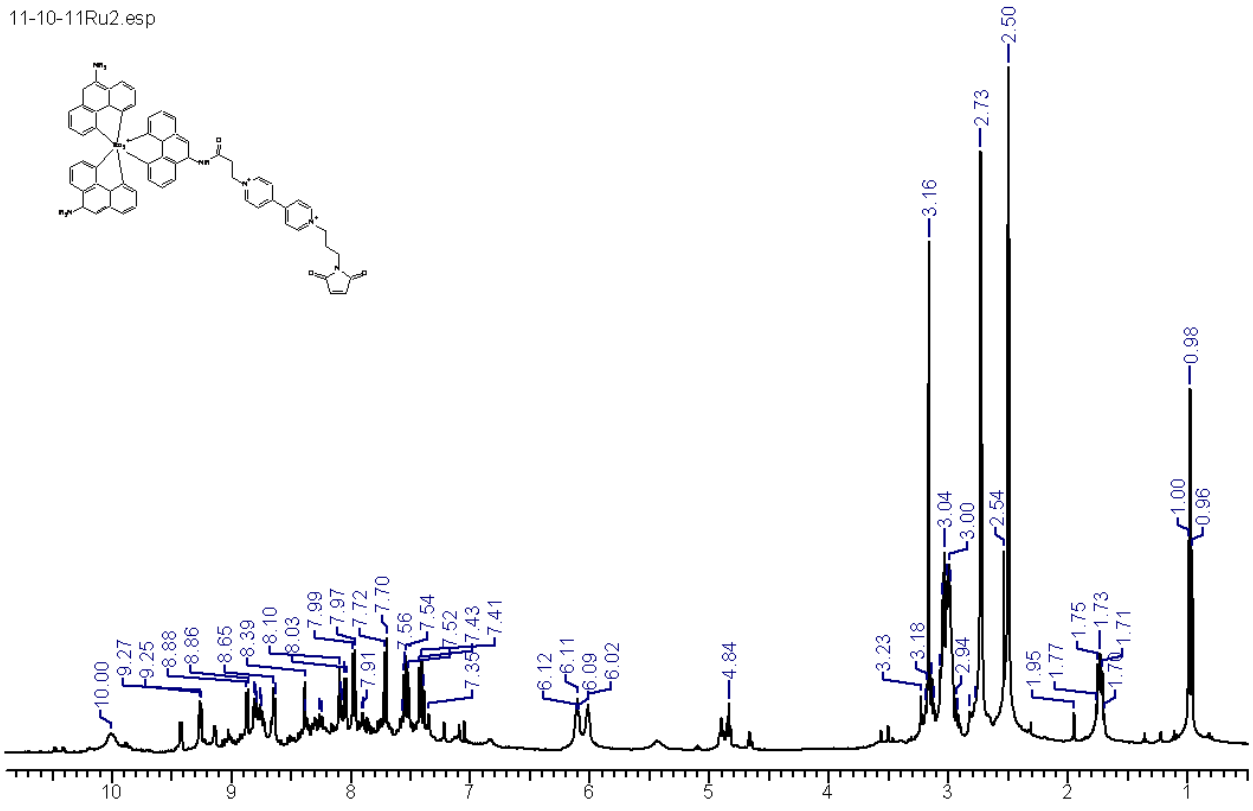


**Figure B. 5: $^{1}$H NMR of Ru2**

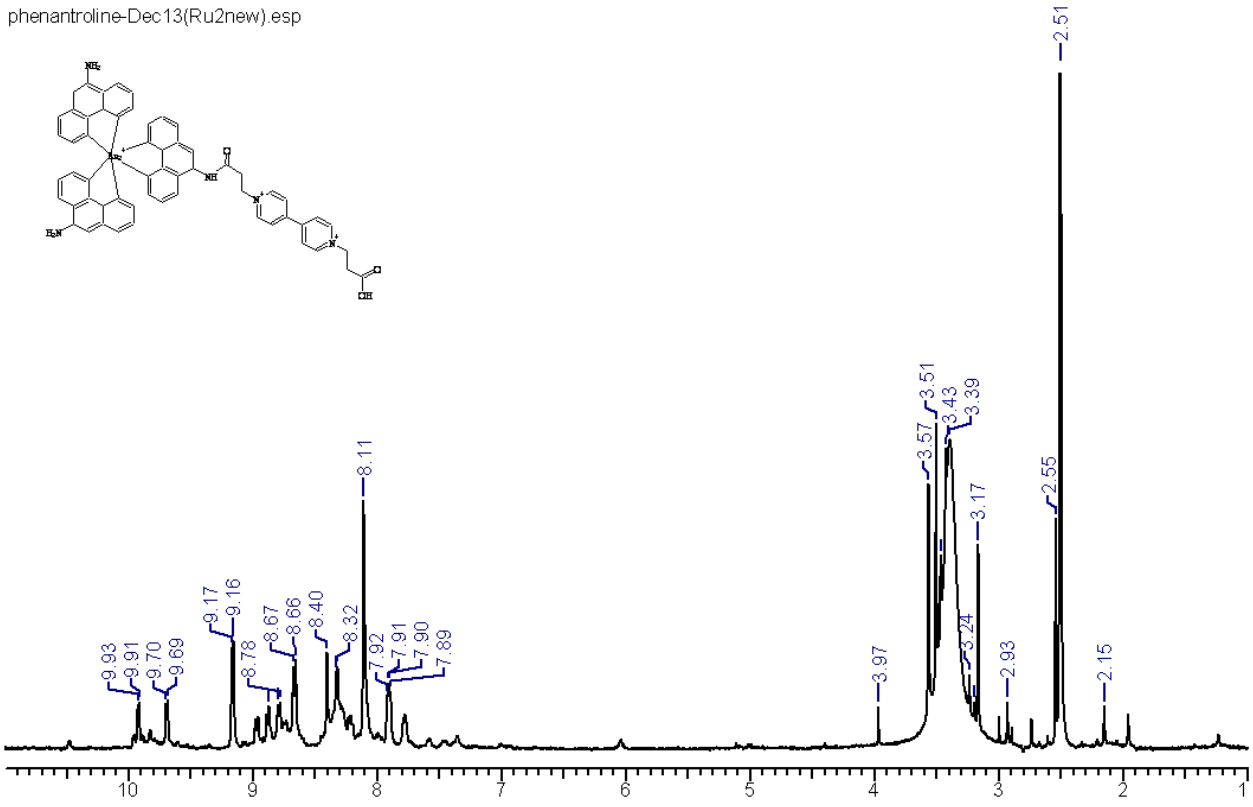


**Figure B. 6: $^{1}$H NMR of Ru3**

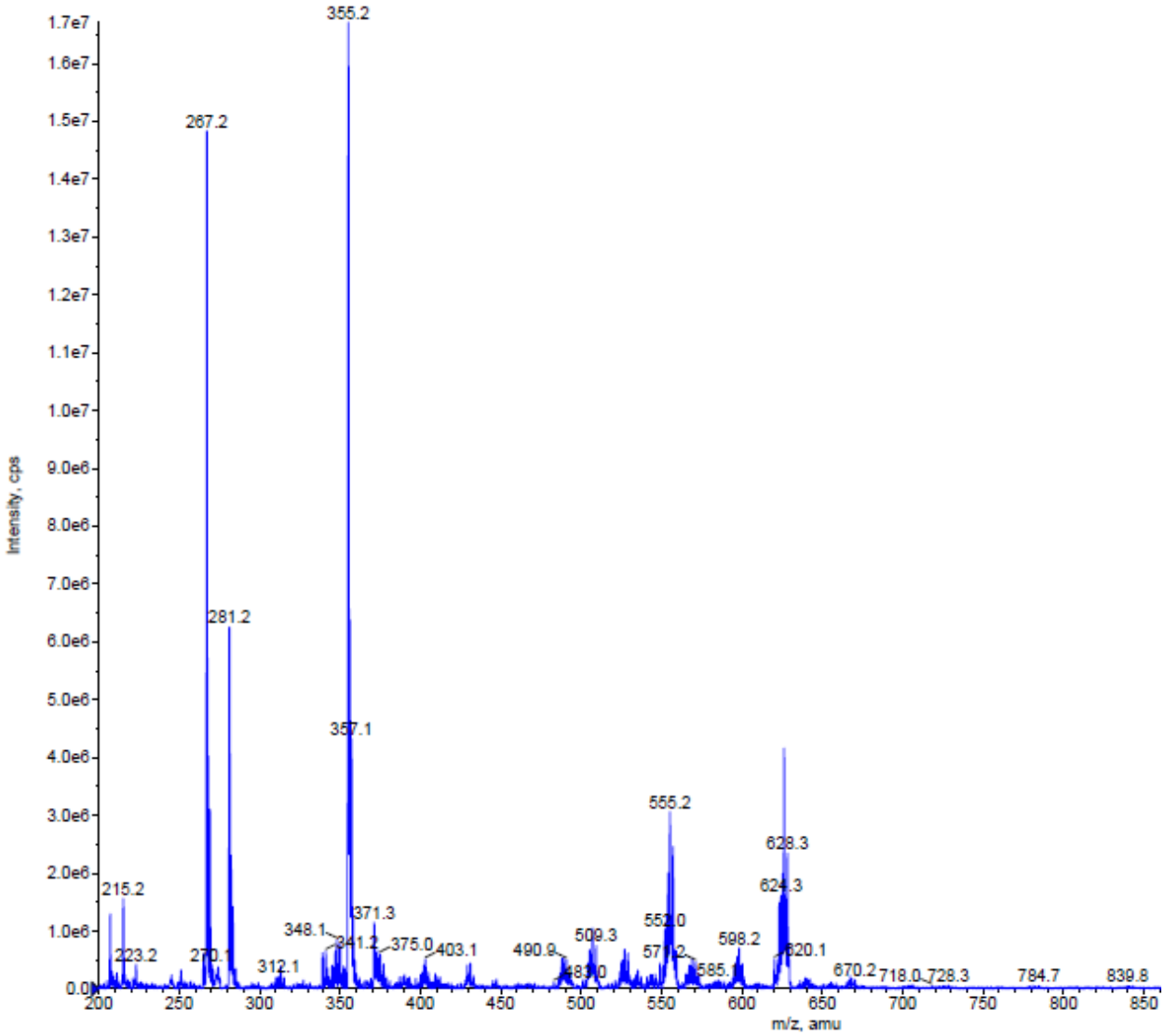


**Figure B. 7: Mass spectrum of Ru1**

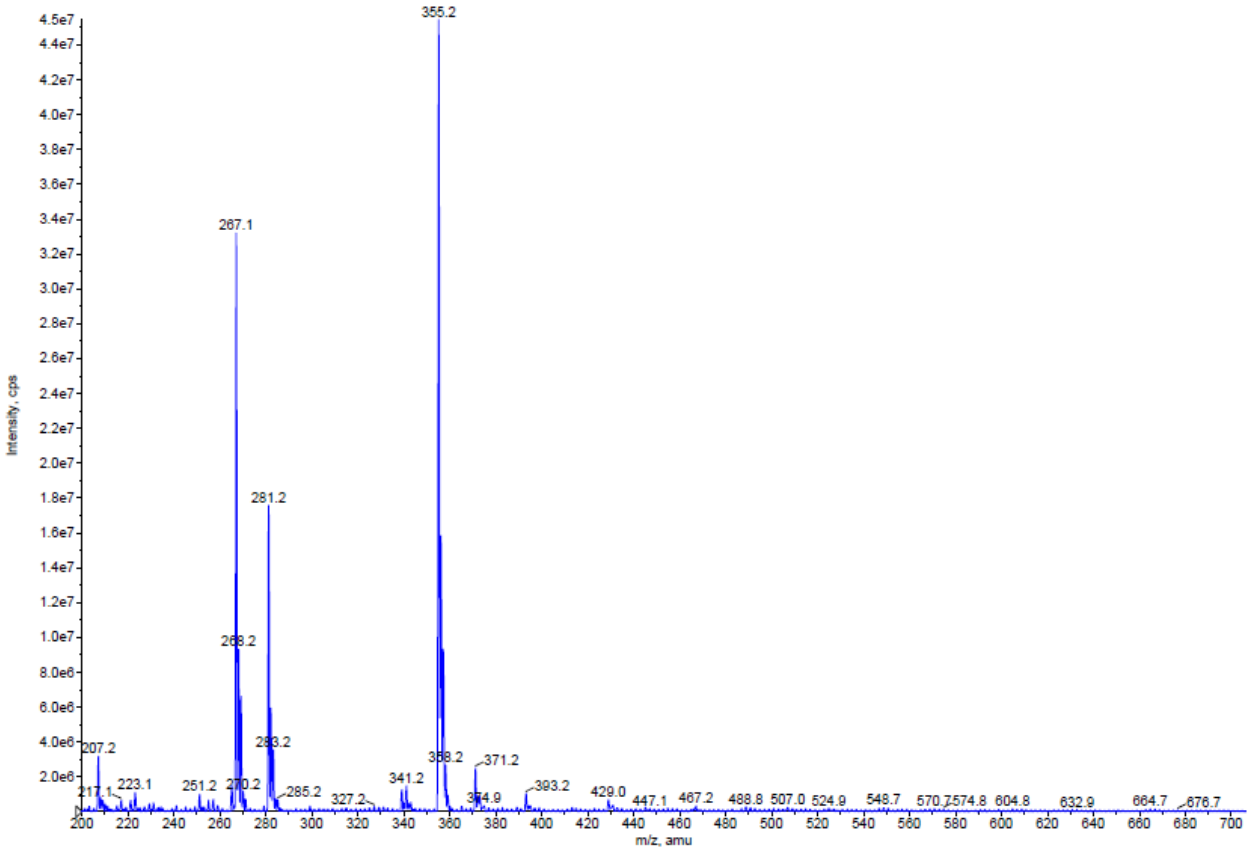


**Figure B. 8: Mass spectrum of Ru2**

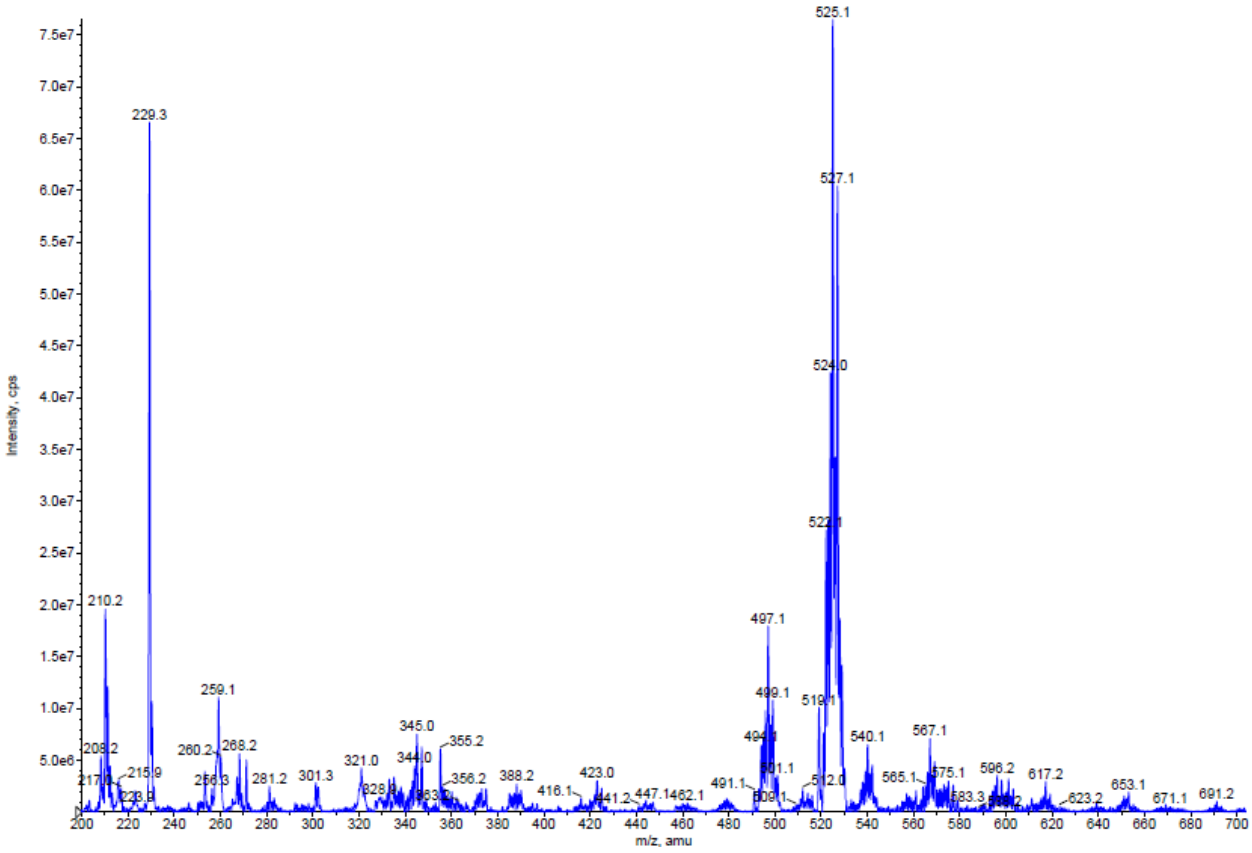


**Figure B. 9: Mass spectrum of Ru3**